LIPID BIOMARKERS FOR CANINE ATOPIC DERMATITIS

by

Jackeline Franco Marmolejo

A Dissertation

Submitted to the Faculty of Purdue University

In Partial Fulfillment of the Requirements for the degree of

Doctor of Philosophy

Department of Comparative Pathobiology

West Lafayette, Indiana

May 2019

THE PURDUE UNIVERSITY GRADUATE SCHOOL
STATEMENT OF COMMITTEE APPROVAL

Dr. Harm HogenEsch, Chair
College of Veterinary Medicine
Dr. Christina R Ferreira
College of Science
Dr. Yava L Jones-Hall
College of Veterinary Medicine
Dr. Stephen Hooser
College of Veterinary Medicine

Approved by:

Dr. Sanjeev K. Narayanan
Head of the Graduate Program

To my mother who never gave up, to my beloved husband who has always supported me and to Octavio and Amelia who push me to be better every day.

ACKNOWLEDGMENTS

I am very thankful to my advisor Dr. Harm HogenEsch for giving me the opportunity to undertake this research and for his support and guidance. I would like to thank Dr. Christina R. Ferreira who taught me a new area of research that I now love and who motivated me to keep growing in it.

I would like to thank my committee members, Dr. Yava L Jones-Hall and Dr. Stephen Hooser for their valuable time and advice.

I want to thank Dr Paulo Gomes and Lara Luke for their essential participation in this research making possible the recruitment of the dogs. As well, I am thankfull to Dr. Bartek Rajwa, who's data analysis input deeply improved the results of the study. I want to thank Dr. Bruce Cooper and Amber Hopf Jannasch for accepting me in the Metabolite Profiling Facility and allowing me to learn from their experience.

To my lab members, Dr. Yung-Yi Mosley, Dr Fangjia Lu, Anisa Dunhan and Juan Fernandez, I have nothing more than gratitude for sharing their knowledge and supporting me for the past 4 years.

Finally, I am thankful for the Colciencias fellowship which opened the door for me to come to Purdue University**.** This research was supported in part by grants from the National Institutes of Health (AR049288) and the Purdue Institute of Inflammation, Immunology and Infectious Disease (PI4D).

TABLE OF CONTENTS

LIST OF TABLES

LIST OF FIGURES

ABBREVIATIONS

AA	Arachidonic acid
AC	Acylcarnitines
ASC	Apoptosis-associated speck-like protein containing C-terminal caspase recruitment domain
ACOX	Acyl-CoA oxidase
AD	Atopic dermatitis
ANOVA	Analysis of variance
APC	Antigen-presenting cells
AUC	Area under the curve
CAD	Canine Atopic dermatitis
CADESI	Canine atopic dermatitis extent and severity index
CD	Cluster of differentiation
CE	Cholesterol esters
Cer	Ceramides
CerAP	Ceramide alpha-hydroxylated phytosphingosine
CerAS	Ceramide alpha-hydroxylated sphingosine
CerNP	Ceramide non-hydroxylated phytosphingosine
CerNS	Ceramide non-hydroxylated sphingosine
CER S	Sphingosine ceramides
CLE	Corneocyte-bound lipid envelope
COX	Cyclooxygenases
CPC	Compositional principal component
cPLA2	Cytosolic phospholipases A2
CPDM	Chronic proliferative dermatitis
CTACK	Cutaneous T-cell-attracting chemokine
DAG	Diacylglycerol
DAMPs	Danger-associated molecular patterns
DHA	Docosahexaenoic acid
E-net	Elastic-net

ELOVL	Elongation of very long chain fatty acids protein
ePC	Alkelnyl-acyl PC
ESI	Electrospray ionization
FA	Fatty acids
FABP	Fatty acid binding protein
FASN	Fatty acid synthase
FC	Fold change
FDR	False discovery rate
FFA	Free fatty acids
FLG	Higher filaggrin
GBA	Beta acid glucosidase
HDM	House dust mite
HEPES	Piperazineethanesulfonic acid
Ig	Immunoglobuline
IL	Interleukin
ILC	Innate lymphoid cells
LB	Lamellar bodies
LC-MS/MS	Liquid chromatography tandem mass spectrometry
LDA	Linear discriminant analysis
LPC	Lysophosphatidylcholines
LOX	Lipoxygenases
MRM	Multiple reaction monitoring
m/z	Mass-to-charge ratio
MS	Mass spectrometry
NF-kB	Nuclear factor kappa-light-chain-enhancer of activated B cells
NL	Neutral loss
NLRP	Nucleotide-Binding Oligomerization Domain, Leucine Rich Repeat And Pyrin Domain Containing
oxPL	Oxidized phospholipids
PPARs	Peroxisome proliferator-activated receptors
PACUC	Purdue University Animal Care and Use Committee

PC	Phosphatidylcholine
PCA	Principal component analysis
PDE	Phosphodiesterase
PE	Phosphatidylethanolamine
PI	Phosphatidylinositol
PL	Glycerophospholipids
PLS-DA	Partial least square – discriminant analysis
PS	Phosphatidylserine
Prec	Precursor ion
PRR	Pattern recognition receptor
PUFAs	Polyunsaturated fatty acids
qPCR	Quantitative polymerase chain reaction or real-time polymerase chain reaction
RF	Random forest
RT-PCR	Reverse transcription polymerase chain reaction
ROC	Receiver Operating Characteristic
Sharpin	Shank-associated RH-domain-interacting protein
SC	Stratum corneum
SIM	Single ion monitoring
SL	Glycerolipids, polyketides, sphingolipids
SM	Sphingomyelin
TAG	Triacylglycerol
TARC	Thymus and activation-regulated chemokine
TEWL	Transepidermal water loss
TLR	Toll-like receptor
TNF	Tumor necrosis factor
VLCFA	Very-long chain fatty acids
WT	Wild-type

ABSTRACT

Author: Franco Marmolejo, Jackeline. PhD
Institution: Purdue University
Degree Received: May 2019
Title: Lipid Biomarkers for Canine Atopic Dermatitis
Committee Chair: Harm HogenEsch

Atopic dermatitis (AD) is a common pruritic skin disease in people and domestic animals that can be severely debilitating and stressful to the patient and the caregiver. The diagnosis of AD requires time consuming and expensive procedures, and treatment is often lifelong at considerable cost. Alterations in the lipid composition of the epidermis are a hallmark of the disease, and these may represent changes caused by the inflammation and defects in the lipid barrier. Liquid chromatography tandem mass spectrometry (LC-MS/MS) and, more recently, untargeted profiling using high-resolution time-of-flight instruments have been used to quantify the lipid composition in skin and other tissues, but these approaches are highly demanding in sample preparation and instrument time. In addition, these methods either detect only a limited number of lipids at the time or the identification of detected mass-to-charge ratio (*m/z*) is problematic when untargeted profiling is used. New lipidomic approaches that generate lipid profiles in a faster and more efficient manner can lead to a better understanding of these lipid changes.

The mass spectrometry analytical strategy used in this study, multiple reaction monitoring (MRM)-profiling, rapidly identifies discriminant lipids of the epidermis by flow injection. MRM-profiling is a small molecule accelerated discovery workflow performed in two parts using a triple quadrupole mass spectrometer with electrospray ionization as the ion source. Briefly, the first step consists of discovery experiments based on neutral loss and precursor ion scans to detect lipids in pooled samples by targeting class-specific chemical motifs such as polar heads of phospholipids or sphingoid bases of ceramides. The second step of the MRM-profiling is the screening of individual samples for the transitions detected in the discovery phase.

We first developed the experimental approach of the MRM-profiling methodology using epidermal samples of mice with AD-like inflammatory skin disease (chronic proliferative dermatitis, *cpdm*). Subsequently, we investigated lipid changes as the disease in mice progressed from minimal to severe. In order to select the most relevant ions, we utilized a two-tiered

filter/wrapper feature-selection strategy. First, we built linear models linking the presence of every lipid monitored to disease stage information. The top 10 lipids, ranked based on η^2 effect size, were used to build a predictive elastic-net (E-net) regression model linking the lipid ions detected by MRM-profiling with disease progression. The developed model accurately identified disease stages based on the variations in relative amounts of lipid ions corresponding to phosphatidylcholines, cholesterol esters, and glycerolipids-containing and eicosapentaenoic acid fatty acyl residues. Finally, we investigated the lipid profile of the epidermis in dogs with canine AD using the previously developed methodology. Epidermis from client owned patients and healthy controls were collected. Patients were sampled from affected and unaffected skin avoiding areas with secondary infections and the canine atopic dermatitis extent and severity index (CADESI-4) was recorded. The monitored lipids substantially separated the samples of healthy dogs from atopic dogs and distinguished the affected from the unaffected skin of patients. Samples were grouped into two cohorts for low-score and high-score CADESI-4, the first principal component was able to differentiate the control group from the low and high-score group. Differences in the lipid composition associated with low and high score CADESI-4 were significantly different only after separating the samples by sex of the dogs, demonstrating sexual dimorphism in the lipid changes associated with disease. The compositional data was feature extracted using the CADESI-4 to build linear models that identified oleic acid-containing triacylglycerides, long-chain acylcarnitines and sphingolipids as highly predictive lipids and were subsequently used to construct a predictive E-net regression. The lipid fingerprint obtained from the MRM-profiling was highly correlated (R^2=0.89) with the classification of the standardized CADESI-4 score.

This research showed that changes in the lipid composition of the epidermis can be detected by MRM-profiling in atopic dogs even when the skin looks clinically healthy and that sex is a modifying factor in the lipid profile of canine atopic dermatitis (CAD). We expect that this research leads to a better understanding of the lipid changes in the epidermis during the onset of AD and as the chronic inflammatory process develops. The high prediction rate given by the lipid biomarkers for disease progression identified here by the machine learning strategy provides a potential molecular assessment tool for the diagnosis and monitoring of atopic dermatitis and the patient response to treatment.

CHAPTER 1. INTRODUCTION

1.1 Lipids

Lipids are a heterogeneous group of molecules with complex structures and multiple functions. Historically, lipids have been defined as “any biological substance that is hydrophobic and soluble in organic solvents” (1). The term “lipidome” was coined by Kishimoto *et al*. in 2001 (2) and is now widely used to refer to the whole composition of lipids in a cell, tissue or organism (3). Lipidomics is the research field where soft ionization mass spectrometry (MS) permits the identification and quantitation of lipids at their chemical level (4). The development of soft ionization techniques enabled the identification of previously unknown lipids and has contributed to the recognition of the important and diverse roles that lipids have across cell biology (5,6). Lipidomics analysis can be targeted or untargeted depending on the goal of the study and the type of instrument used (7). Usually targeted analysis is quantitative and only determines a few molecules at a time, while untargeted or profiling analysis is qualitative and aims to detect as many lipids as possible in the sample (8). Untargeted analysis improves the odds of new molecular findings, but the actual identification of the lipid molecule remains a challenge.

The advancement of lipidomics required the unification and standardization of concepts, so lipids were redefined as “hydrophobic or amphipathic small molecules that originate entirely or in part by carbanion-based condensations of thioesters and/or by carbocation-based condensations of isoprene units” (9). Based on this definition and according to the building blocks that constitute them, lipids were divided into eight categories: glycerophospholipids (PL), fatty acids (FA), glycerolipids, polyketides, sphingolipids (SL), sterol lipids, saccharolipids and prenol lipids. Each of these major categories are subdivided into classes and sub-classes based on backbones, head groups, sugar residues or number of fatty acyl residues, which in turn have different lengths, number and position of unsaturations and hydroxyl-, peroxide-, and epoxide- groups (9). Currently, over 43,000 lipids have been identified or predicted to their molecular species (www.lipidmaps.org) and it is now known that their structure has a strong influence on their physical, chemical and biological properties (10,11).

Lipids are ubiquitous and fundamental components of plasma membrane, organelles, trafficking vesicles and extracellular spaces, and their composition varies considerably from one

to the other (12). These differences have been attributed to the particularities and different functions of each compartment (13). Lipid homeostasis is strictly regulated by enzymes that control the flux of lipids throughout synthesis, hydrolysis, remodeling and turnover (5,6,12,14). These hydrolytic and transferring enzymes can cause a lipid belonging to one category to be remodeled and moved into another one with different functional capabilities and roles at a very fast pace (6,12,14). Currently, lipidomics techniques provide a snapshot of the molecular phenotype but the ability to follow these dynamic processes is very limited. Hopefully with the further development of fluxomics we can monitor these inter-category or inter-class movements in order to better understand their effects on health and disease states (3,15).

Knowledge of roles of lipids in biological processes is expanding quickly. Each lipid class was thought to have a defined task, such as energy storage for triacylglycerols (TAGs), structural components for phospholipids (PL) and signaling for eicosanoids, steroids and isoprenoids, but it is now known that a single lipid can have different biological, physical and chemical roles simultaneously and act in membrane permeability, trafficking, and signal transduction (5,6).

Phospholipids (PL), sphingolipids (SL) and cholesterol are abundant in plasma membranes and their molecular conformation determines the biophysical characteristics of the membrane (16). The head groups of the lipids influence the surface charge of the membrane, where negative charge is given by anionic lipids like phosphatidylserines or phosphatidylinositides (6,14). The length of the acyl chains regulates the fluidity of the membrane and whether they are unsaturated or saturated. Increased saturation leads to a non-fluid and tightly packed membrane (14,17,18). The degree of unsaturation also shapes differently the curvature of the membrane and so does the presence of lyso-PL which are PL with only one acyl residue (14). PL and SL are not passive components of lipid bilayers, but they have active roles in signal transduction by supporting conformational changes necessaries for activation of protein receptors. These changes are caused by alterations of lipid packaging and the charge and space between head groups of PL in the membrane (6). In order to activate transmembrane proteins, the lipid packaging needs to be fluid and therefore lipids change from saturated to unsaturated around the target protein (14). Additionally, PL and SL can be reservoirs of FA residues in their sn positions which can be cleaved by enzymes such as phospholipase A2 (PLA2). The released FA can become lipid mediators such as eicosanoids or specialized pro-resolving mediators fundamental in inflammation (19). Fatty acids can undergo modifications, act as first and second messengers for intracellular processes or act as lipokines that

regulate biological processes outside the cell (6,10,17,20). Fatty acids can be modified to different lipids like cardiolipin or acylcarnitines that have a particular distribution in membranes like mitochondria and play specific roles in metabolic pathways like fatty acid oxidation (21–23). Furthermore, lipids can be used for post-translational modification of proteins, called lipidation, which is fundamental to regulation of protein-membrane interactions, protein stability and enzymatic activity with important effects in cell biology (24,25).

1.2 Lipids in epidermis

The skin is the body's most extensive organ which serves as the first barrier of defense against pathogens and irritants and prevents water loss (26). Among the several function of lipids, they play a fundamental role in the formation and maintenance of this barrier (27).

Three main layers compose the skin: epidermis, dermis and subcutaneous fat. The layer in charge of maintaining the barrier against the environment is the epidermis, which is the outermost in direct contact with the external milieu. The epidermis is composed mostly of keratinocytes although there are other cells that reside in it such as melanocytes, Langerhans cells, dendritic cells and resident T cells (26). The epidermis is subdivided into layers according to the state of differentiation of keratinocytes. The first and deepest layer, the stratum basale, consist of basal cells that divide and push cells upwards as they mature. The stratum spinosum is comprised of mature keratinocytes connected by a large number of desmosomes and with emerging epidermal lamellar bodies (LB) in their cytoplasm. The LB are structures that contains a lipid mixture of cholesterol, SL, PL and sphingomyelins, and enzymes necessaries for the formation of the cornified envelope and the lipid matrix (28). The stratum spinosum also houses immune cells that surveil both internal and external surroundings (26). In the stratum granulosum, the keratinocytes elongate and are filled with keratohyalin granules, fully developed LB and profilaggrin, loricrin and involucrin, proteins necessary for the formation of the cornified envelope. At this level, the terminal differentiation of keratinocytes to corneocytes starts with the formation of the cornified envelope and the disappearance of the plasma membrane (28, 29). As part of the programmed cell death of keratinocytes, pro-filaggrin is cleaved to filaggrin, a precursor of natural moisturizers factors, and organelles undergo degradation. The LB secrete their content into the extracellular space and the cornified envelope is formed by the transglutaminase-mediated crosslinking of involucrin and loricrin. At the same time, the corneocyte-bound lipid envelope (CLE) is generated,

which consists of a monolayer of omega-acylceramides and ultra-long chain FA that are covalently bound to involucrin and loricrin and serves as a scaffold for the lipid matrix (24,25,26). The stratum corneum, the most external layer of the epidermis is a very cohesive layer of corneocytes derived from the dead keratinocytes. The lipid content of the LB that is released into the extracellular space undergoes further remodeling and give rise to the lipid matrix. This fills the intercellular spaces between the corneocytes in a "brick and mortar" configuration and underlies the epidermal barrier function (31). However, the SC is not only a structural component of the skin, but more of a "smart material" that is responsive to its surroundings (28).

The lipid matrix is a carefully balanced mixture of ceramides, cholesterol and fatty acids among other less abundant lipids (32), the properties of which, like the plasma membrane, will depend on the composition and the molecular configuration of the lipids (33). The lipid composition of the matrix is enriched in saturated FA with lengths ranging from C14 to C34 and up to 14 different species of ceramides (34). Ceramides can have different sphingoid bases that can be sphingosine, phytosphingosine, dihydrosphingosine or 6-hydroxy-sphingosine. The base is acylated with a FA that can be non-hydroxylated, alfa-hydroxylated or ester linked-omega-hydroxylated (32,35). The large number of potential combinations has made it possible to identify up to 182 different species of ceramides in the human skin (36). The lipid organization of the matrix is in bilayers that can have an orthorhombic, hexagonal or liquid lateral organization, and form two lamellar phases with short and long periodicity (35). At the initial formation of the bilayer, glycosylceramides are in a hairpin conformation. Subsequent dehydration and deglycosylation change this towards an extended configuration. The extended conformation helps to maintain a tight organization by locating cholesterol and free fatty acids in balanced positions arranged along the extended ceramide and, keeps all the sphingoid moieties in the same layer (32,37).

Changes in the composition or organization of the lipid matrix of the epidermis have been linked to reduced skin barrier function which in turn can lead to development of diseases (32,38–41). Studies of the lipid composition of the skin have found alterations in skin diseases such as lamellar ichthyosis, psoriasis, Netherton syndrome, Chanarin-Dorfman syndrome and atopic dermatitis (32,42–44).

1.3 Atopic dermatitis

Atopic dermatitis is a multifactorial inflammatory skin disease that commonly affects people and domestic animals worldwide (45). The pathogenesis is not completely understood, but it involves an aberrant immune response to percutaneously adsorbed antigens in genetically predisposed individuals.

The prevalence of the AD in children is up to 25% in the US (46), where 60% of the cases develop between birth and 5 years of age and about 2-10% persist into adulthood (47–49). It is unknown what determines if a person outgrows the disease, or what contributes to the development of other allergic states, like rhinitis, allergic asthma or food allergy on what has been called the atopic march. The consecutive initiation of these allergic disorders, along with the increased risk of other comorbidities like cardiovascular disease, suggest that a systemic disease process underlies AD (50–52). Since most AD cases occur before 5 years of age, early detection and treatment has been a major goal for intervention of the atopic march. Atopic dermatitis is characterized by dry and pruritic skin that leads to lichenification and hyperplasia after constant scratching. Lesions include dry scaly, papular and eczematous, erythematous plaques that can have serous exudate. The clinical appearance depends on whether the disease phase is acute or chronic with differences at light microscopic accumulations of inflammatory and immune cells and skin barrier function (53,54). Affected areas usually locate on the forehead, scalp and neck in infantile AD (less than two years of age). Childhood and adult AD distribution of lesions include wrist, ankles, hands, feet, elbows and knees, particularly in flexor areas that are not well delineated and usually superinfected with staphylococcus and herpes simplex virus (55–57).

In veterinary dermatology, the prevalence of canine atopic dermatitis (CAD) is 10-15% and the frequency of diagnosis seems to be increasing, like in humans (58,59). The clinical presentation of CAD is very similar to AD in people, since dogs share the same environment, CAD can be a valuable source of comparative and translatable information (60,61). The typical age of onset is from 6 months to 3 years of age and the predisposed breeds are Chinese Shar Pei, Labrador Retriever, West Highland White Terrier, Boxer, and Yorkshire Terrier, among others (62,63). The most commonly involved body sites are distal limbs and paws, face and neck, abdomen and ears with presence of erythema, self-induced alopecia, excoriations, hyperpigmentation and lichenification (64,65). Canine atopic dermatitis patients are prone to secondary infections result from *Malassezia* and *Staphylococcus pseudintermedius* and *Corynebacterium* spp. (63,66).

Atopic dermatitis is a heterogeneous disease with multiple variants (endotypes) due to differences in genetic background, environment, immune activation pathways and epidermal barrier status (45,54,67,68). In CAD, endotypes are also present and are clinically indistinguishable (59,69).

Atopic dermatitis in humans and dogs can be extrinsic or intrinsic depending on the presence or absence of IgE (59). It is reported that 80% of human patients have the extrinsic phenotype with high IgE serum levels, increased prevalence of filaggrin (FLG) mutations producing skin barrier abnormalities and increased susceptibility to *S. aureus* (53,54,70). However, is important to note that about 40% of FLG mutation carriers do not develop AD and 10 to 20% of AD patients actually have the mutation (53,71). Intrinsic AD or atopic-like dermatitis represent 20% of patients who have normal IgE, later disease onset, milder severity and no association with FLG mutation or impairment of the skin barrier function measured by transepidermal water loss (TEWL) (72).

In addition to an IgE-based classification, other endotypes are centered on the genetic background which is highly correlated with ethnicity (67,73). A genome-wide association study including European, Japanese, African and Hispanic populations found 31 AD risk loci the importance of which varied by ethnic group (74). The differences between races were mostly observed in immune function and skin barrier defect suggesting that not all patients developed the disease by the same pathophysiological mechanisms or respond to insults in the same way (54,67,73). In general, histological features of AD include epidermal hyperplasia, accumulation of mast cells, eosinophils, T helper type 2 (Th2) cells and dendritic cells with increase of type 2 cytokines such as interleukin (IL)-4, IL-5, IL-13 and TSLP (18,29,31). However, in the Asian type of AD a greater increase of Th22 and Th17 polarization is observed rather than the well-known Th2/Th22 increased response (54,73). Also, the proteins required for barrier function were conserved even though a more noticeable parakeratosis was in place (76). This presentation of AD has been suggested as a non-type 2 immune response AD (51).

Interestingly, a feature that has been observed in all AD patients examined is the altered lipid composition of their skin (77). Ceramides and free fatty acids (FFA) on the stratum corneum of AD patients have been investigated across different analytical platforms. These studies have led to the following observations in atopic compared to healthy skin: lower level of total ceramides and FFAs, altered composition and shorter length in the acyl-chain of ceramides, changes in the

ratios of sphingoid bases, increased unsaturation in FFAs, increase of shorter FFAs and decrease of FFAs with more than 26 carbons (35,78–82). Other less abundant lipids have been studied in atopic skin, sweat and sebum such as PL, CE, TAG also showing alteration in their amounts compared to healthy skin (83–86). Similar skin lipid alterations have been described in skin from atopic dogs (87–94).

The basis for these lipid changes are still not fully elucidated, however several genetics and cellular mechanisms have been implicated (95). Loss-of-function mutation of filaggrin contributes to barrier abnormalities by interfering with the extracellular secretion of LB content contributing to an overall reduced lipid content in the stratum corneum (96). A reduction of filaggrin-derivatives has also been related to an increase in stratum corneum pH which activates serine proteases which can degrade enzymes necessaries for the proper formation of the barrier function of the epidermis and stimulate thymic stromal lymphopoietin (TSLP) and IL-1a secretion (97,98). Although significant, these changes can also occure in the absence of filaggrin mutations (99). Ceramide processing enzymes and elongation fatty acid enzymes are downregulated by type 2 cytokines resulting from inflammation contributes to the lipid changes in the epidermis of atopic patients (100,101).

Whether the impaired barrier function is a primary defect or a result of inflammation is not yet determined (59,102) but many studies support the hypothesis of a “outside-inside-outside” pathogenic mechanism (77,95,98). This hypothesis proposes that a primary alteration in the lipid composition leads to a disorganized lipid matrix and an impaired barrier function (35) which in turn permits an increased allergen penetration that shifts the immune response towards type 2 and induces and aggravates the inflammation (89,103,104). The fact that replacement lipid therapy aimed atimproving the barrier function corrects the skin impairment, alleviates symptoms in human and canine AD patients and delays the onset in predisposed children (87,92,95,105–107) points toward the skin barrier impairment as an important step in the pathogenesis of the disease. On the other hand, the success of biologicals targeting the immune response seems to favor a primary role for the immune response and inflammation in the impairment of the barrier function (108–110). However, it is important to keep in mind that lipid alterations in human and dog AD patients have been detected beyond the stratum corneum including sweat, sebum and blood (83,84,111,112). This, in addition to reported alterations in expression of lipid metabolism genes (113–120) point to a possible underlying systemic lipid metabolism defect.

1.4 **Diagnosis** and disease severity assessment in atopic dermatitis: the need for biomarkers.

The definition of AD has changed over the years as new molecular characteristics have been discovered (68,121–123). The phenotypic and endotypic heterogeneity of the disease and the lack of a pathognomonic clinical features make the diagnosis of AD a challenging task in both human and dog patients (122,124,125). Clinicians have addressed this fact by developing evolving sets of clinical criteria to diagnose human and canine AD patients based on practical expertise (122,124,126). In general, these diagnostic criteria for human and canine AD include glucocorticoid-responsive pruritus as a hallmark sign, followed by eczema with location patterns and chronic relapsing history (122). The physical examination remains the principal diagnostic tool as no biomarkers exist to confirm the diagnosis (127). Even though increased IgE levels and FLG mutations can be informative, they are not considered of diagnostic relevance since a significant number of patients do not exhibit them (125). In dogs, other parameters to consider are onset of the disease before three years of age and mostly indoor living conditions (126). More importantly, AD is diagnosis of exclusion, as several conditions need to be ruled out in order to make the diagnosis. In dogs these include ecto-parasites such as scabies and fleas, bacterial and yeast infections, contact allergies and food allergies (124). In humans, besides the ecto-parasites, yeast and bacterial infections to be ruled out, the differential diagnosis includes seborrhoeic dermatitis, impetigo, allergic contact dermatitis, congenital immune-deficiencies, keratinization disorders, nutritional deficiencies and cutaneous T-cell lymphoma (128). Therefore, AD diagnosis is unreliable (129), expensive, time consuming and sometimes frustrating for the human patient, the pet owner, and the clinician.

For the clinical assessment of the AD disease severity score there exist about 20 different indexes for people and one scoring index for dogs called canine atopic dermatitis extent and severity index (CADESI) which has 4 iterations (130,131). These indexes are difficult to perform and interpret and are susceptible to inter-observer and inter-index variability, generating results that are not useful to compare when evaluating treatment responses (132–134). In addition, they do not reflect changes over a short period of time (135). Many attempts have been made to find biomarkers to assess the severity of AD. Possible biomarkers that have been identified include IgE, eosinophilic cationic protein, IL-2R, thymus and activation-regulated chemokine (TARC) (136), (CTACK) (137) and sE-selectin (138), among others (127,139,140). However, the variability between patients in different cohorts limits their success as biomarkers (139). In dogs,

unfortunately, analyses of molecules were not correlated with disease severity, therefore no biomarker has been successfully found yet. Transepidermal water loss (TEWL) is a biophysical variable of the skin that measures the amount of water lost across the stratum corneum and is increased in dog and human atopic patients (59,141–144). In people, this measurement has proven useful to predict disease development in children when measured under 2 months of age (145,146). In dogs, a positive correlation between TEWL and CADESI has been found (147), however, this measurement is not reproducible and varies between body sites (144,148), suggesting that the use of these measurements in dogs is not reliable.

The lack of an objective standardized test that can diagnose and monitor disease severity is consider to be an urgent matter in AD research (149,150). Biomarkers for AD are necessary for several reasons. First, for diagnosis, so this process can be more efficient and less subjective. Second, to screen patients aiming to prevent or delay the onset of a disease that, so far, has no cure. Third, to select the most appropriate treatment course for a patient that often does not get the treatment needed for its underlying molecular mechanism of disease and to assess the treatment response. Fourth, biomarkers can classify patients into cohorts with similar disease mechanisms speeding the development of new therapeutics by selecting the right patients for a specific clinical trial. In general, biomarkers are important as common reliable standards comparable across practice, trials or experiments that provide meaningful and useful data for the management of AD (127,139,149–152).

Systems biology approaches are increasingly used to identify novel biomarkers. However, while genes and proteins reside in the spectrum of what may happen, lipids and metabolites are the endpoint result of metabolism (153). This and the consistently observed lipid alterations throughout atopic patients, makes the analysis of the lipidome a very important tool for the discovery of new biomarkers for AD (153,154). New advances in lipidomics have unraveled the importance of lipids and provided valuable information on their roles in cellular physiology and in its mechanisms of action (3,155). Lipid profiling can identify sets of lipid changes (fingerprints) that reflect changes generated by the underlying molecular mechanisms of disease (156–158). Lipid profiling of AD patients has the potential to produce a fingerprint that allows both diagnosis and stratification of patients according to their endotype (154).

1.5 SHARPIN-deficient *cpdm* mouse

Shank-associated RH-domain-interacting protein (SHARPIN) is ubiquitously expressed and is a member of the linear ubiquitin chain assembly complex (LUBAC) (159–161) involved in cell signaling through NF-κB (162,163). SHARPIN-deficient *cpdm* mice have a spontaneous mutation of the *Sharpin* gene (C57BL/KaLawRij-Sharpin^{cpdm}/Sharpin^{cpdm} RijSunJ) that results in loss of the protein and development of a chronic proliferative dermatitis phenotype (164,165).

The onset of the dermatitis is approximately at five weeks of age with hair loss and erythema around the eyes and on the chest becoming very severe by 10 to 12 weeks when euthanasia is required (165). Skin inflammation in *cpdm* is characterized by epidermal hyperplasia, infiltration of the dermis by eosinophils, neutrophils, mast cells and macrophages (165). Neovascularization is also observed with progression of the dermatitis (166). Transplantation of skin grafts from *cpdm* mice to wild type C57BL mice maintained the phenotype indicating that the dermatitis is not caused by a systemic dysregulation but rather by a defect in the skin that stimulates infiltration of immune cells (167). Increased expression of IL-5 and IL-13 and Chitinase-like proteins CHI3L3 and CHI3L4 are consistent with a type 2 inflammatory phenotype (168,169). Cpdm mice deficient in IL-5 had a reduced infiltration and circulation of eosinophils but it did not affect the onset and severity of the dermatitis indicating they are not the drivers of the disease (170). Dendritic cells of *cpdm* mice have an impaired production of IL-12 after stimulation with TLR ligands. Interestingly, systemic administration of IL-12 rescues the phenotype suggesting that a reduced production of IL-12 contributes to the development of the dermatitis. . This is further supported by the finding that dendritic cells are unable to polarize $CD4^+$ T cells to Th1 T cells. The dermatitis in *cpdm* mice recapitulates many aspects of the inflammation in AD. Decreased expression of the SHARPIN protein was recently reported in the skin of human AD patients (171).

Mitochondria of keratinocytes of *cpdm* mice have round electron dense inclusions in the inner membrane that increase with disease progression and causes loss of mitochondria membrane potential (172). There is marked apoptotic cell death in the *cpdm* epidermis and this is accompanied by increased cleavage of Caspase-3 as disease progresses (165,172). *Cpdm* mice with deletion of TNF and cell death signaling pathways components do not develop or have a delay in the inflammation in the skin suggesting that the dermatitis is dependent on the TNF signaling pathway (160,173–175).

Additionally, *Cdpm* mice exhibit a multi-organ inflammation, that includes esophagus, lungs and liver (164,165). Development of secondary lymphoid organs is impaired based on the absence of marginal zones in the spleen and the lack of definition in the separation between B cells and T cells areas in the white pulp (176). Lymphoid follicles in the lymph nodes and the nasal associated lymphoid tissues are not developed, and Peyer's patches are absent (176,177). There is general immune dysregulation of *cpdm* mice reflected in a reduced concentration of IgG, IgA and IgE are observed while IgM remain normal, indicating a defect in isotype switching (164).

1.6 References

1. Smith A. Oxford Dictionary of Biochemistry and Molecular Biology . Cammack R, Atwood T, Campbell P, Parish H, Smith A, Vella F, et al., editors. Oxford University Press; 2008.
2. Kishimoto K, Urade R, Ogawa T, Moriyama T. Nondestructive quantification of neutral lipids by thin-layer chromatography and laser-fluorescent scanning: Suitable methods for "lipidome" analysis. Biochem Biophys Res Commun. 2001;281(3):657–62.
3. Ferraz EG, Henrique-Araújo R, Fernandez LG, Rolim AEH, de Araújo Alves Dultra FK. Lipidomics in the study of lipid metabolism: Current perspectives in the omic sciences. Gene. 2014;554(2):131–9.
4. Han X, Gross RW. Global analyses of cellular lipidomes directly from crude extracts of biological samples by ESI mass spectrometry. J Lipid Res. 2003;44(6):1071–9.
5. Furse S, Shearman GC. Do lipids shape the eukaryotic cell cycle? Biochim Biophys Acta - Mol Cell Biol Lipids. 2018;1863(1):9–19.
6. Bou Khalil M, Hou W, Zhou H, Elisma F, Swayne LA, Blanchard AP, et al. Lipidomics era: Accomplishments and challenges. Mass Spectrom Rev. 2010;29(6):877–929.
7. Jurowski K, Kochan K, Walczak J, Barańska M, Piekoszewski W, Buszewski B. Analytical Techniques in Lipidomics: State of the Art. Vol. 47, Critical Reviews in Analytical Chemistry. 2017. p. 418–37.
8. Han X, Gross RW. Shotgun lipidomics: Electrospray ionization mass spectrometric analysis and quantitation of cellular lipidomes directly from crude extracts of biological samples. Mass Spectrom Rev. 2005;24(3):367–412.
9. Fahy E, Subramaniam S, Brown H, Glass C, Merrill A, Murphy R, et al. A Comprehensive Classification System for Lipids. Handb Biochem Mol Biol Fourth Ed. 2013;46:165–88.

10. Lizardo DY, Parisi LR, Li N, Atilla-Gokcumen GE. Noncanonical Roles of Lipids in Different Cellular Fates. Biochemistry. 2018;57(1):22–9.
11. Grösch S, Schiffmann S, Geisslinger G. Chain length-specific properties of ceramides. Prog Lipid Res. 2012;51(1):50–62.
12. Jacquemyn J, Cascalho A, Goodchild RE. The ins and outs of endoplasmic reticulum-controlled lipid biosynthesis. EMBO Rep. 2017;18(11):1905–21.
13. Muro E, Atilla-Gokcumen GE, Eggert US. Lipids in cell biology: how can we understand them better? Bement W, editor. Mol Biol Cell. 2014;25(12):1819–23.
14. Holthuis JCM, Menon AK. Lipid landscapes and pipelines in membrane homeostasis. Nature. 2014;510(7503):48–57.
15. Cortassa S, Caceres V, Bell LN, O'Rourke B, Paolocci N, Aon MA. From metabolomics to fluxomics: A computational procedure to translate metabolite profiles into metabolic fluxes. Biophys J. 2015;108(1):163–72.
16. Murate M, Kobayashi T. Revisiting transbilayer distribution of lipids in the plasma membrane. Chem Phys Lipids. 2016;194:58–71.
17. Ray S, Kassan A, Busija AR, Rangamani P, Patel HH. The plasma membrane as a capacitor for energy and metabolism. Am J Physiol Physiol. 2015;310(3):C181–92.
18. Sezgin E, Levental I, Mayor S, Eggeling C. The mystery of membrane organization: composition, regulation and roles of lipid rafts. Nat Rev Mol Cell Biol. 2017;18(6):361–74.
19. Spite M, Clària J, Serhan CN. Resolvins, specialized proresolving lipid mediators, and their potential roles in metabolic diseases. Cell Metab. 2014;19(1):21–36.
20. Ertunc ME, Hotamisligil GS. Lipid signaling and lipotoxicity in metaflammation: indications for metabolic disease pathogenesis and treatment. J Lipid Res. 2016;57(12):2099–114.
21. Okun JG, Kölker S, Schulze A, Kohlmüller D, Olgemöller K, Lindner M, et al. A method for quantitative acylcarnitine profiling in human skin fibroblasts using unlabelled palmitic acid: Diagnosis of fatty acid oxidation disorders and differentiation between biochemical phenotypes of MCAD deficiency. Biochim Biophys Acta - Mol Cell Biol Lipids. 2002;1584(2–3):91–8.

22. Thompson Legault J, Strittmatter L, Tardif J, Sharma R, Tremblay-Vaillancourt V, Aubut C, et al. A Metabolic Signature of Mitochondrial Dysfunction Revealed through a Monogenic Form of Leigh Syndrome. Cell Rep. 2015;13(5):981–9.

23. Indiveri C, Iacobazzi V, Tonazzi A, Giangregorio N, Infantino V, Convertini P, et al. The mitochondrial carnitine/acylcarnitine carrier: Function, structure and physiopathology. Mol Aspects Med. 2011;32(4–6):223–33.

24. Nguyen MT, Hanzelmann D, Härtner T, Peschel A, Götz F. Skin-Specific Unsaturated Fatty Acids Boost the Staphylococcus aureus Innate Immune Response. Infect Immun. 2015;84(1):205–15.

25. Jiang H, Zhang X, Chen X, Aramsangtienchai P, Tong Z, Lin H. Protein Lipidation: Occurrence, Mechanisms, Biological Functions, and Enabling Technologies. Chem Rev. 2018;118(3):919–88.

26. Chuong C, Nickoloff B, Elias P, Goldsmith L, Macher E. What is the ‘ true ’ function of skin ? Exp Dermatol. 2002;(11):159–87.

27. Feingold KR, Elias PM. Role of lipids in the formation and maintenance of the cutaneous permeability barrier. Biochim Biophys Acta - Mol Cell Biol Lipids. 2014;1841(3):280–94.

28. Menon GK. Skin Basics; Structure and Function. In: Lipids and Skin Health. Cham: Springer International Publishing; 2015. p. 9–23.

29. Elias PM, Gruber R, Crumrine D, Menon G, Williams ML, Wakefield JS, et al. Formation and functions of the corneocyte lipid envelope (CLE). Biochim Biophys Acta - Mol Cell Biol Lipids. 2014;1841(3):314–8.

30. Kezic S, O’Regan GM, Lutter R, Jakasa I, Koster ES, Saunders S, et al. Filaggrin loss-of-function mutations are associated with enhanced expression of IL-1 cytokines in the stratum corneum of patients with atopic dermatitis and in a murine model of filaggrin deficiency. J Allergy Clin Immunol. 2012;129(4):1031–40.

31. Elias PM. Epidermal lipids, barrier function, and desquamation. J Invest Dermatol. 1983;80(1 Suppl):44s–9s.

32. Sahle FF, Gebre-Mariam T, Dobner B, Wohlrab J, Neubert RHH. Skin diseases associated with the depletion of stratum corneum lipids and stratum corneum lipid substitution therapy. Skin Pharmacol Physiol. 2015;28(1):42–55.

33. Janssens M, van Smeden J, Gooris GS, Bras W, Portale G, Caspers PJ, et al. Lamellar lipid organization and ceramide composition in the stratum corneum of patients with atopic eczema. J Invest Dermatol. 2011;131(10):2136–8.

34. Mojumdar EH, Gooris GS, Barlow DJ, Lawrence MJ, Deme B, Bouwstra JA. Skin Lipids: Localization of Ceramide and Fatty Acid in the Unit Cell of the Long Periodicity Phase. Biophys J. 2015;108(11):2670–9.

35. Janssens M, van Smeden J, Gooris GS, Bras W, Portale G, Caspers PJ, et al. Increase in short-chain ceramides correlates with an altered lipid organization and decreased barrier function in atopic eczema patients. J Lipid Res. 2012;53(12):2755–66.

36. Masukawa Y, Narita H, Sato H, Naoe A, Kondo N, Sugai Y, et al. Comprehensive quantification of ceramide species in human stratum corneum. J Lipid Res. 2009;50(8):1708–19.

37. Iwai I, Han H, Hollander L Den, Svensson S, Öfverstedt LG, Anwar J, et al. The human skin barrier is organized as stacked bilayers of fully extended ceramides with cholesterol molecules associated with the ceramide sphingoid moiety. J Invest Dermatol. 2012;132(9):2215–25.

38. Školová B, Januìššová B, Zbytovská J, Gooris G, Bouwstra J, Slepička P, et al. Ceramides in the skin lipid membranes: Length matters. Langmuir. 2013;29(50):15624–33.

39. Behne M, Uchida Y, Seki T, de Montellano PO, Elias PM, Holleran WM. Omega-Hydroxyceramides are Required for Corneocyte Lipid Envelope (CLE) Formation and Normal Epidermal Permeability Barrier Function. J Invest Dermatol. 2000;114(1):185–92.

40. Uchiyama M, Oguri M, Mojumdar EH, Gooris GS, Bouwstra JA. Free fatty acids chain length distribution affects the permeability of skin lipid model membranes. Biochim Biophys Acta - Biomembr. 2016;1858(9):2050–9.

41. Loiseau N, Obata Y, Moradian S, Sano H, Yoshino S, Aburai K, et al. Altered sphingoid base profiles predict compromised membrane structure and permeability in atopic dermatitis. J Dermatol Sci. 2013;72(3):296–303.

42. van Smeden J, Janssens M, Gooris GS, Bouwstra JA. The important role of stratum corneum lipids for the cutaneous barrier function. Biochim Biophys Acta - Mol Cell Biol Lipids. 2014;1841(3):295–313.

43. De Benedetto A, Kubo A, Beck LA. Skin barrier disruption: A requirement for allergen sensitization. J Invest Dermatol. 2012;132(3 PART 2):949–63.

44. Olivry T, Wofford J, Paps JS, Dunston SM. Stratum corneum removal facilitates experimental sensitization to mite allergens in atopic dogs. Vet Dermatol. 2011;22(2):188–96.

45. Thijs JL, Strickland I, Bruijnzeel-Koomen CAFM, Nierkens S, Giovannone B, Csomor E, et al. Moving toward endotypes in atopic dermatitis: Identification of patient clusters based on serum biomarker analysis. J Allergy Clin Immunol. 2017;140(3):730–7.

46. Malajian D, Guttman-Yassky E. New pathogenic and therapeutic paradigms in atopic dermatitis. Cytokine. 2014;73(2):311–8.

47. Brunner PM. "Early Immunologic Changes During the Onset of Atopic Dermatitis." Ann Allergy, Asthma Immunol. 2019; pii: S1081-1206(19)30255-8

48. Bieber T. Atopic dermatitis. Ann Dermatol. 2008;22(2):1483–94.

49. Sacotte R, Silverberg JI. Epidemiology of adult atopic dermatitis. Clin Dermatol. 2018;36(5):595–605.

50. Paller AS, Spergel JM, Mina-Osorio P, Irvine AD. The atopic march and atopic multimorbidity: Many trajectories, many pathways. J Allergy Clin Immunol. 2019;143(1):46–55.

51. Werfel T, Allam JP, Biedermann T, Eyerich K, Gilles S, Guttman-Yassky E, et al. Cellular and molecular immunologic mechanisms in patients with atopic dermatitis. J Allergy Clin Immunol. 2016;138(2):336–49.

52. Brunner PM, Silverberg JI, Guttman-Yassky E, Paller AS, Kabashima K, Amagai M, et al. Increasing Comorbidities Suggest that Atopic Dermatitis Is a Systemic Disorder. J Invest Dermatol. 2017;137(1):18–25.

53. Malajian D, Guttman-Yassky E. New pathogenic and therapeutic paradigms in atopic dermatitis. Cytokine. 2015;73(2):311–8.

54. Czarnowicki T, He H, Krueger JG, Guttman-Yassky E. Atopic dermatitis endotypes and implications for targeted therapeutics. J Allergy Clin Immunol. 2019;143(1):1–11.

55. Ahn C, Huang W. Clinical Presentation of Atopic Dermatitis. In: Indian Journal of Practical Pediatrics. 2017. p. 39–46.

56. Boguniewicz M, Leung DYM. Recent insights into atopic dermatitis and implications for management of infectious complications. J Allergy Clin Immunol 2010;125(1–3):4–13.

57. Stambovsky M, dos Santos KR, Vidal F, Cavalcante FS, Saintive S, C Ferreira D de, et al. What is the role of Staphylococcus aureus and herpes virus infections in the pathogenesis of atopic dermatitis? . Future Microbiol. 2017;12(14):1327–34.

58. Hillier a, Griffin CE. The ACVD task force on canine atopic dermatitis (I): incidence and prevalence. Vet Immunol Immunopathol. 2001;81(3–4):147–51.

59. Marsella R, De Benedetto A. Atopic Dermatitis in Animals and People: An Update and Comparative Review. Vet Sci. 2017;4(3):37.

60. Martel BC, Lovato P, Bäumer W, Olivry T. Translational animal models of atopic dermatitis for preclinical studies. Vol. 90, Yale Journal of Biology and Medicine. 2017. p. 389–402.

61. Marsella R, Girolomoni G. Canine models of atopic dermatitis: a useful tool with untapped potential. J Invest Dermatol. 2009;129(10):2351–7.

62. Griffin CE, DeBoer DJ. The ACVD task force on canine atopic dermatitis (XIV): clinical manifestations of canine atopic dermatitis. Vet Immunol Immunopathol. 2001;81(3–4):255–69.

63. Santoro D. Therapies in Canine Atopic Dermatitis. Vet Clin North Am Small Anim Pract. 2019;49(1):9–26.

64. Bizikova P, Santoro D, Marsella R, Nuttall T, Eisenschenk MNC, Pucheu-Haston CM. Review: Clinical and histological manifestations of canine atopic dermatitis. Vet Dermatol. 2015;26(2):79-e24.

65. Jaeger K, Linek M, Power HT, Bettenay S V., Zabel S, Rosychuk RAW, et al. Breed and site predispositions of dogs with atopic dermatitis: A comparison of five locations in three continents. Vet Dermatol. 2010;21(1):118–22.

66. Bradley CW, Morris DO, Rankin SC, Cain CL, Misic AM, Houser T, et al. Longitudinal evaluation of the skin microbiome and association with microenvironment and treatment in canine atopic dermatitis. J Invest Dermatol. 2016;136(6):1182–90.

67. Brunner PM, Guttman-Yassky E. Racial differences in atopic dermatitis. Ann Allergy, Asthma Immunol. 2018:1–6.

68. Ardern-Jones MR, Bieber T. Biomarkers in atopic dermatitis: it is time to stratify. Br J Dermatol. 2014;171(2):207–8.

69. Marsella R, Sousa CA, Gonzales AJ, Fadok VA. Current understanding of the pathophysiologic mechanisms of canine atopic dermatitis. J Am Vet Med Assoc. 2012;241(2):194–207.

70. Ong PY, Leung DYM. The infectious aspects of atopic dermatitis. Immunol Allergy Clin North Am. 2010;30(3):309–21.

71. O'Regan GM, Sandilands A, McLean WHI, Irvine AD. Filaggrin in atopic dermatitis. J Allergy Clin Immunol. 2008;122(4):689–93.

72. Tokura Y. Extrinsic and intrinsic types of atopic dermatitis. J Dermatol Sci. 2010;58(1):1–7.

73. Kaufman BP, Guttman-Yassky E, Alexis AF. Atopic dermatitis in diverse racial and ethnic groups—Variations in epidemiology, genetics, clinical presentation and treatment. Exp Dermatol. 2018;27(4):340–57.

74. Paternoster L, Standl M, Waage J, Baurecht H, Hotze M, Strachan DP, et al. Multi-ancestry genome-wide association study of 21,000 cases and 95,000 controls identifies new risk loci for atopic dermatitis. Nat Genet. 2015;47(12):1449–56.

75. Jaeger K, Linek M, Power HT, Bettenay S V., Zabel S, Rosychuk RAW, et al. Breed and site predispositions of dogs with atopic dermatitis: A comparison of five locations in three continents. Vet Dermatol. 2010;21(1):118–22.

76. Guttman-Yassky E, Krueger JG. Atopic dermatitis and psoriasis: two different immune diseases or one spectrum? Curr Opin Immunol. 2017;48:68–73.

77. Elias PM, Hatano Y, Williams ML. Basis for the barrier abnormality in atopic dermatitis: Outside-inside-outside pathogenic mechanisms. J Allergy Clin Immunol. 2008;121(6):1337–43.

78. Yamamoto A, Serizawa S, Ito M, Sato Y. Stratum corneum lipid abnormalities in atopic dermatitis. Arch Dermatol Res. 1991;283(4):219–23.

79. Imokawa G, Abe A, Jin K, Higaki Y, Kawashima M, Hidano A. Decreased level of ceramides in stratum corneum of atopic dermatitis: an etiologic factor in atopic dry skin? J Invest Dermatol. 1991;96(4):523–6.

80. Di Nardo A, Wertz P, Giannetti A, Seidenari S. Ceramide and cholesterol composition of the skin of patients with atopic dermatitis. Acta Derm Venereol. 1998;78(1):27–30.

81. Macheleidt O, Kaiser HW, Sandhoff K. Deficiency of epidermal protein-bound omega-hydroxyceramides in atopic dermatitis. J Invest Dermatol. 2002;119(1):166–73.

82. van Smeden J, Janssens M, Kaye ECJ, Caspers PJ, Lavrijsen AP, Vreeken RJ, et al. The importance of free fatty acid chain length for the skin barrier function in atopic eczema patients. Exp Dermatol. 2014;23(1):45–52.

83. Agrawal K, Hassoun LA, Foolad N, Pedersen TL, Sivamani RK, Newman JW. Sweat lipid mediator profiling: a noninvasive approach for cutaneous research. J Lipid Res. 2017;58(1):188–95.

84. Agrawal K, Hassoun LA, Foolad N, Borkowski K, Pedersen TL, Sivamani RK, et al. Effects of atopic dermatitis and gender on sebum lipid mediator and fatty acid profiles. Prostaglandins Leukot Essent Fat Acids. 2018;134:7–16.

85. Schafer L, Kragballe K. Abnormalities in epidermal lipid metabolism in patients with atopic dermatitis. J Invest Dermatol. 1991;96(1):10–5.

86. Fluhr JW, Kao J, Ahn SK, Feingold KR, Elias PM, Jain M. Generation of Free Fatty Acids from Phospholipids Regulates Stratum Corneum Acidification and Integrity. J Invest Dermatol. 2001;117(1):44–51.

87. Popa I, Remoue N, Osta B, Pin D, Gatto H, Haftek M, et al. The lipid alterations in the stratum corneum of dogs with atopic dermatitis are alleviated by topical application of a sphingolipid-containing emulsion. Clin Exp Dermatol. 2012;37(6):665–71.

88. Reiter L V, Torres SMF, Wertz PW. Characterization and quantification of ceramides in the nonlesional skin of canine patients with atopic dermatitis compared with controls. Vet Dermatol. 2009;20(4):260–6.

89. Marsella R, Olivry T, Carlotti D-N. Current evidence of skin barrier dysfunction in human and canine atopic dermatitis. Vet Dermatol. 2011;22(3):239–48.

90. Chermprapai S, Broere F, Gooris G, Schlotter YM, Rutten VPMG, Bouwstra JA. Altered lipid properties of the stratum corneum in Canine Atopic Dermatitis. Biochim Biophys Acta - Biomembr. 2018;1860(2):526–33.

91. Yoon J-SS, Nishifuji K, Sasaki A, Ide K, Ishikawa J, Yoshihara T, et al. Alteration of stratum corneum ceramide profiles in spontaneous canine model of atopic dermatitis. Exp Dermatol. 2011;20(9):732–6.

92. Piekutowska a, Pin D, Rème C a, Gatto H, Haftek M. Effects of a topically applied preparation of epidermal lipids on the stratum corneum barrier of atopic dogs. J Comp Pathol. 2008;138(4):197–203.

93. Olivry T. Is the skin barrier abnormal in dogs with atopic dermatitis? Vet Immunol Immunopathol. 2011;144(1–2):11–6.

94. Angelbeck-Schulze M, Mischke R, Rohn K, Hewicker-Trautwein M, Naim HY, Bäumer W. Canine epidermal lipid sampling by skin scrub revealed variations between different body sites and normal and atopic dogs. BMC Vet Res. 2014;10(1):152.

95. Elias PM. Lipid abnormalities and lipid-based repair strategies in atopic dermatitis. Biochim Biophys Acta - Mol Cell Biol Lipids. 2014;1841(3):323–30.

96. Scharschmidt TC, Man MQ, Hatano Y, Crumrine D, Gunathilake R, Sundberg JP, et al. Filaggrin deficiency confers a paracellular barrier abnormality that reduces inflammatory thresholds to irritants and haptens. J Allergy Clin Immunol. 2009;124(3).

97. Jang H, Matsuda A, Jung K, Karasawa K, Matsuda K, Oida K, et al. Skin pH is the Master Switch of Kallikrein 5-Mediated Skin Barrier Destruction in a Murine Atopic Dermatitis Model. J Invest Dermatol. 2015;136:1–32.

98. Elias PM. Primary role of barrier dysfunction in the pathogenesis of atopic dermatitis. Exp Dermatol. 2018;27(8):847–51.

99. van Drongelen V, Alloul-Ramdhani M, Danso MO, Mieremet A, Mulder A, van Smeden J, et al. Knock-down of filaggrin does not affect lipid organization and composition in stratum corneum of reconstructed human skin equivalents. Exp Dermatol. 2013;22(12):807–12.

100. Danso MO, van Drongelen V, Mulder A, van Esch J, Scott H, van Smeden J, et al. TNF-α and Th2 cytokines induce atopic dermatitis-like features on epidermal differentiation proteins and stratum corneum lipids in human skin equivalents. J Invest Dermatol. 2014;134(7):1941–50.

101. Danso MMO, Boiten W, van Drongelen V, Gmelig KM, Gooris G, El Ghalbzouri A, et al. Altered expression of epidermal lipid bio-synthesis enzymes in atopic dermatitis skin is accompanied by changes in stratum corneum lipid composition. J Dermatol Sci. 2017;88(1):57–66.

102. Santoro D, Marsella R, Pucheu-Haston CM, Eisenschenk MNCC, Nuttall T, Bizikova P. Review: Pathogenesis of canine atopic dermatitis: skin barrier and host-micro-organism interaction. Vet Dermatol. 2015;26(2):n/a-n/a.

103. Newell L, Polak ME, Perera J, Owen C, Boyd P, Pickard C, et al. Sensitization via healthy skin programs Th2 responses in individuals with atopic dermatitis. J Invest Dermatol. 2013;133(10):2372–80.

104. Elias PM, Schmuth M. Abnormal skin barrier in the etiopathogenesis of atopic dermatitis. Curr Opin Allergy Clin Immunol. 2009;9(5):437–46.

105. Chamlin SL, Kao J, Frieden IJ, Sheu MY, Fowler AJ, Fluhr JW, et al. Ceramide-dominant barrier repair lipids alleviate childhood atopic dermatitis: Changes in barrier function provide a sensitive indicator of disease activity. J Am Acad Dermatol. 2002;47(2):198–208.

106. Na J-I, Hwang J-S, Park H-J, Kim D-H, Park W-S, Youn S-W, et al. A new moisturizer containing physiologic lipid granules alleviates atopic dermatitis. J Dermatolog Treat. 2010;21(1):23–7.

107. Marsella R. Fixing the skin barrier: past, present and future--man and dog compared. Vet Dermatol. 2013;24(1):73-6.e17-8.

108. Hamilton JD, Suárez-Fariñas M, Dhingra N, Cardinale I, Li X, Kostic A, et al. Dupilumab improves the molecular signature in skin of patients with moderate-to-severe atopic dermatitis. J Allergy Clin Immunol. 2014;134(6):1293–300.

109. Beck LA, Thaçi D, Hamilton JD, Graham NM, Bieber T, Rocklin R, et al. Dupilumab Treatment in Adults with Moderate-to-Severe Atopic Dermatitis. N Engl J Med. 2014;371(2):130–9.

110. Weiss D, Schaschinger M, Ristl R, Gruber R, Kopp T, Stingl G, et al. Ustekinumab treatment in severe atopic dermatitis: Down-regulation of T-helper 2/22 expression. J Am Acad Dermatol. 2017;76(1):91–97.e3.

111. Ottas A, Fishman D, Okas T-L, Püssa T, Toomik P, Märtson A, et al. Blood serum metabolome of atopic dermatitis: Altered energy cycle and the markers of systemic inflammation. Motta A, editor. PLoS One. 2017;12(11):e0188580.

112. Mihály J, Sonntag D, Krebiehl G, Szegedi a, Töröcsik D, Rühl R. Steroid concentrations in atopic dermatitis patients: Reduced plasma DHEAS and increased cortisone levels. Br J Dermatol. 2014;285–8.

113. Ewald DA, Malajian D, Krueger JG, Workman CT, Wang T, Tian S, et al. Meta-analysis derived atopic dermatitis (MADAD) transcriptome defines a robust AD signature highlighting the involvement of atherosclerosis and lipid metabolism pathways. BMC Med Genomics. 2015;8(1):60.

114. Mathay C, Pierre M, Pittelkow MR, Depiereux E, Nikkels AF, Colige A, et al. Transcriptional profiling after lipid raft disruption in keratinocytes identifies critical mediators of atopic dermatitis pathways. J Invest Dermatol. 2011;131(1):46–58.

115. Friedenberg S, Olby NJ, Meurs KM, Olivry T, Agler CS. Genome-wide association analysis in West Highland White Terriers with atopic dermatitis. Vet Immunol Immunopathol. 2019;209:1–6.

116. Sääf AM, Tengvall-Linder M, Chang HY, Adler AS, Wahlgren CF, Scheynius A, et al. Global expresion profiling in atopic eczema reveals reciprocal expression of inflammatory and lipid genes. PLoS One. 2008;3(12):e4017.

117. Ding Y, Shao X, Li X, Zhai Y, Zhang Y, Wang S, et al. Identification of candidate genes in atopic dermatitis based on bioinformatic methods. Int J Dermatol. 2016;55(7):791–800.

118. Blunder S, Kõks S, Kõks G, Reimann E, Hackl H, Gruber R, et al. Enhanced Expression of Genes Related to Xenobiotic Metabolism in the Skin of Patients with Atopic Dermatitis but Not with Ichthyosis Vulgaris. J Invest Dermatol. 2018;138(1):98–108.

119. Ghosh D, Ding L, Sivaprasad U, Geh E, Myers JB, Bernstein JA, et al. Multiple transcriptome data analysis reveals biologically relevant atopic dermatitis signature genes and pathways. PLoS One. 2015;10(12):1–23.

120. Nuttall T. The genomics revolution: Will canine atopic dermatitis be predictable and preventable? Vet Dermatol. 2013;24(1).

121. Marsella R, Sousa CA, Gonzales AJ, Fadok VA. Current understanding of the pathophysiologic mechanisms of canine atopic dermatitis. J Am Vet Med Assoc. 2012;241(2):194–207.

122. Andersen RM, Thyssen JP, Maibach HI. Qualitative vs. quantitative atopic dermatitis criteria - In historical and present perspectives. J Eur Acad Dermatology Venereol. 2016;30(4):604–18.

123. Nakamura T, Haider S, Colicino S, Murray CS, Holloway J, Simpson A, et al. Different definitions of atopic dermatitis: Impact on prevalence estimates and associated risk factors. Br J Dermatol. 2019;0–2. [Epub ahead of print] doi: 10.1111/bjd.17853

124. DeBoer DJ, Hillier a. The ACVD task force on canine atopic dermatitis (XV): fundamental concepts in clinical diagnosis. Vet Immunol Immunopathol. 2001;81(3–4):271–6.

125. Schneider L, Tilles S, Lio P, Boguniewicz M, Beck L, Lebovidge J, et al. Atopic dermatitis: A practice parameter update 2012. J Allergy Clin Immunol. 2013;131(2).

126. Olivry T. New diagnostic criteria for canine atopic dermatitis. Vol. 21, Veterinary Dermatology. 2010. p. 123–6.

127. Thijs J, van Seggelen W, Bruijnzeel-Koomen C, de Bruin-Weller M, Hijnen D. New Developments in Biomarkers for Atopic Dermatitis. J Clin Med. 2015;4(3):479–87.

128. Weidinger S, Novak N. Atopic dermatitis. Lancet. 2016;387(10023):1109–22.

129. Laly MJ, Combarros D, Bourdeau PJ, Bruet V, Guillemaille D. Reliability of different sets of criteria in diagnosing canine atopic dermatitis applied to a population of 250 dogs seen in a veterinary teaching hospital. 2019;1–9. [Epub ahead of print] doi:10.1111/vde.12729

130. Schmitt J, Langan S, Williams HC. What are the best outcome measurements for atopic eczema? A systematic review. J Allergy Clin Immunol. 2007;120(6):1389–98.

131. Olivry T, Marsella R, Iwasaki T, Mueller R. Validation of CADESI-03, a severity scale for clinical trials enrolling dogs with atopic dermatitis. Vet Dermatol. 2007;18(2):78–86.

132. Chopra R, Vakharia PP, Sacotte R, Patel N, Immaneni S, White T, et al. Severity strata for Eczema Area and Severity Index (EASI), modified EASI, Scoring Atopic Dermatitis (SCORAD), objective SCORAD, Atopic Dermatitis Severity Index and body surface area in adolescents and adults with atopic dermatitis. Br J Dermatol. 2017;177(5):1316–21.

133. Silverberg J, Gelfand J, Margolis D, Fonacier L, Boguniewicz M, Schwartz L, et al. Severity strata for POEM, PO-SCORAD and DLQI in US adults with atopic dermatitis. Ann Allergy, Asthma Immunol. 2018;121(4):464–71.

134. Futamura M, Leshem YA, Thomas KS, Nankervis H, Williams HC, Simpson EL. A systematic review of Investigator Global Assessment (IGA) in atopic dermatitis (AD) trials: Many options, no standards. J Am Acad Dermatol. 2016;74(2):288–94.

135. Olivry T. Could we use the erythema grading of the CADESI4 as a simple instrument for future short-duration clinical trials of dogs with atopic dermatitis? Vet Dermatol. 2018;80–1.

136. Kou K, Aihara M, Matsunaga T, Chen H, Taguri M, Morita S, et al. Association of serum interleukin-18 and other biomarkers with disease severity in adults with atopic dermatitis. Arch Dermatol Res. 2012;304(4):305–12.

137. Vestergaard C, Bang K, Gesser B, Yoneyama H, Matsushima K, Larsen CG. A Th2 chemokine, TARC, produced by keratinocytes may recruit CLA+CCR4+ lymphocytes into lesional atopic dermatitis skin. J Invest Dermatol. 2000;115(4):640–6.

138. de Vries IJM, Langeveld-Wildschut EG, van Reijsen FC, Dubois GR, van den Hoek JA, Bihari IC, et al. Adhesion molecule expression on skin endothelia in atopic dermatitis: Effects of TNF-α and IL-4. J Allergy Clin Immunol. 1998 Sep;102(3):461–8.

139. Thijs JL, de Bruin-Weller MS, Hijnen DJ. Current and Future Biomarkers in Atopic Dermatitis. Immunol Allergy Clin North Am. 2017;37(1):51–61.

140. Thijs JL, Nierkens S, Herath A, Bruijnzeel-Koomen CAF, Knol EF, Giovannone B, et al. A panel of biomarkers for disease severity in atopic dermatitis. Clin Exp Allergy. 2015;45(3):698–701.

141. Furue M, Matsumoto T, Yamamoto T, Takeuchi S, Esaki H, Chiba T, et al. Correlation between serum thymus and activation-regulated chemokine levels and stratum corneum barrier function in healthy individuals and patients with mild atopic dermatitis. J Dermatol Sci. 2012;66(1):60–3.

142. Shimada K, Yoshihara T, Yamamoto M, Konno K, Momoi Y, Nishifuji K, et al. Transepidermal water loss (TEWL) reflects skin barrier function of dog. J Vet Med Sci. 2008;70(8):841–3.

143. Shimada K, Yoon J-S, Yoshihara T, Iwasaki T, Nishifuji K. Increased transepidermal water loss and decreased ceramide content in lesional and non-lesional skin of dogs with atopic dermatitis. Vet Dermatol. 2009;20(5–6):541–6.

144. Cobiella D, Archer L, Bohannon M, Santoro D. Pilot study using five methods to evaluate skin barrier function in healthy dogs and in dogs with atopic dermatitis. Vet Dermatol. 2019;20–2.

145. Kelleher M, Dunn-Galvin A, Hourihane JO, Murray D, Campbell LE, McLean WHI, et al. Skin barrier dysfunction measured by transepidermal water loss at 2 days and 2 months predates and predicts atopic dermatitis at 1 year. J Allergy Clin Immunol. 2015;135(4):930–935.e1.

146. Horimukai K, Morita K, Narita M, Kondo M. Transepidermal water loss measurement during infancy can predict the subsequent development of atopic dermatitis regardless of filaggrin mutations. Allergol Int. 2016;65(1):103–8.

147. Zając M, Szczepanik MP, Wilkołek PM, Adamek ŁR, Pomorski ZJH, Sitkowski W, et al. Assessment of the relationship between transepidermal water loss (TEWL) and severity of clinical signs (CADESI-03) in atopic dogs. Vet Dermatol. 2014;25(6):503-e83.

148. Zając M, Szczepanik MP, Wilkołek PM, Adamek ŁR, Pomorski ZJH, Sitkowski W, et al. Assessment of a correlation between Canine Atopic Dermatitis Extent and Severity Index (CADESI-03) and selected biophysical skin measures (skin hydration, pH, and erythema intensity) in dogs with naturally occurring atopic dermatitis. Can J Vet Res. 2015;79(2):136–40.

149. Kabashima K, Biedermann T. A new era for translational atopic dermatitis research and management. Exp Dermatol. 2018;27(4):313–7.

150. Moyle M, Cevikbas F, Harden JL, Guttman-Yassky E. Understanding the Immune Landscape in Atopic Dermatitis: The Era of Biologics and Emerging Therapeutic Approaches. Exp Dermatol. 2019; [Epub ahead of print] doi:10.1111/exd.13911.

151. Cabanillas B, Brehler AC, Novak N. Atopic dermatitis phenotypes and the need for personalized medicine. Vol. 17, Current Opinion in Allergy and Clinical Immunology. 2017. p. 309–15.

152. Thijs JL, Strickland I, Bruijnzeel-Koomen CAFM, Nierkens S, Giovannone B, Knol EF, et al. Serum biomarker profiles suggest that atopic dermatitis is a systemic disease. J Allergy Clin Immunol. 2018;141(4):1523–6.

153. Stephenson DJ, Hoeferlin LA, Chalfant CE. Lipidomics in translational research and the clinical significance of lipid-based biomarkers. Transl Res. 2017;189:13–29.

154. Kendall AC, Koszyczarek MM, Jones EA, Hart PJ, Towers M, Griffiths CEM, et al. Lipidomics for translational skin research: A primer for the uninitiated. Exp Dermatol. 2018;1–8.

155. Han X. Lipidomics for studying metabolism. Nat Rev Endocrinol. 2016;12(11):668–79.

156. Haslam RP, Feussner I. Green light for lipid fingerprinting. Biochim Biophys Acta - Mol Cell Biol Lipids. 2017;1862(8):782–5.

157. Wu Z, Shon JC, Liu K-H. Mass Spectrometry-based Lipidomics and Its Application to Biomedical Research. J lifestyle Med. 2014;4(1):17–33.

158. Zhao YY, Miao H, Cheng XL, Wei F. Lipidomics: Novel insight into the biochemical mechanism of lipid metabolism and dysregulation-associated disease. Chem Biol Interact. 2015;240:220–38.

159. Rieser E, Cordier SM, Walczak H. Linear ubiquitination: A newly discovered regulator of cell signalling. Trends Biochem Sci. 2013;38(2):94–102.

160. Ikeda F, Deribe YL, Skånland SS, Stieglitz B, Grabbe C, Franz-Wachtel M, et al. SHARPIN forms a linear ubiquitin ligase complex regulating NF-κB activity and apoptosis. Nature. 2011;471(7340):637–41.

161. Tokunaga F, Nakagawa T, Nakahara M, Saeki Y, Taniguchi M, Sakata S, et al. SHARPIN is a component of the NF-κB-activating linear ubiquitin chain assembly complex. Nature. 2011;471(7340):633–6.

162. Iwai K. Linear polyubiquitin chains: A new modifier involved in NFκB activation and chronic inflammation including dermatitis. Cell Cycle. 2011;10(18):3095–104.

163. Gerlach B, Cordier SM, Schmukle AC, Emmerich CH, Rieser E, Haas TL, et al. Linear ubiquitination prevents inflammation and regulates immune signalling. Nature. 2011;471(7340):591–6.

164. Seymour RE, Hasham MG, Cox GA, Shultz LD, HogenEsch H, Roopenian DC, et al. Spontaneous mutations in the mouse Sharpin gene result in multiorgan inflammation, immune system dysregulation and dermatitis. Genes Immun. 2007;8(5):416–21.

165. HogenEsch H, Gijbels MJ, Offerman E, van Hooft J, van Bekkum DW, Zurcher C. A spontaneous mutation characterized by chronic proliferative dermatitis in C57BL mice. Am J Pathol. 1993;143(3):972–82.

166. HogenEsch H, Sola M, Stearns TM, Silva KA, Kennedy VE, Sundberg JP. Angiogenesis in the skin of SHARPIN-deficient mice with chronic proliferative dermatitis. Exp Mol Pathol. 2016;101(3):303–7.

167. Gijbels MJJ, HogenEsch H, Bruijuzeel PLB, Elliott GR, Zurcher C. Maintenance of Donor Phenotype After Full-Thickness Skin Transplantation from Mice with Chronic Proliferative Dermatitis (cpdm/dpdm) to C57BL/Ka and Nude Mice and Vice Versa. J Invest Dermatol. 1995;105(6):769–73.

168. HogenEsch H, Torregrosa SE, Boggess D, Sundberg BA, Carroll J, Sundberg JP. Increased expression of type 2 cytokines in chronic proliferative dermatitis (cpdm) mutant mice and resolution of inflammation following treatment with IL-12. Eur J Immunol. 2001;31(3):734–42.

169. HogenEsch H, Dunham A, Seymour R, Renninger M, Sundberg JP. Expression of chitinase-like proteins in the skin of chronic proliferative dermatitis (cpdm/cpdm) mice. Exp Dermatol. 2006;15(10):808–14.

170. Renninger ML, Seymour RE, Whiteley LO, Sundberg JP, HogenEsch H. Anti-IL5 decreases the number of eosinophils but not the severity of dermatitis in Sharpin-deficient mice. Exp Dermatol. 2010;19(3):252–8.

171. Tang L, Wang J, Zhu J, Liang Y. Down-regulated SHARPIN may accelerate the development of atopic dermatitis through activating interleukin-33/ST2 signalling. Experimental Dermatology [Internet]. 2018 Dec 19;1328–35. Available from: http://doi.wiley.com/10.1111/exd.13784

172. Liang Y, Sundberg JP. SHARPIN regulates mitochondria-dependent apoptosis in keratinocytes. J Dermatol Sci. 2011;63(3):148–53.

173. Kumari S, Bonnet MC, Ulvmar MH, Wolk K, Karagianni N, Witte E, et al. Tumor necrosis factor receptor signaling in keratinocytes triggers interleukin-24-dependent psoriasis-like skin inflammation in mice. Immunity. 2013;39(5):899–911.

174. Kumari S, Redouane Y, Lopez-Mosqueda J, Shiraishi R, Romanowska M, Lutzmayer S, et al. Sharpin prevents skin inflammation by inhibiting TNFR1-induced keratinocyte apoptosis. Elife. 2014;3:e03422.

175. Rickard J a, Anderton H, Etemadi N, Nachbur U, Darding M, Peltzer N, et al. TNFR1-dependent cell death drives inflammation in Sharpin-deficient mice. Elife. 2014;3:1–23.

176. HogenEsch H, Janke S, Boggess D, Sundberg JP. Absence of Peyer's patches and abnormal lymphoid architecture in chronic proliferative dermatitis (cpdm/cpdm) mice. J Immunol. 1999;162(7):3890–6.

177. Seymour R, Shirley BJ, HogenEsch H, Shultz LD, Sundberg JP. Loss of Function of the Mouse Sharpin Gene Results in Peyer's Patch Regression. PLoS One. 2013;8(2).

CHAPTER 2. PROFILING OF EPIDERMAL LIPIDS IN A MOUSE MODEL OF DERMATITIS: IDENTIFICATION OF POTENTIAL BIOMARKERS

A version of this chapter has been previously published at

DOI: 10.1371/journal.pone.0196595

2.1 Abstract

Lipids are important structural and functional components of the skin. Alterations in the lipid composition of the epidermis are associated with inflammation and can affect the barrier function of the skin. Shank-associated RH-domain-interacting protein (SHARPIN)-deficient chronic proliferative dermatitis (*cpdm*) mice develop a chronic dermatitis with similarities to atopic dermatitis in humans. Here, we used a recently-developed approach named multiple reaction monitoring (MRM)-profiling and single ion monitoring to rapidly identify discriminative lipid ions. Shorter fatty acyl residues and increased relative amounts of sphingosine ceramides were observed in *cpdm* epidermis compared to wild type mice. These changes were accompanied by downregulation of the *Fasn* gene which encodes fatty acid synthase. Fast screening of over 300 transitions (ion pairs) generated a profile of diverse lipids. Tentative attribution of the most significant transitions was confirmed by product ion scan (MS/MS), and the MRM-profiling linear intensity response was validated with a C17-ceramide lipid standard. Relative quantification of sphingosine ceramides Ceramide alpha-hydroxylated sphingosine (CerAS) (d18:1/24:0)2OH, CerAS(d18:1/16:0)2OH and Ceramide non-hydroxylated sphingosine (CerNS) (d18:1/16:0) discriminated between the two groups with 100% accuracy, while the free fatty acids cerotic acid, 16-hydroxy palmitic acid, and docosahexaenoic acid (DHA) had 96.4% of accuracy. Validation by liquid chromatography tandem mass spectrometry (LC-MS/MS) of the above-mentioned ceramides was in agreement with MRM-profiling results. Identification and rapid monitoring of these lipids represent a tool to assess therapeutic outcomes in SHARPIN-deficient mice and other mouse models of dermatitis and may have diagnostic utility in atopic dermatitis.

2.2 Introduction

Lipids play an important role in maintaining the integrity of the skin and in inflammatory skin diseases, phototoxicity, and wound healing (1). They form a critical structural component of the epidermal barrier which prevents water loss and limits the penetration of pathogens, ultraviolet light, and chemicals. The barrier is formed by the outermost layer of the epidermis and consists of anucleated flattened keratinocytes (corneocytes) with abundant keratin filaments cross-linked by envelope proteins embedded in a lamellar lipid matrix (2). The lipid matrix consists of lipids secreted by terminally differentiated keratinocytes in the granular layer through exocytosis of lamellar bodies along with enzymes that can alter the lipid structure. The main classes of lipids that make up the epidermal lipid matrix are fatty acids, cholesterol esters, and ceramides (2). Lipids also have antimicrobial activity and can enhance the effect of antimicrobial peptides (3). Furthermore, lipid mediators play an important role in activation and signaling of innate and adaptive immune cells (1). Although there is increasing appreciation of the role of lipids in the biology of the skin, knowledge of the lipid composition in healthy and diseased conditions is incomplete.

Atopic dermatitis (AD) is an inflammatory skin disease that affects up to 20% of Caucasian children and 2-10% of adults (4), and greatly impacts the quality of life of patients and their families (5,6). Atopic dermatitis is a complex disease with a broad spectrum of clinical phenotypes. It has a large heritable component and more than 30 susceptibility genetic loci have been identified (7). Impairment of the barrier function of the skin and deviation of the immune system are thought to be key components of the pathogenesis of AD. Changes in the lipid barrier may underlie susceptibility to AD, and the inflammation associated with AD can induce changes which sustain and further aggravate the disease (8,9). These lipid changes are mainly attributed to a decrease of ultra-long chain ceramides and free fatty acids (>26 carbons) with subsequent less dense and less organized lipid lamellae (10). This creates gaps in the lipid arrangement of the extracellular spaces between the corneocytes (2,11). However, the exact nature of the changes in the lipid matrix across the spectrum of AD remains to be determined.

Liquid chromatography tandem mass spectrometry (LC-MS/MS) techniques have traditionally been used to quantify the lipid composition in skin and other tissues (12), but these approaches are highly demanding in sample preparation and instrument time, and can only screen for a limited number of lipid features. Therefore, new lipidomic approaches (13,14) that provide

an overview of lipid profiles in a faster and more efficient manner could lead to better understanding of these lipid changes and may result in new diagnostic biomarkers to classify disease phenotypes that drive therapeutic development and personalized medicine for AD (15,16). With the goal of enhancing the knowledge of lipids in the skin and to rapidly identify discriminant lipids, we used an MS analytical strategy named multiple reaction monitoring (MRM)-profiling (17) associated with the monitoring of lipids observed by full mass scan MS as well as free fatty acid profiling by flow injection MS. Multiple reaction monitoring-profiling is a small molecule discovery workflow performed in two phases. Briefly, the first phase consists of discovery experiments based on neutral loss (NL) and precursor ion (Prec) scan experiments to detect lipids and metabolites in the samples by targeting class-specific chemical motifs such as polar heads of phospholipids or sphingoid bases of ceramides. The second phase of the MRM-profiling is the screening of a larger set of samples for the transitions detected in the discovery phase (18–20). Thus, the screening phase consists of a profile of the transitions found in the discovery phase for each sample.

Data analysis considers relative amounts of the lipids since the skin barrier lipid metabolism is determined by the relative amounts of different lipids rather than their absolute amounts. The interaction of the lipids themselves is important and this interaction is independent of the cellular total protein content or the tissue weight (20). The MRM-profiling workflow has been benchmarked in the full mass profiling/fingerprinting screening commonly used for small molecules in ambient ionization and MALDI studies (21,22). For some ion classes such as free fatty acids (FFA), collision-induced fragmentation is not informative, precluding the use of NL and Prec scans. Therefore, we monitored these in the lipid extracts by single ion monitoring (SIM). We also considered ions present in the full mass scan. All MS experiments were performed using flow injection to a QqQ mass spectrometer with electrospray ionization (ESI) as the ion source.

This study was based on lipid extracts from the epidermis of wild type mice and SHARPIN-deficient *cpdm* mice, which have a spontaneous mutation in exon 1 of the *Sharpin* gene that results in loss of the SHARPIN protein (23). SHARPIN-deficient mice develop a chronic proliferative dermatitis with morphological and molecular similarities to the intrinsic form of AD. Clinical features include pruritus, progressive alopecia, thickening of the skin, and no increase of total serum IgE (23,24). Diffuse ortho- and focal parakeratosis is observed along with scattered keratinocyte apoptosis. The dermatitis is characterized by accumulation of eosinophils, mast cells,

and type 2 macrophages, and increased expression of cytokines including IL5, IL13, IL33, and TSLP (25–27). Epidermal samples from wild-type (WT) and *cpdm* mice were subjected to selected Prec and NL scans to profile diverse phospholipids (PL), ceramides, and cholesterol esters (CE). Several hundred transitions were detected in the discovery phase using a subset of animals, and these were used in the screening phase for fast screening of all samples. Data generated clearly discriminated WT and *cpdm* phenotypes based on relative amounts of specific epidermal lipids. A set of discriminating lipids was identified and validated by LC-MS/MS, and comprised three sphingosine ceramides, which could discriminate between WT and *cpdm* mice with 100% accuracy. These lipids will be helpful for the development and assessment of novel therapies in this mouse model. They could also be used to establish and validate a panel of biomarkers for AD in domestic animals and humans to perform patient classification, assess disease progression, and response to treatments.

2.3 Materials and methods

2.3.1 Mice

36 female C57BL/KaLawRij-Sharpin^{cpdm}/Sharpin^{cpdm} RijSunJ (*cpdm*) mice and control littermates (WT) were obtained from The Jackson Laboratory and housed at 2 to 4 animals per box with food (Envigo) and water ad libitum. Room temperature was maintained at 20 ± 2 °C and relative humidity at 50 ± 15% with a 12/12 hour light/dark cycle. For the biomarker discovery experimental design, two experiments involving two groups of animals were carried out: the first group (analyzed as a testing set) comprised 7 *cpdm* and 8 WT, and the second group (validation set) had 10 *cpdm* and 11 WT mice. Mice were euthanized at 8 to 9 weeks of age by CO2 asphyxiation and cervical dislocation. The animal experiments and procedures were conducted in accordance with the Guide for the Care and Use of Laboratory Animals of the National Institutes of Health. The protocol was approved by the Purdue University Animal Care and Use Committee (PACUC protocol 111001019).

2.3.2 Sample collection

The skin was shaved, a 2x1 cm skin sample collected from each mouse, and the subcutaneous adipose tissue was removed. The epidermis was separated from the dermis by floating the skin samples in a 5 ml petri dish containing 2.5mL of 500 µg/ml Thermolysin (from

Geobacillus stearothermophilus, Sigma-Aldrich, St. Louis, MO) supplemented with 10 mM 4-(2-hydroxyethyl)-1-piperazineethanesulfonic acid (HEPES), 132 mM NaCl, 2.7 mM KCl, 0.4 mM NaOH.7H2O, 1.8 mM CaCl2.2H2O, 1.3 mM MgSO4 at pH 7.4 for 2 h at 37ºC (adapted from (28)). After incubation, the epidermis was peeled off from the dermis with forceps and stored at -80º until lipid extraction. For gene expression analysis, skin samples were collected and stored in RNAlater (Qiagen, Valencia, CA) at − 80 °C until samples from all replicates were collected.

2.3.3 Lipid Extraction

Samples were individually weighed and 10 mg of dry tissue was homogenized in 2mL vials with 1.4mm ceramic (zirconium oxide) beads with 250uL of water using Precellys24 tissue homogenizer (Bertin Technologies, Rockville, MD, USA). The homogenate was transferred and the Precellys tube was rinsed with 200 µL of methanol (MeOH). The total volume of the homogenate was collected and submitted to lipid extraction using Bligh and Dyer method (29). By this protocol, phase separation was performed using CHCl3/MeOH/H2O (1:2:0.8) and the combined organic fractions were centrifuged; the bottom phase was transferred and evaporated. Dried lipid extracts were reconstituted in 40 µL of acetonitrile (ACN)/chloroform at 3:1 volume ratio and stored at -20°C. The reconstituted extracts were individually diluted 50X with ACN/methanol/ammonium acetate 300mM at 3:6.65:0.35 volume ratio and used for MS analysis.

2.3.4 MRM-Profiling

2.3.4.1 Discovery

Samples assigned to the testing set were used for the discovery experiments. The volume of 6µL of lipid extract from individual samples was directly delivered through a micro-autosampler (G1377A) into a QQQ6460 triple quadrupole mass spectrometer (Agilent Technologies, San Jose, CA) equipped with Jet Stream ESI ion source for each of the NL and Prec scans to profile phospholipids (30,31), acylcarnitines (32), cholesterol esters (33,34), ceramides (12,35), diverse fatty acid acyl residues (36), and free fatty acids in positive and negative ion modes (S1 Table). Briefly, phosphatidylcholines were profiled by precursor ion mode of mass-to-charge ratio (*m/z*) 184, and phosphatidylserine (PS), phosphatidylinositol (PI), and phosphatidylethanolamine (PE) were profiled using neutral loss of 185 mass units, 277 mass units, and 141 mass units, respectively. Ceramides were scanned using precursor ion of *m/z* 264.3 for

sphingosine ceramides, precursor ion of *m/z* 266.4 for sphinganine ceramides, and precursor ion of *m/z* 282.4 for phytosphingosine ceramides. Two fatty acid acyl residues, oleate and arachidonate, were profiled using neutral loss of 299 and 321 mass units, respectively. Scan for precursor ion of *m/z* 303.1 was used as well for arachidonate acyl residues. Acylcarnitines were detected by precursor ion of *m/z* 85 and cholesterol esters by precursor ion of *m/z* 369.1 and MRM. Cholesterol esters were selected to be monitored instead of free cholesterol because they have a constant ion loss that can be used by MRM profiling for analysis in the same fashion as the other lipids monitored in this study. In contrast, free cholesterol needs derivatization and LC-MS analysis since it does not ionize well and is not associated with either a precursor ion or ion loss that can be monitored by MRM profiling. For FFA profiling, the *m/z* of each free fatty acid was monitored in Q1 and Q3 at the negative ion mode to detect deprotonated FFAs. Values of ion intensity of each lipid ion were normalized by the total ion intensity of each sample. The solvent pumped between injections was ACN + 0.1% formic acid. Initial data processing of the profiles obtained was carried out by using MassHunter (B.06.00).

2.3.4.2 Screening

The 300 molecular features detected in all scans were organized into two methods for targeted lipidomics by flow injection using multiple reaction monitoring (MRM), where each ion was detected by a specific parent and a fragment ion in positive or negative mode. The use of two methods was necessary because of the time and signal requirements to examine all MRMs in a single sample injection. For the MRM scan, the selection for the *m/z* of the parent ion occurs at the first quadrupole (Q1) of a triple quadrupole mass spectrometer, the second quadrupole (Q2) is set to apply collision induced dissociation to cause fragmentation of the parent ion and the third quadrupole (Q3) is set to monitor the fragment. A total of 217 transitions were monitored in the positive and 83 in the negative ion mode (S2 and S3 Tables). These methods were applied to all samples (testing and validation sets, n=36) so that each sample was individually screened in a high-throughput manner (circa 5 min/sample) by injecting 12µL of lipid extract from each sample into the ESI-MS for the positive ion mode method and 8 µL for the negative ion mode. A blank sample was run in between the samples to avoid carryover. The binary pump flow rate was set at 0.05mL/min, the capillary voltage and the multiplier voltage at the source was 3500 V and 300 V, respectively. For the negative ion mode method, the collision energy voltage was 2 V. Collision

energy for the ions detected in positive ion mode varied according to the lipid class as follow: ceramides, PE, lipids with arachidonate acyl residue and oleate acyl residue were set at 22 V, PC and SM at 20 V, PS and PI at 16 V, CE at 17V and acylcarnitines at 30 V. The fragmentation voltage was 100 V for both methods. The raw mass spectrometry data have been deposited in the public proteomics repository MassIVE (http://massive.ucsd.edu) using the identifier: MSV000080197. The data is accessible at ftp://massive.ucsd.edu/MSV000080197. The informative values of *m/z* were tentatively identified by accurate mass measurement against values in online reference databases, the Lipid Maps database (http://www.lipidmaps.org/) and METLIN (https://metlin.scripps.edu), as well as submitted to product ion scan (MS/MS) for attribution confirmation (S1 Fig). The dynamic range and linear ion intensity response of the MRM-profiling were evaluated with C17-ceramide (860517 Avanti Polar Lipids) spiked into 50X diluted pooled epidermis lipid extract. A linear ion intensity response was observed for four orders of magnitude, 1 to 10,000 ppm. Although our experiments were aimed at relative amounts, a calibration curve of C17-ceramide demonstrated excellent linearity and dynamic range exceeding 3 orders of magnitude (S2 Fig).

2.3.5 LC-MS/MS validation

The validation set of samples (n=19) were re-extracted following a protocol for high-throughput analysis of sphingolipids by liquid chromatography tandem mass spectrometry (LC-MS/MS) (adapted from (12)). Briefly, samples were homogenized following the above-mentioned procedure with the addition of internal standard of ceramide/sphingolipid mixture I (LM-6002 Advanti Polar Lipids, USA) with 0.5 nmol of each sphingolipid. The total volume of the homogenate was collected and MeOH/CHCl3 (2:1) was added. The mixtures were sonicated and incubated overnight at 48 °C in a heating block. After cooling to room temperature, 75µL of 1M KOH in MeOH was added, followed by sonication and incubation for 2 hours at 37 °C in a heating block. The sample was cooled down to room temperature, transferred and evaporated. The extract was reconstituted in 200µL of 80:20 mobile phases RA/RB, where RA is 74:25:1 (v/v/v) of MeOH:H2O:Formic Acid plus 5nM of ammonium formate and RB is 99:1 (v/v) of MeOH: Formic Acid plus 5nM of ammonium formate. The LC column used was 2.1x100 Xbridge C18 (Waters, Milford, MA). The binary pump flow rate was set at 0.3mL/min, the capillary voltage was positive 4000 V and negative 3500 V. The collision energy voltage was 12 V, the fragmentation voltage

was 100 and the cell accelerator voltage was 7 V. Seven µL of the reconstituted sample was delivered to the column through a micro-autosampler (G1377A) into a QQQ6460 triple quadrupole mass spectrometer (Agilent Technologies, San Jose, CA) equipped with Jet Stream ESI ion source. The LC column was pre-equilibrated with 100% RA for 1 min. The binary pump was set in a linear gradient to 100% RB in 9 min and held for 3 min. It was then returned to 100% RA in 2 min and re-equilibrated for 5 min. The MRMs (parent-fragment) for the acquisition included the ones found as highly discriminatory by ROC curve analysis (666.3-264.1; 554.3-264.1 and 538.3-264.1). Data processing was carried out by using MassHunter (B.06.00). Concentrations in nmol/mg of tissue were obtained by normalizing by the dried weight of the sample homogenized and by the concentration of the internal standard.

2.3.6 Quantitative Reverse transcription polymerase chain reaction (RT-PCR)

Quantitative RT-PCR was performed as previously described (37). RNA was extracted using a Quick-RNA MiniPrep (Zymo Research, Irvine, CA). For each RT-PCR, a 20µl reaction was run with 4µl iScript RT supermix (Bio-Rad Laboratories Inc., Hercules, CA), 100ng RNA template and nuclease free water. For each qPCR, a 10µl reaction was run with 5 µl iTaq Universal Probe SuperMix (2x) (Bio-Rad Laboratories Inc., Hercules, CA), 0.5µl 20x TaqMan Gene Expression Assays primer and probe set for *Gba*, *Pde12*, *Fasn*, and *Elovl1* (ThermoFisher Scientific, Waltham, MA), 1µl cDNA and 3.5µl nuclease-free water. The qRT-PCR was performed at 40 cycles of 95°C for 30 min, 95°C for 15 min and 60 °C for 1 min. Ct values of each gene were normalized by subtracting the Ct values of the housekeeping gene beta-actin (*Actb*) (ΔCt). The relative fold change in mRNA expression between wild-type mice and *cpdm* mice was calculated and expressed as $2^{-\Delta\Delta Ct}$ (38).

2.3.7 Statistical analysis

The files generated by the mass spectrometer were converted to mzML format using MSConvert (http://proteowizard.sourceforge.net), and an in-house script was developed to obtain the ion intensity of each *m/z* values monitored. Relative amounts of ion abundances were used for statistics. Values of ion intensities for each of the MRMs monitored were normalized by total ion intensity of all MRMs in the method for a given sample. The differences in the mean values for relative amounts of ceramides and free fatty acids were determined by unpaired t-tests with Holm-

Sidak correction for multiple comparisons and alpha set at 5% (Graphpad Prism 6.0). Further statistical analysis was performed using MetaboAnalyst 3.0 software (http://www.metaboanalyst.ca) (39). Data was auto scaled for principal component analysis (PCA), volcano plots and heat maps. The performance of the identified metabolites and their ratios in discriminating WT from *cpdm* samples was evaluated by constructing receiver operating characteristic (ROCs) curves using the testing set and including the validation set as unknowns for classification. Fold change of mRNA expression on the analyzed genes is presented as geometric means with standard error bars. The statistical significance of fold change in *cpdm* to WT mice were calculated by Student's t-test for unpaired samples.

2.4 Results

2.4.1 MRM-Profiling

Epidermal samples of 7 *cpdm* and 8 WTmice were individually subjected to flow injection experiments by ESI-MS in positive and negative ion mode for the discovery of molecular features by chemically supervised scans. Therefore, full mass scans in both polarities, FFA profiling by single ion monitoring (SIM), and Prec and NL scans (S1 Table) targeted to profile phospholipids, cholesterol esters (CE), ceramides (Cer), and acylcarnitines (AC), were used.

Phospholipid profiles were represented by phosphatidylserine (PS), phosphatidylinositol (PI), and phosphatidylethanolamine (PE), which were detected by NL scans of *m/z* 185, *m/z* 277 and *m/z* 141, respectively. Phosphatidylcholine (PC) lipids were profiled by the Prec of *m/z* 184 (30). Since each phospholipid contains two fatty acids esterified to a glycerol, lipids are attributed by their class abbreviation (PS, PI, PE, PC) followed by the number of carbon atoms in the esterified fatty acid, a colon, and the number of carbon-carbon double bonds in parentheses, such as PC(34:1). The profiles for phospholipids identified 68 molecular features. CE were screened by the Prec of *m/z* 369.1 (34) and individually screened by the related MRMs as previously described (33), providing a total of 32 molecular features. Acylcarnitines, metabolites essential in fatty acid metabolism, were detected by the Prec of *m/z* 85 (32) yielding 21 transitions. Ceramides were analyzed by three separate Prec scan modes based on the sphingoid base. Sphingosine ceramides (Cer[S]) were detected by the Prec of *m/z* 264.3, dihydroceramide (Cer[DS]) by the Prec of *m/z* 266.4, and phytosphingosine ceramide (Cer[P]) by the Prec of *m/z* 282.4 based on typical

fragments as previously reported (12). A total of 33 molecular features were recovered from these scans. Sixty-three transitions were produced by the NL of *m/z* 299 for oleic acyl residues and the NL of *m/z* 321 and Prec scans of *m/z* 303.1 for arachidonate acyl residues. In the negative ion mode, 83 molecular features were discovered after analysis of FFA by SIM.

The transitions isolated from the discovery methods (S1 Table) as well as the full mass scan ions and FFA as SIM were organized into two fast (2 min of data acquisition) MRM methods, one for each ion mode, for individual sample screening. In total, the discovery methods revealed 217 ions in positive ion mode and 83 ions in negative ion mode as shown in S2 and S3 Tables.

For the screening phase, a total of 36 samples were used. The lipids were re-extracted from the first group of samples used for the discovery analysis (N=15; 7 *cpdm* and 8 WT) and these samples were considered a testing set (i.e., were used to build a classification system). The new samples (N=21; 10 *cpdm* and 11 WT) were introduced in the data analysis as a validation set (blind samples). Clear discrimination of the phenotypes of WT and *cpdm* mouse strains was observed by PCA and cluster analysis (Fig 1A). In the positive ion mode, PC1 explained 47.1% of the variability of the data. When PC2 was included, the explained variance increased to 65.7% (S3 Fig). Consistent with the PCA, clustering analysis based on different groups of lipid ions shown as a heat map revealed clear differentiation of *cpdm* from WT mice (Figure 1B).

The structural attribution of the relevant transitions was performed by reference database analysis and by product ion scan (MS/MS) (S1 Fig). Table 1 lists the attribution of significant lipids from the targeted analysis by MRM-profiling as detected by Volcano plot with a *p*-value of 0.05 and at least a two-fold change.

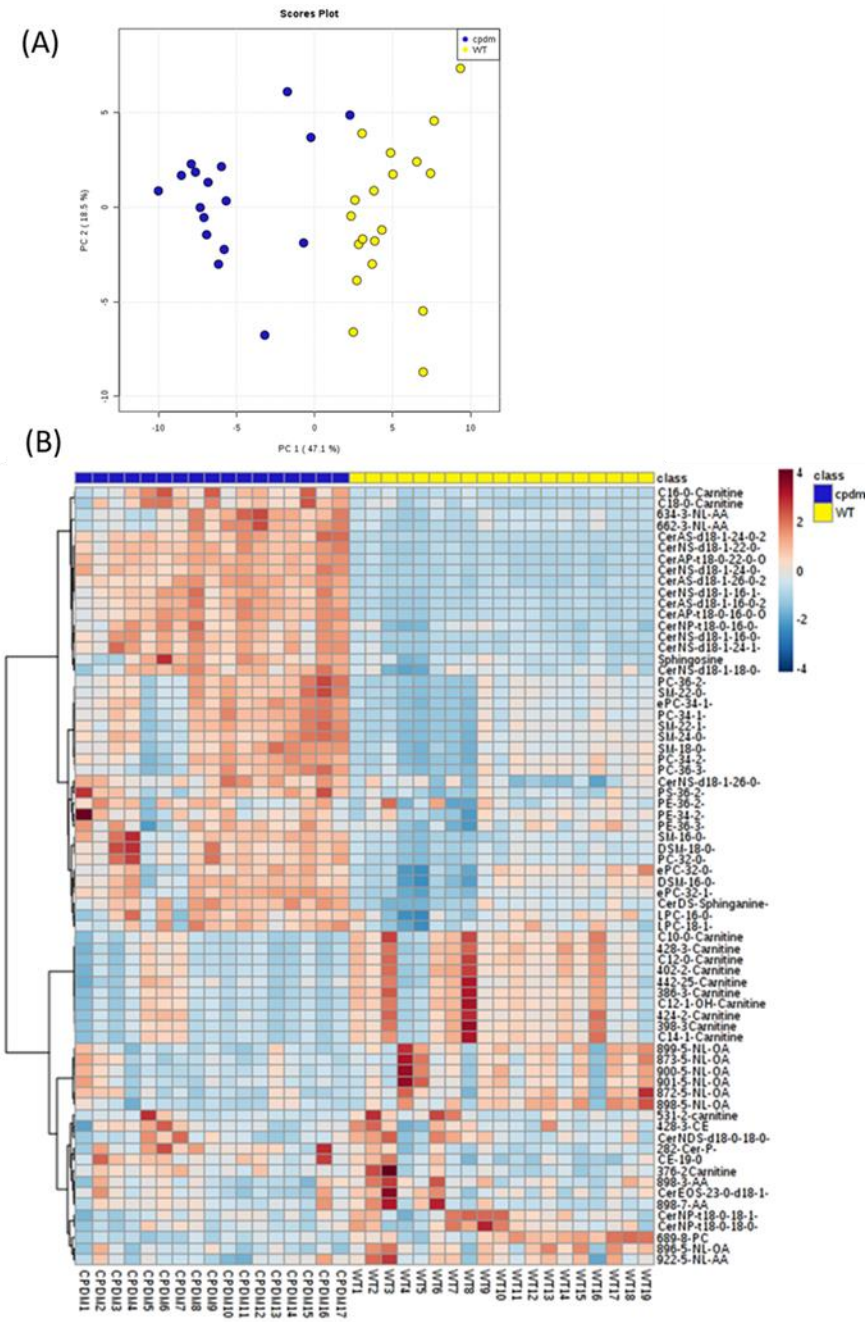

Figure 1**. Monitored lipid ions in *cpdm* and WT epidermis by MRM scans in positive ion mode.** Clear discrimination of the phenotypes of WT and cpdm mouse strains was observed by PCA and cluster analysis. (A) Score plot of principal component analysis (PCA). PC1 explained 47.1% of the variability of the data. When PC2 was included, the explained variance increased to 65.7%. (B) Heat map with the distribution of lipids monitored individually in 36 samples. Lipids not identified are shown with their m/z and corresponding lipid class. Color of each cell corresponds to the relative abundance of the lipid feature monitored in the sample.

Table 1 **Tentative attribution of significant molecular features.** List of ion pairs (parent and fragment), ion mode of detection, scan description, tentative attribution, fold change (FC) and significance (p-values) resulting from the MRM profiling of WT and *cpdm* mice epidermis. For attribution based on the LipidMaps database, one mass unit has been subtracted of the *m/z* observed in order to obtain the neutral mass of the lipid.

Parent ion	Fragment	Ion Mode	Scan description	Tentative Attribution	Fold Change	p.value
650.3	282.1	$[M+H]^+$	Ceramide	CerAP(t18:0/22:0)2OH	5.24	3.67E-21
650.4	264.1	$[M+H]^+$	Ceramide	CerNS(d18:1/24:0)	7.31	5.40E-19
622.1	264.1	$[M+H]^+$	Ceramide	CerNS(d18:1/22:0)	5.76	4.61E-18
694.15	264.1	$[M+H]^+$	Ceramide	CerAS(d18:1/26:0)2OH	4.85	1.54E-17
554.2	264.1	$[M+H]^+$	Ceramide	CerAS(d18:1/16:0)2OH	5.23	1.22E-15
554.2	282.1	$[M+H]^+$	Ceramide	CerAP(t18:0/16:0)2OH	4.48	6.96E-15
536.1	264.1	$[M+H]^+$	Ceramide	CerNS(d18:1/16:1)	4.66	8.34E-15
538.3	264.1	$[M+H]^+$	Ceramide	CerNS(d18:1/16:0)	4.89	1.02E-14
666.35	264.1	$[M+H]^+$	Ceramide	CerAS(d18:1/24:0)2OH	18.73	1.25E-14
648.4	264.1	$[M+H]^+$	Ceramide	CerNS(d18:1/24:1)	3.64	1.64E-12
271.3	271.3	$[M-H]^-$	FFA	16-hydroxy (16:0)	2.31	7.67E-12
761.9	184.1	$[M+H]^+$	PC	SM(d18:0/20:0) SM(d16:0/22:0) posible isotope PC(34:1)	2.62	4.01E-09
538.2	282.1	$[M+H]^+$	Ceramide	CerNP(t18:0/16:0)	2.03	2.21E-08
484	85.1	$[M+H]^+$	Acylcarnitine	AC(18:0)	2.73	5.31E-08
703.8	184.1	$[M+H]^+$	PC	SM(16:0)	2.41	7.37E-08
456.3	85.1	$[M+H]^+$	Acylcarnitine	AC(16:0)	4.02	1.32E-07
438.05	266.1	$[M+H]^+$	Ceramide	CerDS(18:0/10:0)	2.26	1.37E-07
746.8	184.1	$[M+H]^+$	PC	ePC(34:1) / pPC(34:0)[a]	2.01	7.87E-07
734.8	184.1	$[M+H]^+$	PC	PC(32:0)	2.23	9.37E-07
662.3	341.3	$[M+H]^+$	NL AA	Not attributted	3.44	1.82E-06
760.8	184.1	$[M+H]^+$	PC	PC(34:1)	2.12	2.85E-06
758.8	184.1	$[M+H]^+$	PC	PC(34:2)	2.11	5.11E-06
634.3	313.3	$[M+H]^+$	NL AA	Not attributed	2.81	6.20E-06
487.5	487.5	$[M-H]^-$	FFA	Not attributed	0.42	7.40E-06
689.8	184.1	$[M+H]^+$	PC	PG(30:3) SM(d16:1/17:0) SM(d18:1/15:0)	0.50	8.68E-06
788.9	184.1	$[M+H]^+$	PC	PC(36:1)	2.02	1.32E-05
787.9	184.1	$[M+H]^+$	PC	SM(d18:1/22:0) SM(d16:1/24:0)	2.06	1.95E-05
395.4	395.4	$[M-H]^-$	FFA	C26:0	0.23	3.85E-05
372.2	85.1	$[M+H]^+$	Acylcarnitine	AC(10:0)	0.49	5.94E-05
400.3	85.1	$[M+H]^+$	Acylcarnitine	AC(12:0)	0.48	6.53E-05
414.3	85.1	$[M+H]^+$	Acylcarnitine	AC(12:1)OH	0.48	2.63E-04
426.3	85.1	$[M+H]^+$	Acylcarnitine	AC(14:1)	0.48	4.44E-04

[a]The 'e-'prefix is used to indicate the presence of an alkyl ether substituent e.g. ePC(34:1), whereas the 'p-'prefix is used for the 1Z-alkenyl ether (plasmalogen) substituent e.g. pPC(34:0)

In general, more sphingosine ceramides (Cer[S]) than phytoceramides (Cer[P]) and sphinganine ceramides (Cer[DS]) were detected by MRM-profiling. The overall profile of ceramide composition by sphingoid base showed that relative amounts of phytosphingosine and sphinganine ceramides were decreased in *cpdm* epidermis compared to WT, while sphingosine ceramides were increased. Sphinganine ceramides were omitted from further comparison because of the small amounts in the samples and it was not possible to attribute all detected. The profiling showed a higher proportion of ceramides with hydroxylated fatty acid residues (Cer[AS] or Cer[AP]) in *cpdm* compared to WT. This finding was independent of the sphingoid base, as it was observed for both sphingosines and phytosphingosines. Sphingosine ceramides carrying fatty acid residues of 16 - 18 and 22 - 24 carbons were increased in *cpdm* samples compared to WT, while those longer than 26 were reduced (Fig 2).

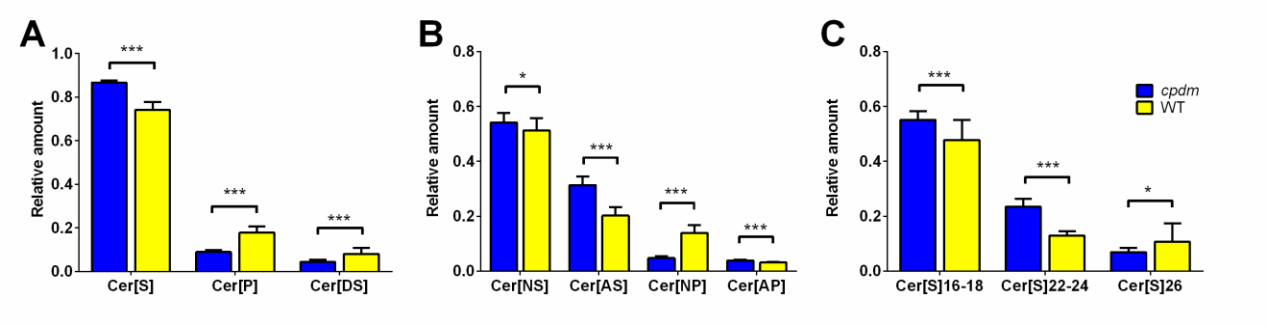

Figure 2**. Ceramide profile in *cpdm* and WT epidermis by MRM-profiling**. (A) There was an increase of Cer[S] and a decrease of Cer[P] and Cer[DS] in the *cpdm* epidermis. (B) The relative amount of ceramides with α-hydroxy-fatty acid residues was larger in cpdm compared to WT. This finding was independent of the sphingoid base as it was observed for both Cer[S] and Cer[P]. (C) Cer[S] carrying fatty acid residues of 16 - 18 and 22 -24 carbons were increased and those with 26 carbons were reduced in *cpdm* samples compared to WT. The vertical axis represents the relative amounts of ceramides detected in the epidermis of *cpdm* and WT mice (horizontal axis). Bars represent the mean +SE of 7 (*cpdm*) or 8 (WT) mice. * $p < 0.05$; *** $p < 0.001$, based on unpaired t-test with Holm-Sidak correction for multiple comparisons.

Principal component analysis of FFA profiles in negative ion mode revealed an explained variance for PC1 of 57.3% giving a clear separation of the two groups (Fig S2). The PCA and the heat map suggest that poly-unsaturated fatty acids such as DHA (22:6), AA (20:4), adrenic acid (22:4) and dihomo-γ-linoleic acid (20:3) are determinants of the score plot position of *cpdm* samples and had higher relative ion abundances when compared to WT (Fig 3). In addition, univariate statistics revealed that epidermal samples from WT mice had more saturated and monounsaturated fatty acids while the epidermis of *cpdm* mice contained more polyunsaturated fatty acids. The relative amounts of FFAs with a length of 20 – 24 carbons were increased in *cpdm* compared to WT, whereas FFAs with 12 – 18 and longer than 26 carbons were reduced in *cpdm* mice (Fig 4).

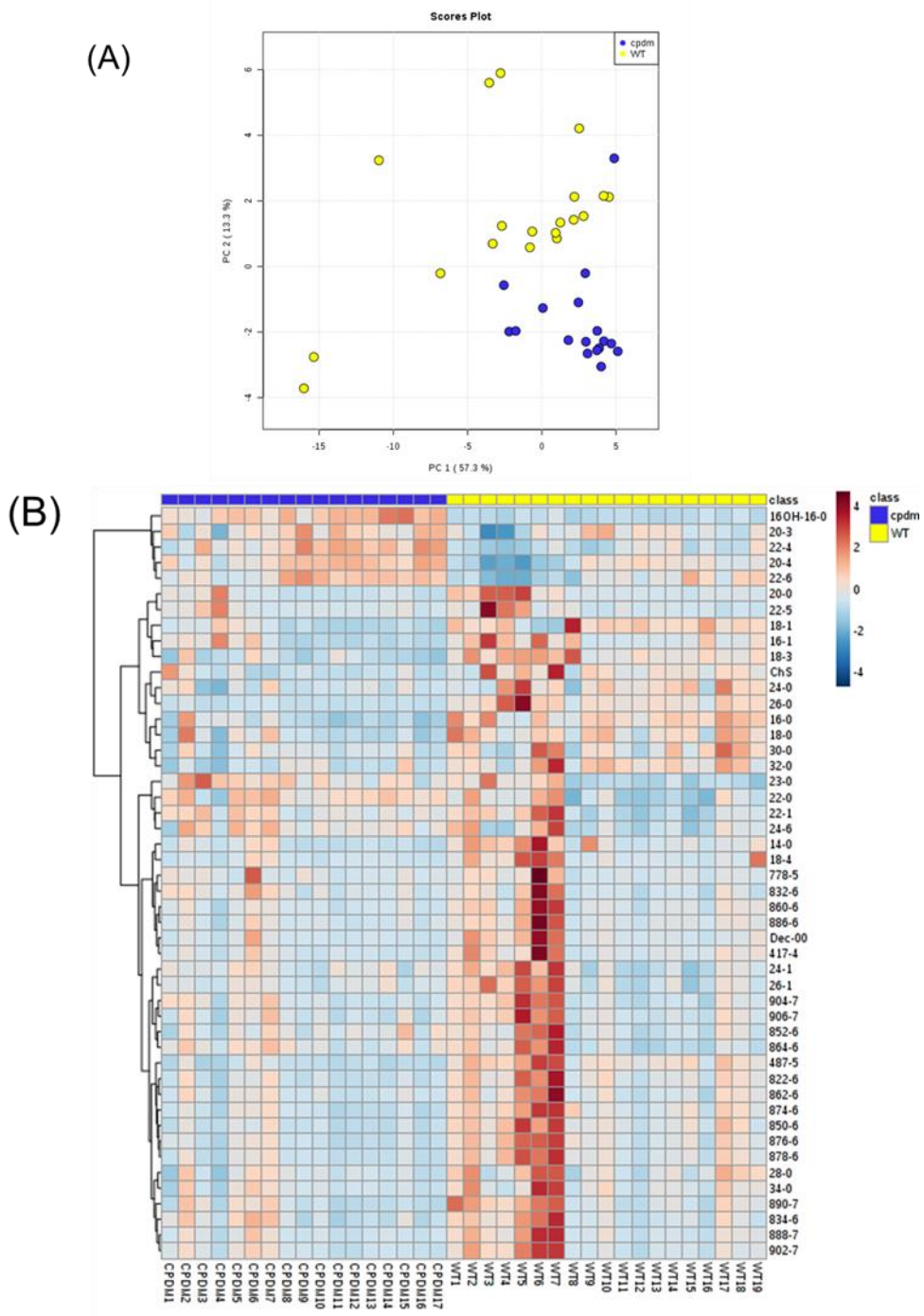

Figure 3**. Monitored lipid ions in *cpdm* and WT epidermis by MRM scans in negative ion mode.** Clear discrimination of the phenotypes of WT and *cpdm* mouse strains was observed by PCA and cluster analysis. (A) Score plot of principal component analysis (PCA). PC1 explained 57.3% of the variability of the data. When PC2 was included, the explained variance increased to 70.6% (B) Heat map with the distribution of lipids monitored individually in 36 samples. Lipids no identified are shown with their *m/z*. Color of each cell corresponds to the relative abundance of the lipid feature monitored in the samples.

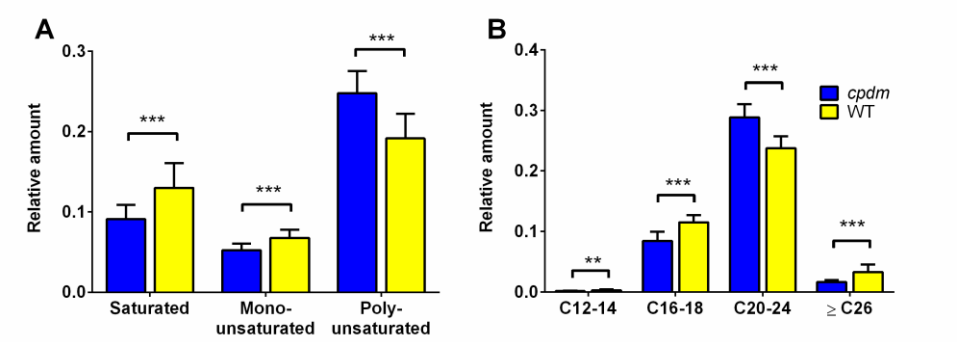

Figure 4**. FFA profile in *cpdm* and WT epidermis by MRM-profiling**. (A) Relative amounts of polyunsaturated FFAs were increased and saturated and monounsaturated FFAs were decreased in the *cpdm* epidermis. (B) The relative amounts of FFAs with chain length of 12 – 18 and longer than 26 carbons were reduced in *cpdm* samples compared to WT, instead FFAs with 22 -24 carbons were increased. Lipid ions were detected in negative ion mode with *m/z* 199-600 range and normalized by the total ion count. Values are means of 7 (*cpdm*) or 8 (WT) mice. ** $p < 0.01$; *** $p < 0.001$, based on unpaired t-test with Holm-Sidak correction for multiple comparisons.

2.4.2 Expression of lipid synthesis enzymes

Based on the results from MRM profiling, we examined the expression levels of two enzymes involved in biosynthesis and elongation of fatty acids, namely fatty acid synthase (FASN) and elongation of very long fatty acids-like 1 (ELOVL1), and two enzymes of the sphingolipid pathway, phosphodiesterase 12 (PDE12) and beta acid glucosidase (GBA). The expression of FASN mRNA was lower in *cpdm* mice compared with WT mice ($p < 0.05$) (S5 Fig). Changes in the expression of the other enzymes did not reach statistical significance ($p > 0.05$).

2.4.3 Receiver Operating Characteristic (ROC) curve analysis

The discriminative values of ceramides and FFA monitored were assessed by developing ROC curves using the initial test samples (n=15) to model the classification and the validation set (N=21) as unknowns. The sphingosine ceramides CerAS(d18:1/24:0)2OH, CerAS(d18:1/16:0)2OH and CerNS(d18:1/16:0) discriminated between WT and *cpdm* mice with 100% accuracy (Fig 5) using partial least square – discriminant analysis (PLS-DA) as the algorithm for the multivariate ROC curve. The area under the curve (AUC) score for the model was 1, and the predicted class probability for the testing samples was precise, with no errors in the attribution (S6 Fig). All new samples were correctly classified with high-predicted probabilities

for each sample (>0.99) using random forest (RF) or PLS-DA as algorithms for the multivariate ROC curve (S4 Table). Another ROC was modeled with FFA selected from the targeted negative ion mode method, namely, DHA (22:6), ω-hydroxyl palmitic acid (16OH-16:0) and cerotic acid (26:0). The AUC score for the univariate ROC curve for the training group had a value of 1 for the first two fatty acids and a value of 0.964 for the cerotic acid (Fig 6). The overall model had an AUC of 1 and the class prediction probability of the testing samples was high (S7 Fig). For the new samples there was misclassification of two of the validation set samples using RF and one using PLS-DA, giving an AUC value of 0.964 for the multivariate ROC curve (S5 Table).

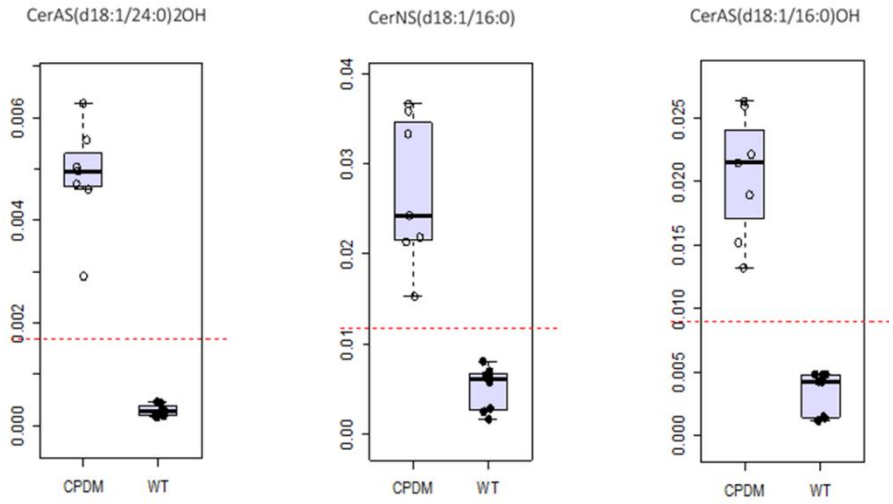

Figure 5 **Discriminative value of a set of three ceramides**. ROC curve analysis of sphingosine ceramides CerAS(d18:1/24:0)2OH, CerAS(d18:1/16:0)2OH and CerNS(d18:1/16:0) in *cpdm* and WT epidermis. The threshold (red dotted line) set to differentiate between the two groups is not crossed by any of the samples analyzed for any of the three ceramides.

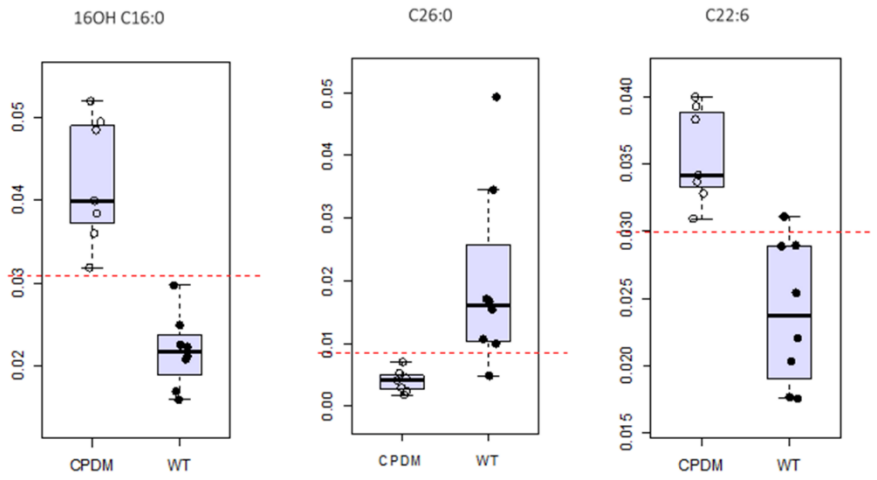

Figure 6 **Discriminative value of a set of three free fatty acids.** ROC curve analysis of free fatty acids (FFAs) ω-hydroxyl palmitic acid (16OH-16:0), cerotic acid (26:0), and DHA (22:6) in *cpdm* and WT epidermis. The threshold (red dotted line) set to differentiate between the two groups is crossed by one sample of the WT group analyzed for cerotic acid (26:0), and DHA (22:6). There was no overlap between the groups for ω-hydroxyl palmitic acid (16OH-16:0).

The sphingolipids that were selected by ROC curve analysis were analyzed by LC-MS (12) to obtain quantitative results in nmol/mg of tissue. The results were analyzed by ROC curve to confirm the outcome of the MRM-profiling approach. The LC-MS/MS results were in agreement with those obtained by MRM-profiling (S8 Fig).

2.5 Discussion

Changes in the composition and structure of epidermal lipids are found in various skin conditions (1). In recent years, the epidermal lipid barrier has received most attention in the context of AD (40,41). Reduced barrier function facilitates penetration by pathogens or irritant molecules that cause an exacerbated inflammatory response characterized by a Th1/Th2 imbalance (42), which in turn can affect the lipid composition and the barrier function of the skin (8,43). We investigated the lipid composition of the epidermis of *cpdm* mice, a mouse model with histological and immunological characteristics of human inflammatory skin diseases (25,26) applying a straightforward workflow mostly based on MRM-profiling. This exploratory approach focused on relative rather than absolute quantification. This is a widely accepted strategy in discovery MS such as liquid-chromatography-high resolution mass spectrometry (44). The relative amounts of

lipids in the epidermis determine their organization, barrier formation, and biological function (45–47).

The *cpdm* epidermis contained more Cer[S] at the expense of Cer[P] compared with WT mice similar to changes observed in human patients with AD (21,43). The increase of α-hydroxylated ceramides and reduction of ω-esterified ceramides in *cpdm* mice, similar to changes observed in human AD (48–51), can contribute to reduced membrane stability of keratinocytes (52) and decreased lipid organization and density of the lipid lamellae (53). Ceramides of 34 carbons were increased in patients with atopic eczema and Netherton syndrome (41,46). Similarly, an increase of ceramides with 16 carbon fatty acid residues (and 18 carbons from the sphingoid base) was observed in the *cpdm* epidermis. A possible common metabolic pathway of ceramides and FFA was suggested as the fatty acid residues on ceramides are related to the FFA chain lengths, and both FFA and ceramides with chain lengths of 20 – 24 carbons were present in increased amounts. On the other hand, there was a clear reduction of ceramides and FFA with more than 26 carbons in their acyl chains. This is in agreement with reports of a reduction of ultra-long ceramides and long chain FFA in human AD and another mouse model of AD (8,40,53).

Disruption of the epidermal barrier induces changes in the expression of enzymes required for the biosynthesis of lipids (54). Conversely, changes in the expression of enzymes may cause changes in the lipid composition of the epidermis. Investigation of the expression of four enzymes involved in the synthesis and of fatty acids and ceramides revealed decreased expression of Fasn mRNA, and no significant changes in the other enzymes. Little is known about the effect of inflammation or inflammatory mediators on the expression of lipid synthesis enzymes in the epidermis. Increased immunohistochemical labeling of the lower epidermis for fatty acid synthase was reported in various forms of dermatitis (55). In addition, treatment of *in vitro* cultures of human skin with tumor necrosis factor (TNF) and IL-31 decreased expression of ELOVL1 (8) and cultures with a Th2 cocktail, including IL-4, IL-13 and IL-31 showed significantly lower mRNA expression of ELOVL1, aSmase and GBA (43). The *cpdm* dermatitis is associated with increased expression of type 2 cytokines, but there was no increase of TNF mRNA in the skin (25).

Sphingomyelin (SM) can give rise only to sphingosine ceramides (Cer[AS] and Cer[NS]) (10) in the sphingolipid pathway. Changes in the structure of ceramides and SM have been observed under pathologic conditions including inflammatory diseases (56,57). Alterations in the

length, hydroxylation state and saturation degree of the fatty acid residues can result from inflammation and can also affect the cellular response to inflammatory stimuli (58).

There was an increase of FFA species with 20 – 24 carbons chain length and a higher degree of unsaturation as reflected in the increase of arachidonic acid (AA) (20:4) and DHA (22:6) and decrease of ultra-long chain fatty acid cerotic acid (C26:0). AA and DHA are important lipid mediators of inflammation having both pro-inflammatory and anti-inflammatory roles (1,59,60). The FFA profile of the *cpdm* epidermis had fewer fatty acids carrying acyl chains of 12, 14, and 16 carbons. Combined with the significant downregulation of the Fasn gene, this indicates alterations in early metabolic pathways in addition to reduced activity of the elongation pathway of the fatty acids. The MRM-profiling in positive mode demonstrated a general increase of PL in the epidermis of *cpdm* mice compared to WT, especially plasmalogens, which can affect the fluidity of cell membranes. Plasmalogens can also incorporate and store AA and DHA which can be released by the action of phospholipase A2 (61,62) suggesting a correlation between the increase of plasmalogens and AA and DHA in the *cpdm* epidermis.

To the best of our knowledge, changes in the structure of acylcarnitines have not been reported in AD. These molecules are involved in fatty acid oxidation disorders, metabolic disease and inflammation (63). Long chain acylcarnitines (16 and 18 carbons) were increased in *cpdm* epidermis while medium chain (10 and 14 carbons) were reduced. Long chain acylcarnitines can activate nuclear factor kappa-light-chain-enhancer of activated B cells (NF-kB) in macrophages resulting in secretion of inflammatory cytokines and chemokines (64). They may contribute to the dermatitis in *cpdm* mice and may also play a role in atopic dermatitis.

Reports of biomarkers in AD have focused mainly on gene mutations or levels of inflammatory mediators, which vary greatly among individuals and do not allow a clear stratification of patients. For example, filaggrin mutations are only present in a small percentage of AD patients (65,66), disease onset may not depend on it (67) and alteration of lipid processing enzymes are not correlated with presence of FLG mutation (9). Serum biomarkers such as IL31, IL33, and CCL17 had a weak correlation with disease severity (68,69) and do not reliably predict severity as a recent computational model based on 30 serum proteins failed to provide acceptable error values (70). However, transcriptome analysis in AD patients showed enrichment of pathways related to lipid biosynthesis and metabolism (71) reinforcing the idea that biochemical dysregulation (72) of multiple pathways and gene defects may underlie the pathogenesis of a

phenotypically diverse and complex disease such as atopic dermatitis. An unbiased methodology, such as MRM-profiling, is able to capture phenotypic information important for the development of techniques to predict high-risk patients and to discriminate between disease progression stages and treatment response beyond clinical assessment (66,69). In this study, the prediction model using sphingosine ceramides CerAS(d18:1/24:0)2OH, CerAS(d18:1/16:0)2OH, and CerNS(d18:1/16:0) showed clear discrimination of the samples with a 100% of accuracy. Such information can lead to the identification of biomarkers that will be instrumental in the development of personalized approaches for the treatment of AD (15).

In summary, we report CerAS(d18:1/24:0)2OH, CerAS(d18:1/16:0)2OH, CerNS(d18:1/16:0), cerotic acid, 16-hydroxy palmitic acid, and docosahexaenoic acid (DHA) as highly discriminative lipids in the dermatitis of SHARPIN-deficient mice. The validation set of this panel of biomarkers confirmed its specificity and sensitivity, with an exact class prediction of new samples based on ceramides and a 90.5% success based on FFA. This panel of lipids may be useful as molecular indicators of treatment effect in this and other mouse models of AD. We also suggest that it would be worthwhile to determine whether the amounts of these lipids are altered in the epidermis of human patients and domestic animals with AD.

2.6 References

1. Kendall AC, Nicolaou A. Bioactive lipid mediators in skin inflammation and immunity. Prog Lipid Res. 2013;52(1):141–64.
2. van Smeden J, Janssens M, Gooris GS, Bouwstra JA. The important role of stratum corneum lipids for the cutaneous barrier function. Biochim Biophys Acta - Mol Cell Biol Lipids. 2014;1841(3):295–313.
3. Fischer CL, Blanchette DR, Brogden K a., Dawson D V., Drake DR, Hill JR, et al. The roles of cutaneous lipids in host defense. Biochim Biophys Acta - Mol Cell Biol Lipids. 2014;1841(3):319–22.
4. Flohr C, Mann J. New insights into the epidemiology of childhood atopic dermatitis. Allergy. 2014;69(1):3–16.
5. Maksimović N, Janković S, Marinković J, Sekulović LK, Zivković Z, Spirić VT. Health-related quality of life in patients with atopic dermatitis. J Dermatol. 2012;39(1):42–7.
6. Weidinger S, Novak N. Atopic dermatitis. Lancet. 2016;387(10023):1109–22.

7. Paternoster L, Standl M, Waage J, Baurecht H, Hotze M, Strachan DP, et al. Multi-ancestry genome-wide association study of 21,000 cases and 95,000 controls identifies new risk loci for atopic dermatitis. Nat Genet. 2015;47(12):1449–56.

8. Danso MO, van Drongelen V, Mulder A, van Esch J, Scott H, van Smeden J, et al. TNF-α and Th2 cytokines induce atopic dermatitis-like features on epidermal differentiation proteins and stratum corneum lipids in human skin equivalents. J Invest Dermatol. 2014;134(7):1941–50.

9. Elias PM, Schmuth M. Abnormal skin barrier in the etiopathogenesis of atopic dermatitis. Curr Opin Allergy Clin Immunol. 2009;9(5):437–46.

10. Breiden B, Sandhoff K. The role of sphingolipid metabolism in cutaneous permeability barrier formation. Biochim Biophys Acta. 2014;1841(3):441–52.

11. Mojumdar EH, Kariman Z, van Kerckhove L, Gooris GS, Bouwstra J a. The role of ceramide chain length distribution on the barrier properties of the skin lipid membranes. Biochim Biophys Acta. 2014;1838(10):2473–83.

12. Merrill AH, Sullards MC, Allegood JC, Kelly S, Wang E. Sphingolipidomics: high-throughput, structure-specific, and quantitative analysis of sphingolipids by liquid chromatography tandem mass spectrometry. Methods. 2005;36(2):207–24.

13. Li S, Ganguli-Indra G, Indra AK. Lipidomic analysis of epidermal lipids: a tool to predict progression of inflammatory skin disease in humans. Expert Rev Proteomics. 2016;13(5):451–6.

14. Sadowski T, Klose C, Gerl MJ, Wójcik-Maciejewicz A, Herzog R, Simons K, et al. Large-scale human skin lipidomics by quantitative, high-throughput shotgun mass spectrometry. Sci Rep. 2017;7:43761.

15. Bieber T, Akdis C, Lauener R, Traidl-Hoffmann C, Schmid-Grendelmeier P, Schäppi G, et al. Global Allergy Forum and 3rd Davos Declaration 2015: Atopic dermatitis/Eczema: challenges and opportunities toward precision medicine. Allergy. 2016;71(5):588–92.

16. Mansouri Y, Guttman-Yassky E. Immune Pathways in Atopic Dermatitis, and Definition of Biomarkers through Broad and Targeted Therapeutics. J Clin Med. 2015;4(5):858–73.

17. Ferreira CR, Yannell KE, Mollenhauer B, Espy RD, Cordeiro FB, Ouyang Z, et al. Chemical profiling of cerebrospinal fluid by multiple reaction monitoring mass spectrometry. Analyst. 2016;141(18):5252–5.

18. Wang M, Wang C, Han RH, Han X. Novel advances in shotgun lipidomics for biology and medicine. Prog Lipid Res. 2016 Jan;61:83–108.

19. Schwudke D, Schuhmann K, Herzog R, Bornstein SR, Shevchenko A. Shotgun lipidomics on high resolution mass spectrometers. Cold Spring Harb Perspect Biol. 2011;3(9):a004614.

20. Cordeiro FB, Ferreira CR, Sobreira TJP, Yannell KE, Jarmusch AK, Cedenho AP, et al. Multiple Reaction Monitoring (MRM)-Profiling for Biomarker Discovery Applied to Human Polycystic Ovarian Syndrome. Rapid Commun Mass Spectrom. 2017;(17):1462-1470.

21. van Smeden J, Janssens M, Kaye ECJ, Caspers PJ, Lavrijsen AP, Vreeken RJ, et al. The importance of free fatty acid chain length for the skin barrier function in atopic eczema patients. Exp Dermatol. 2014;23(1):45–52.

22. Tata A, Sudano MJ, Santos VG, Landim-Alvarenga FDC, Ferreira CR, Eberlin MN. Optimal single-embryo mass spectrometry fingerprinting. J Mass Spectrom. 2013;48(7):844–9.

23. Seymour RE, Hasham MG, Cox GA, Shultz LD, HogenEsch H, Roopenian DC, et al. Spontaneous mutations in the mouse Sharpin gene result in multiorgan inflammation, immune system dysregulation and dermatitis. Genes Immun. 2007;8(5):416–21.

24. HogenEsch H, Gijbels MJ, Offerman E, van Hooft J, van Bekkum DW, Zurcher C. A spontaneous mutation characterized by chronic proliferative dermatitis in C57BL mice. Am J Pathol. 1993;143(3):972–82.

25. HogenEsch H, Torregrosa SE, Boggess D, Sundberg BA, Carroll J, Sundberg JP. Increased expression of type 2 cytokines in chronic proliferative dermatitis (cpdm) mutant mice and resolution of inflammation following treatment with IL-12. Eur J Immunol. 2001;31(3):734–42.

26. Potter CS, Wang Z, Silva K a, Kennedy VE, Stearns TM, Burzenski L, et al. Chronic proliferative dermatitis in Sharpin null mice: development of an autoinflammatory disease in the absence of B and T lymphocytes and IL4/IL13 signaling. Brandner JM, editor. PLoS One. 2014;9(1):e85666.

27. HogenEsch H, Dunham A, Seymour R, Renninger M, Sundberg JP. Expression of chitinase-like proteins in the skin of chronic proliferative dermatitis (cpdm/cpdm) mice. Exp Dermatol. 2006;15(10):808–14.

28. Germain L, Rouabhia M, Guignard R, Carrier L, Bouvard V, Auger F. Improvement of human keratinocyte isolation and culture using thermolysin. Burns. 1993;19(2):99–104.

29. Bligh EG, Dyer WJ. A rapid method of total lipid extraction and purification. Can J Biochem Physiol. 1959 Aug;37(8):911–7.

30. Brugger B, Erben G, Sandhoff R, Wieland FT, Lehmann WD. Quantitative analysis of biological membrane lipids at the low picomole level by nano-electrospray ionization tandem mass spectrometry. Proc Natl Acad Sci. 1997 Mar 18;94(6):2339–44.

31. Taguchi R, Houjou T, Nakanishi H, Yamazaki T, Ishida M, Imagawa M, et al. Focused lipidomics by tandem mass spectrometry. J Chromatogr B Analyt Technol Biomed Life Sci. 2005;823(1):26–36.

32. Han X, Gross RW. Shotgun lipidomics: Electrospray ionization mass spectrometric analysis and quantitation of cellular lipidomes directly from crude extracts of biological samples. Mass Spectrom Rev. 2005;24(3):367–412.

33. Chowdhury B, Porter EG, Stewart JC, Ferreira CR, Schipma MJ, Dykhuizen EC. PBRM1 regulates the expression of genes involved in metabolism and cell adhesion in renal clear cell carcinoma. PLoS One. 2016;11(4):1–20.

34. Liebisch G, Binder M, Schifferer R, Langmann T, Schulz B, Schmitz G. High throughput quantification of cholesterol and cholesteryl ester by electrospray ionization tandem mass spectrometry (ESI-MS/MS). Biochim Biophys Acta. 2006;1761(1):121–8.

35. Colsch B, Afonso C, Popa I, Portoukalian J, Fournier F, Tabet J-C, et al. Characterization of the ceramide moieties of sphingoglycolipids from mouse brain by ESI-MS/MS: identification of ceramides containing sphingadienine. J Lipid Res. 2004;45(2):281–6.

36. Li M, Butka E, Wang X. Comprehensive quantification of triacylglycerols in soybean seeds by electrospray ionization mass spectrometry with multiple neutral loss scans. Sci Rep. 2014;4:6581.

37. Renninger ML, Seymour RE, Whiteley LO, John P, Sundberg JP, HogenEsch H. Anti-IL5 decreases the number of eosinophils but not the severity of dermatitis in SHARPIN-deficient mice. Exp Dermatol. 2010;19(3):252–8.

38. Livak KJ, Schmittgen TD. Analysis of relative gene expression data using real-time quantitative PCR and. Methods. 2001;25:402–8.

39. Xia J, Sinelnikov I V., Han B, Wishart DS. MetaboAnalyst 3.0--making metabolomics more meaningful. Nucleic Acids Res. 2015;43(W1):W251-7.

40. Elias PM. Lipid abnormalities and lipid-based repair strategies in atopic dermatitis. Biochim Biophys Acta - Mol Cell Biol Lipids. 2014;1841(3):323–30.

41. Li S, Villarreal M, Stewart S, Choi J, Indra G, Babineau DC, et al. Altered composition of epidermal lipids correlates with Staphylococcus aureus colonization status in Atopic Dermatitis. Br J Dermatol. 2017;177(4):e125–7.

42. Boguniewicz M, Leung DYM. Atopic dermatitis: A disease of altered skin barrier and immune dysregulation. Immunol Rev. 2011;242(1):233–46.

43.Danso MO, Boiten W, van Drongelen V, Gmelig KM, Gooris G, El Ghalbzouri A, et al. Altered expression of epidermal lipid bio-synthesis enzymes in atopic dermatitis skin is accompanied by changes in stratum corneum lipid composition. J Dermatol Sci. 2017;88(1):57-66.

44. Vinayavekhin N, Homan EA, Saghatelian A. Exploring disease through metabolomics. ACS Chemical Biology. 2010. 5:91–103.

45. Uchiyama M, Oguri M, Mojumdar EH, Gooris GS, Bouwstra JA. Free fatty acids chain length distribution affects the permeability of skin lipid model membranes. Biochim Biophys Acta - Biomembr. 2016;1858(9):2050–9.

46. van Smeden J, Janssens M, Boiten WA, van Drongelen V, Furio L, Vreeken RJ, et al. Intercellular skin barrier lipid composition and organization in Netherton syndrome patients. J Invest Dermatol. 2014;134(5):1238–45.

47. Opálka L, Kováčik A, Maixner J, Vávrová K. Omega-O-Acylceramides in Skin Lipid Membranes: Effects of Concentration, Sphingoid Base, and Model Complexity on Microstructure and Permeability. Langmuir. 2016;32:12894–12904.

48. Tawada C, Kanoh H, Nakamura M, Mizutani Y, Fujisawa T, Banno Y, et al. Interferon-γ decreases ceramides with long-chain fatty acids: possible involvement in atopic dermatitis and psoriasis. J Invest Dermatol. 2014;134(3):712–8.

49. Macheleidt O, Kaiser HW, Sandhoff K. Deficiency of epidermal protein-bound omega-hydroxyceramides in atopic dermatitis. J Invest Dermatol. 2002 Jul;119(1):166–73.

50. Bleck O, Abeck D, Ring J, Hoppe U, Vietzke JP, Wolber R, et al. Two ceramide subfractions detectable in Cer(AS) position by HPTLC in skin surface lipids of non-lesional skin of atopic eczema. J Invest Dermatol. 1999;113(6):894–900.

51. Yamamoto A, Serizawa S, Ito M, Sato Y. Stratum corneum lipid abnormalities in atopic dermatitis. Arch Dermatol Res. 1991;283(4):219–23.

52. Loiseau N, Obata Y, Moradian S, Sano H, Yoshino S, Aburai K, et al. Altered sphingoid base profiles predict compromised membrane structure and permeability in atopic dermatitis. J Dermatol Sci. 2013;72(3):296–303.

53. Janssens M, van Smeden J, Gooris GS, Bras W, Portale G, Caspers PJ, et al. Increase in short-chain ceramides correlates with an altered lipid organization and decreased barrier function in atopic eczema patients. J Lipid Res. 2012;53(12):2755–66.

54. Harris IR, Farrell AM, Grunfeld C, Holleran WM, Elias PM, Feingold KR. Permeability Barrier Disruption Coordinately Regulates mRNA Levels for Key Enzymes of Cholesterol, Fatty Acid, and Ceramide Synthesis in the Epidermis. J Invest Dermatol. 1997;109(6):783–7.

55. Uchiyama N, Yamamoto A, Kameda K, Yamaguchi H, Ito M. The activity of fatty acid synthase of epidermal keratinocytes is regulated in the lower stratum spinousum and the stratum basale by local inflammation rather than by circulating hormones. J Dermatol Sci. 2000;24(2):134–41.

56. Grösch S, Schiffmann S, Geisslinger G. Chain length-specific properties of ceramides. Prog Lipid Res. 2012;51(1):50–62.

57. Hannun YA, Obeid LM. Many ceramides. J Biol Chem. 2011;286(32):27855–62.

58. Köberlin MS, Snijder B, Heinz LX, Baumann CL, Fauster A, Vladimer GI, et al. A Conserved Circular Network of Coregulated Lipids Modulates Innate Immune Responses. Cell. 2015;162(1):170–83.

59. Gil a. Polyunsaturated fatty acids and inflammatory diseases. Biomed Pharmacother. 2002;56(8):388–96.

60. Miki Y, Yamamoto K, Taketomi Y, Sato H, Shimo K, Kobayashi T, et al. Lymphoid tissue phospholipase A2 group IID resolves contact hypersensitivity by driving antiinflammatory lipid mediators. J Exp Med. 2013;210(6):1217–34.

61. Brites P, Waterham HR, Wanders RJA. Functions and biosynthesis of plasmalogens in health and disease. Biochim Biophys Acta - Mol Cell Biol Lipids. 2004;1636(2–3):219–31.

62. Gorgas K, Teigler A, Komljenovic D, Just WW. The ether lipid-deficient mouse: Tracking down plasmalogen functions. Biochim Biophys Acta - Mol Cell Res. 2006;1763(12):1511–26.

63. McCoin CS, Knotts TA, Adams SH. Acylcarnitines -old actors auditioning for new roles in metabolic physiology. Nat Rev Endocrinol. 2015;11(10):617–25.

64. Rutkowsky JM, Knotts T a, Ono-Moore KD, McCoin CS, Huang S, Schneider D, et al. Acylcarnitines activate proinflammatory signaling pathways. Am J Physiol Endocrinol Metab. 2014;306(12):E1378-87.

65. Yokouchi M, Kubo A, Kawasaki H, Yoshida K, Ishii K. Epidermal tight junction barrier function is altered by skin inflammation, but not by filaggrin-deficient stratum corneum. J Dermatol Sci. 2015;77(1):28–36.

66. Ardern-Jones MR, Bieber T. Biomarkers in atopic dermatitis: it is time to stratify. Br J Dermatol. 2014;171(2):207–8.

67. Kelleher M, Dunn-Galvin A, Hourihane JO, Murray D, Campbell LE, McLean WHI, et al. Skin barrier dysfunction measured by transepidermal water loss at 2 days and 2 months predates and predicts atopic dermatitis at 1 year. J Allergy Clin Immunol. 2015;135(4):930–935.e1.

68. Nygaard U, Hvid M, Johansen C, Buchner M, Fölster-Holst R, Deleuran M, et al. TSLP, IL-31, IL-33 and sST2 are new biomarkers in endophenotypic profiling of adult and childhood atopic dermatitis. J Eur Acad Dermatol Venereol. 2016;30(11):1930–8.

69. Thijs J, van Seggelen W, Bruijnzeel-Koomen C, de Bruin-Weller M, Hijnen D. New Developments in Biomarkers for Atopic Dermatitis. J Clin Med. 2015;4(3):479–87.

70. Krause L, Mourantchanian V, Brockow K, Theis FJ, Schmidt-Weber CB, Knapp B, et al. A computational model to predict severity of atopic eczema from 30 serum proteins. J Allergy Clin Immunol.2016 Oct;138(4):1207–1210.e2.

71. Cole C, Kroboth K, Schurch NJ, Sandilands A, Sherstnev A, O'Regan GM, et al. Filaggrin-stratified transcriptomic analysis of pediatric skin identifies mechanistic pathways in patients with atopic dermatitis. J Allergy Clin Immunol. 2014;134(1):82–91.

72. Agrawal K, Hassoun LA, Foolad N, Pedersen TL, Sivamani RK, Newman JW. Sweat lipid mediator profiling: a noninvasive approach for cutaneous research. J Lipid Res. 2017;58(1):188–95.

2.7 Supporting information

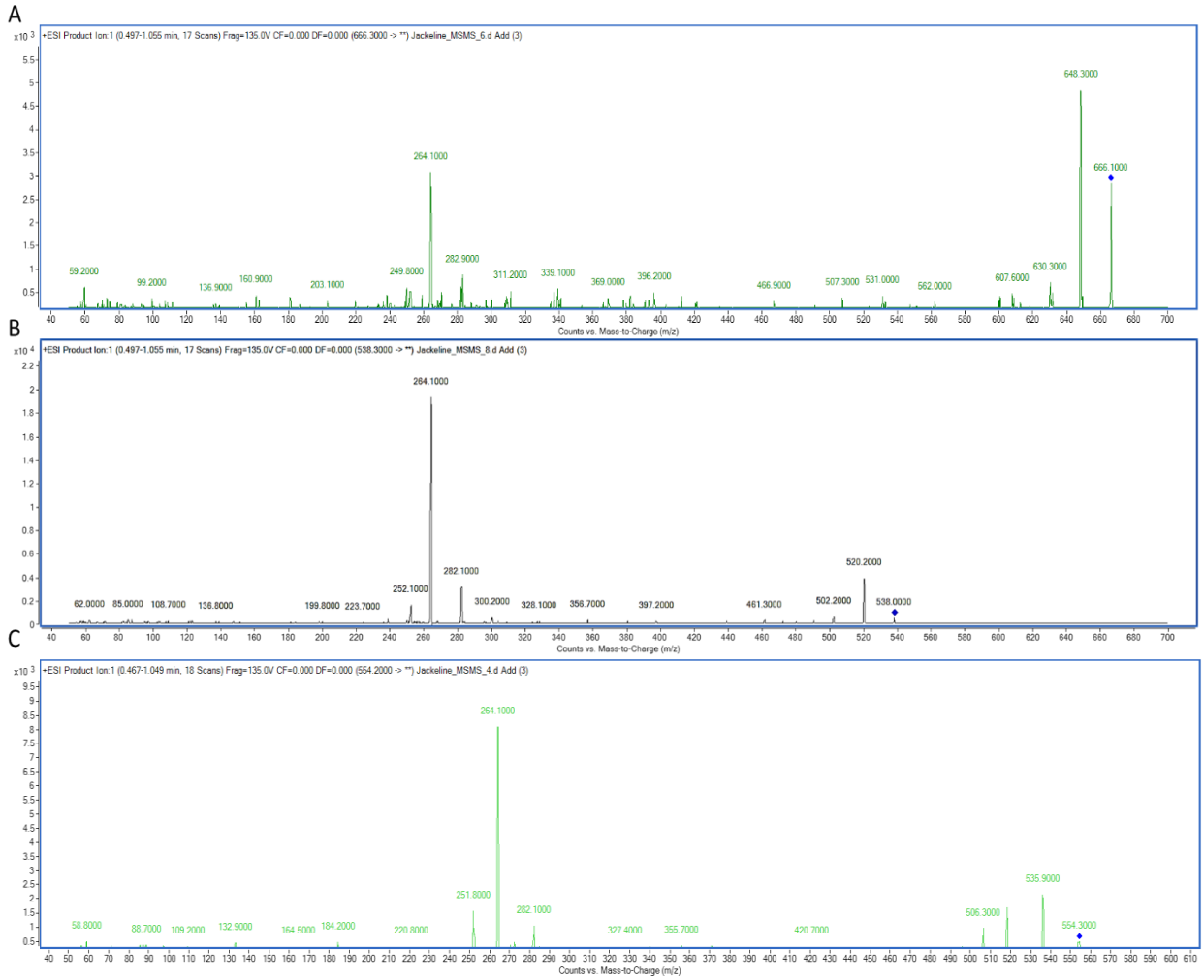

S1 Figure: Representative added MS/MS spectrum for tentative attribution of transitions selected as potential biomarkers by ROC curve analysis.

(A) MS/MS of *m/z* 666.3 corresponding to the sphingosine ceramide Cer(d18:1/24:0)2OH. Three peaks observed correspond to the parent ion (*m/z* 666.3), the release of water with a loss of 18 u (*m/z* 648.3) and the sphingosine base (*m/z* 264.1). The *m/z* difference between *m/z* 648.3 and *m/z* 264.1 correspond to 2-hydroxy-tetracosanoic acid (*m/z* 384.2) (LMFA01050080) (B) MS/MS of *m/z* 538.3 corresponding to the sphingosine ceramide Cer(d18:1/16:0). Three peaks observed correspond to the parent ion (*m/z* 538.3), the release of water with a loss of 18 u (*m/z* 520.2) and the sphingosine base (*m/z* 264.1). The *m/z* difference between *m/z* 520.2 and *m/z* 264.1 correspond to hexadecanoic acid (*m/z* 256.1) (LMFA01010001) (C) MS/MS of *m/z* 554.2 corresponding to the sphingosine ceramide Cer(d18:1/16:0)2OH. Three peaks observed correspond to the parent ion (*m/z* 554.2), the release of water with a loss of 18 u (*m/z* 535.9) and the sphingosine base (*m/z* 264.1). The *m/z* difference between *m/z* 535.9 and *m/z* 264.1 correspond to 2-hydroxy-hexadecanoic acid (*m/z* 271.8) (LMFA01050047). The *m/z* values had a delta +/-0.5. Vertical axis represents the ion intensity response and the horizontal axis is the mass-to-charge (*m/z*) of the ion analized.

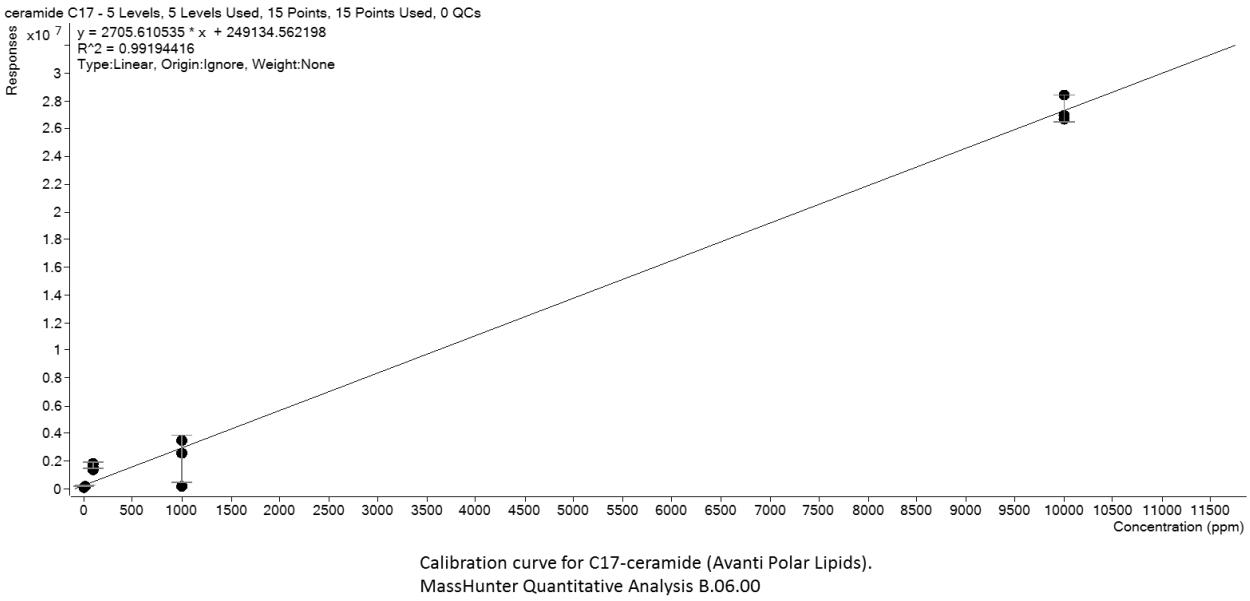

S2 Figure Calibration curve of C17-ceramide lipid standard spiked into pooled lipid extracts from 3 WT and 3 *cpdm* mice.

Assay linearity exceeds 3 order of magnitude and has excellent linearity and dynamic range. Five levels were determined in the MassHunter Quantitative Analysis software method for the calibration curve corresponding to concentrations of 1, 10, 100, 1000 and 10000 ppm. 15 points were created out of 3 replicates for each of the 5 levels, all of them were used to plot the curve as shown in the figure. Vertical axis represents the ion intensity response and the horizontal axis is concentration on ppm.

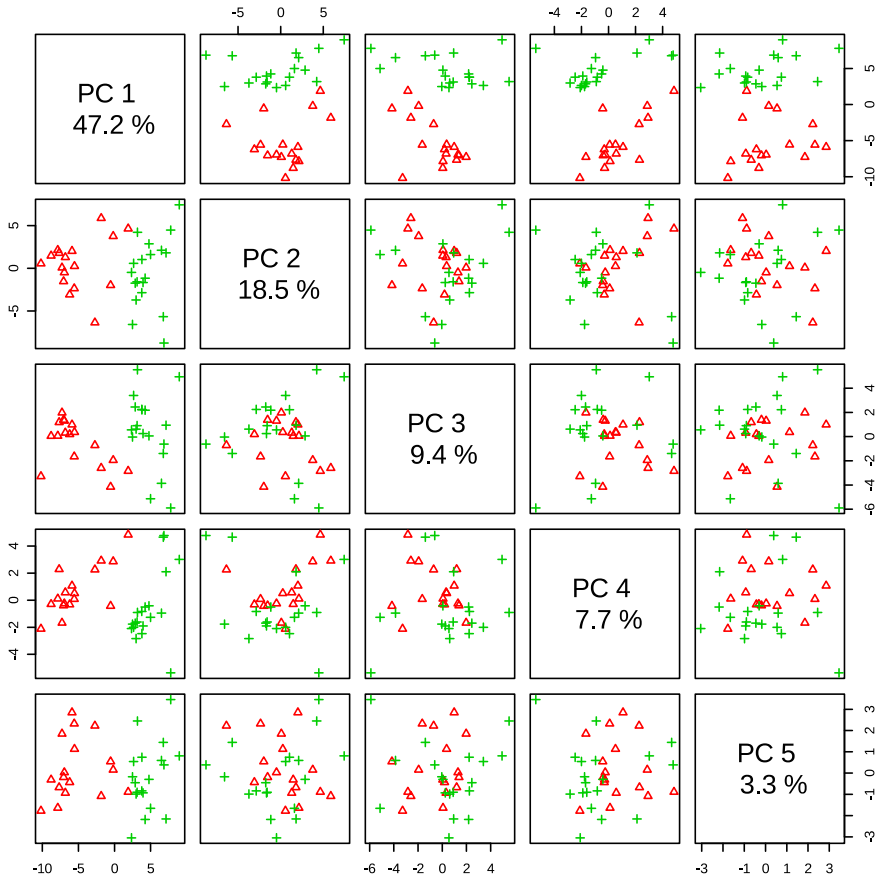

S3 Figure PCA pair plot of MRM-profiling in positive ion mode.

Overview of all combinations for the 5 first principal components (PC) for PCA score plots of MRM profiling data for the method in the positive ion mode (Method 1).

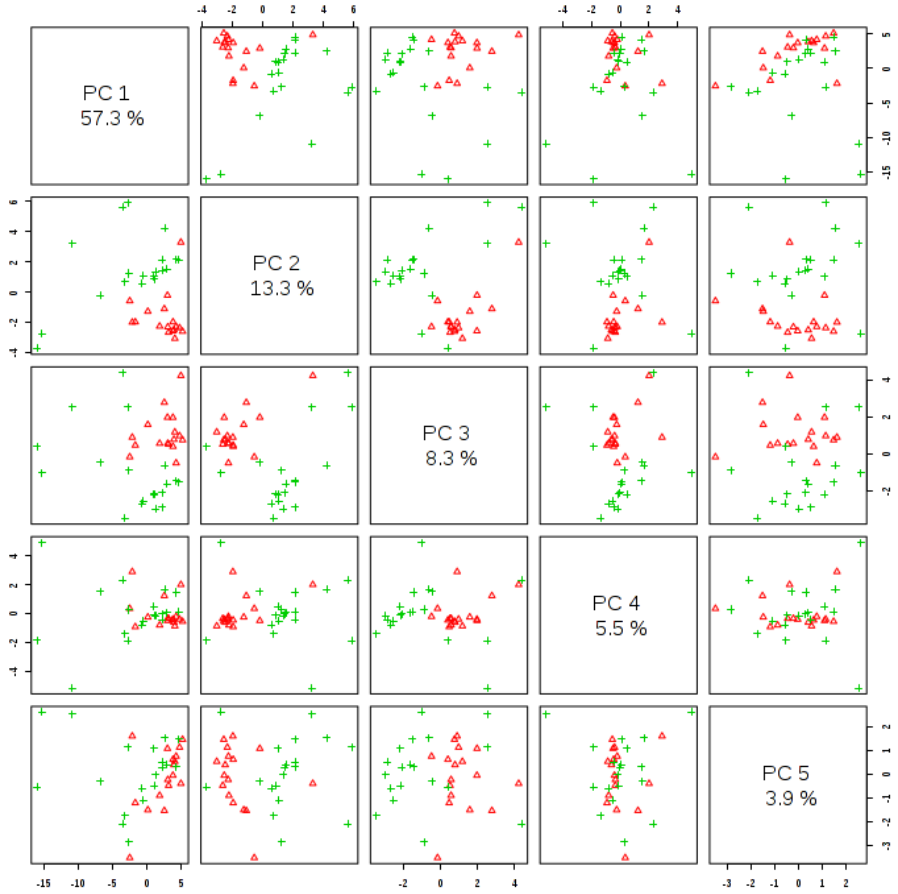

S4 Figure PCA pair plot of MRM-profiling in negative ion mode.

Overview of all combinations for the 5 first principal components (PC) for PCA score plots of MRM profiling data for the method in the negative ion mode (Method 2).

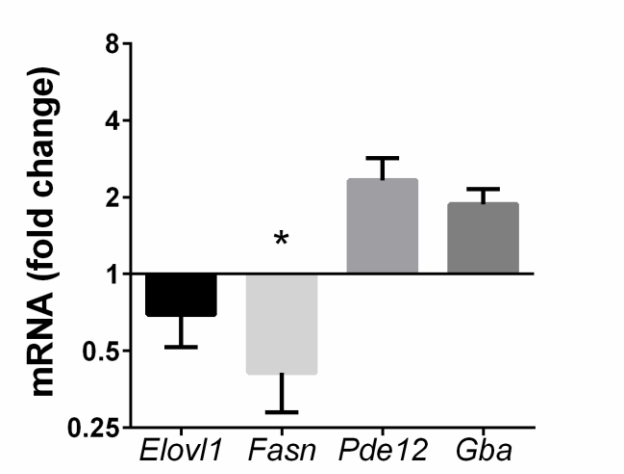

S5 Figure Expression of enzymes involves in lipid synthesis in the skin.

The expression of *Fasn* mRNA was significantly increased (* $p<0.05$) in *cpdm* mice whereas the expression of other enzymes was not changed. The bars represent the mean fold change of mRNA expression in *cpdm* mice versus WT mice (n=8).

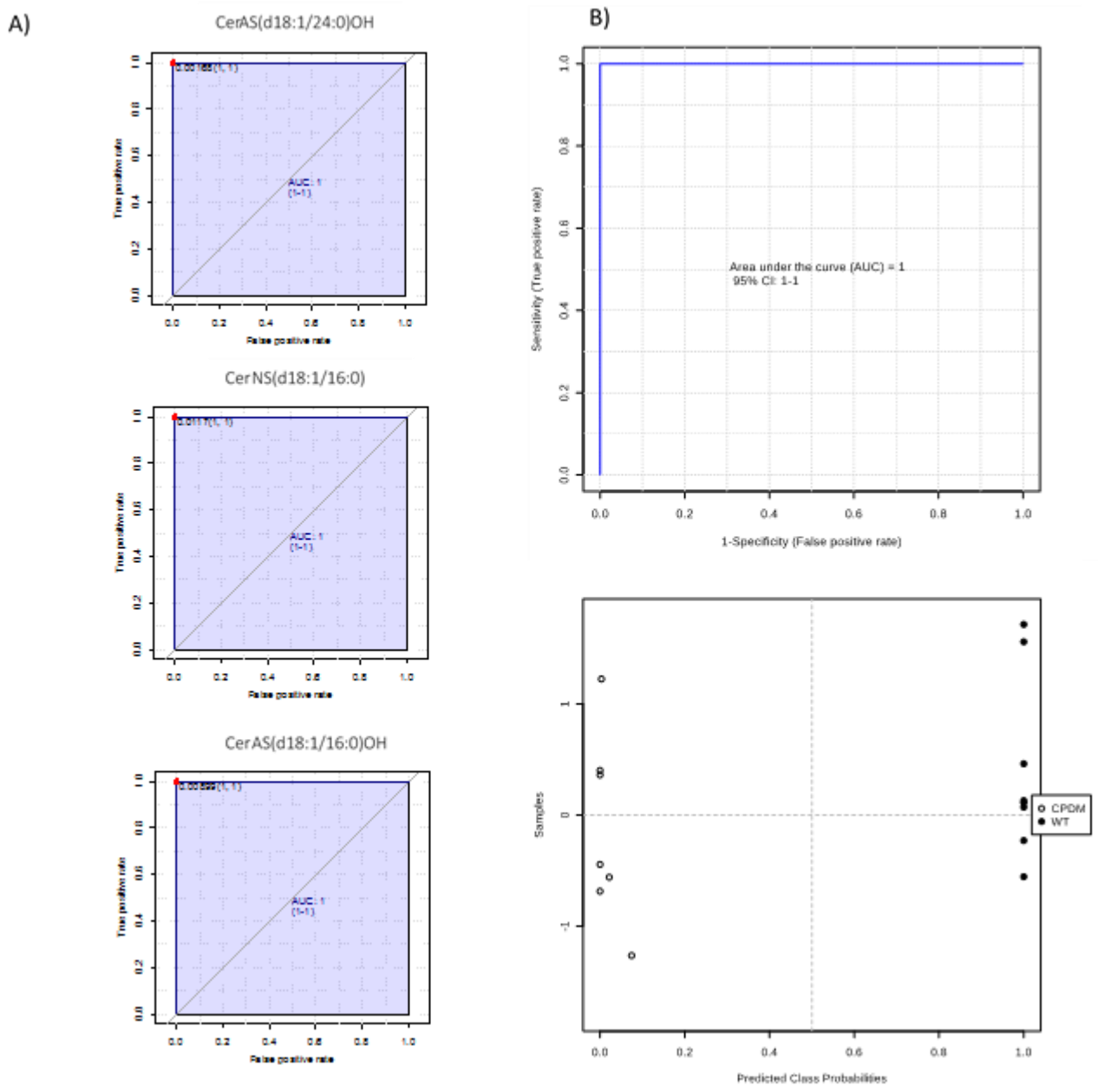

S6 Figure Discriminative value of a set of three ceramides.

(A) ROC curves of sphingosine ceramides CerAS(d18:1/24:0)OH, CerAS(d18:1/16:0)OH and CerNS(d18:1/16:0). (B) Area under the curve (AUC) representation for the testing samples by partial least square – discriminant analysis (PLSA-DA) built with the three selected ceramides; C) Predicted class probability for the testing set of samples of *cpdm* and WT epidermis.

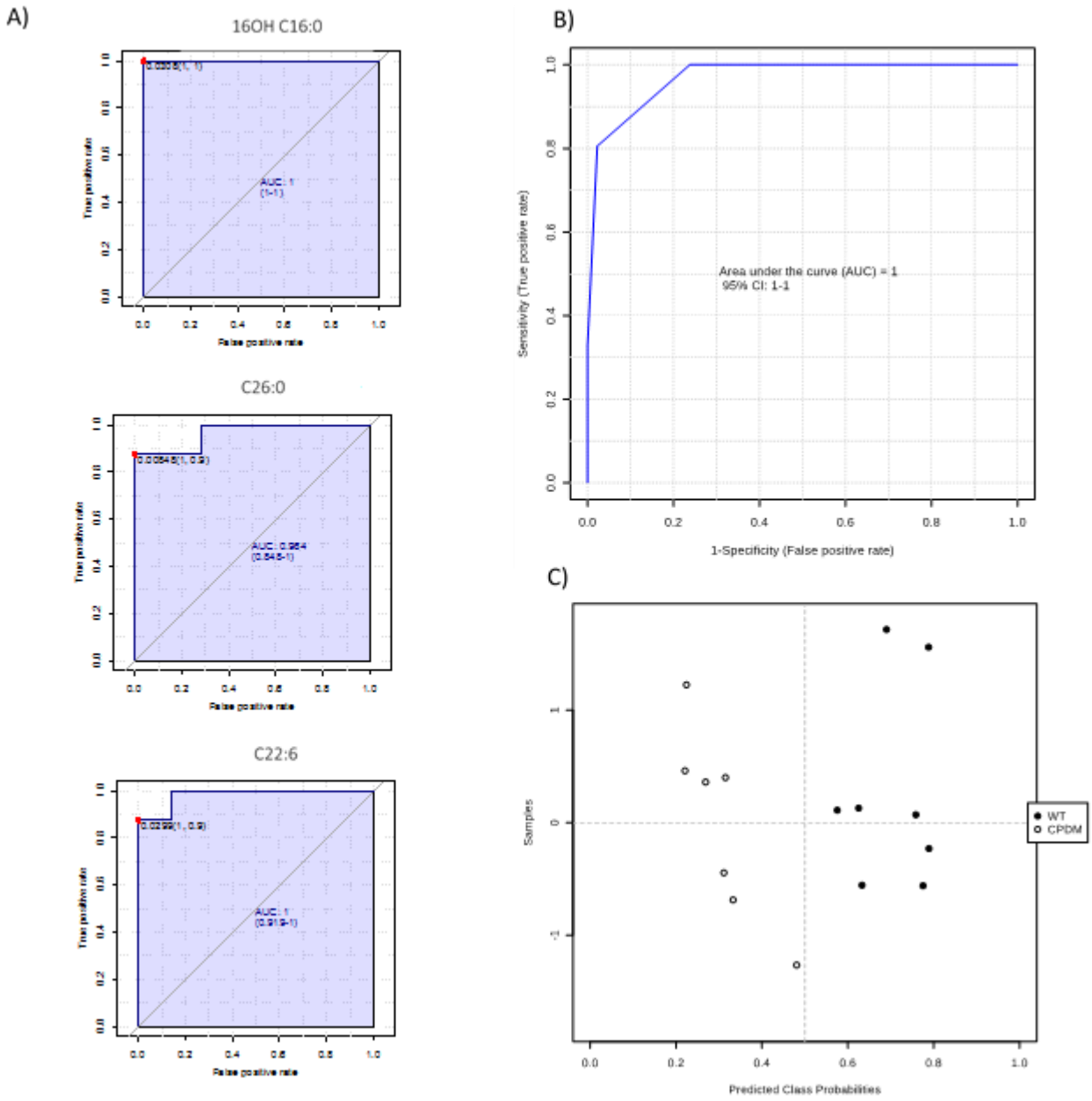

S7 Figure Discriminative value of a set of three free fatty acids.

(A) ROC curves of free fatty acids (FFAs) ω-hydroxyl palmitic acid (16OH-16:0), cerotic acid (26:0), and DHA (22:6); (B) Area under the curve (AUC) representation for the testing samples by partial least square – discriminant analysis (PLSA-DA) built with the three FFAs; (C) Predicted class probability for the testing set of samples of *cpdm* and WT epidermis.

S1 Table. Discovery scans. Multidimensional scan modes used for exploratory detection of lipids in *cpdm* and WT epidermis of the testing set.

Scan Mode	Description	Ion Mode	Ion Detected	Targeted Lipids	Reference	Data Collection Time/Sample
Prec 184	Precursor ion scan for *m/z* 184	(+)	[M+H]+	Phosphatidylcholine (PC), alkelnyl-acyl PC (ePC), sphingomyelin (SM) and LysoPC	*Brugger et al., 1997*	2min
NL 141	Neutral loss of 141 mass units	(+)	[M+H]+	Phosphatidylethanolamine (PE)	*Brugger et al., 1997*	2min
NL 277	Neutral loss of 277 mass units	(+)	[M+NH4]+	Phosphatidylinositol (PI)	*Taguchi et al., 2005*	2min
NL 185	Neutral loss of 185 mass units	(+)	[M+H]+	Phosphatydylserine (PS)	*Brugger et al., 1997*	2min
Prec 369.1	Precursor ion scan for *m/z* 369.1	(+)	[M+NH4]+	Cholesteryl esters (CE)	*Liebisch et al., 2006*	2min
Prec 264.3	Precursor ion scan for *m/z* 264.3	(+)	[M+H]+	Ceramides (d18:1; sphingosines)/Cerebrosides	*Colsch et al, 2004; Merrill et al., 2005*	2min
Prec 266.4	Precursor ion scan for *m/z* 266.4	(+)	[M+H]+	Ceramides (d18:0; Dihydro-ceramides)	*Colsch et al, 2004; Merrill et al., 2005*	2min
Prec 282.4	Precursor ion scan for *m/z* 282.4	(+)	[M+H]+	Ceramides (t18:0; phyto-ceramides)	*Colsch et al, 2004; Merrill et al., 2005*	2min
NL 299	Neutral loss of 299 mass units	(+)	[M+H]+	Oleate (acyl residue)	*Li et al., 2014*	2min
NL 321	Neutral loss of 321 mass units	(+)	[M+H]+	Arachidonate (acyl residue)	*Li et al., 2014*	2min
Prec 85	Precursor ion scan for *m/z* 85	(+)	[M+H]+	Acylcarnitines	*Han & Gross, 2005*	2min
Prec 303.1	Precursor ion scan for *m/z* 303.1	(-)	[M-H]+	Arachidonate (acyl residue)	*Li et al., 2014*	2min
Single ion monitoring (SIM)	*m/z* expected for FFA	(-)	[M-H]+	Free Fatty Acid profiles		2min
MRM		(+)	[M+H]+	Cholesteryl esters Profiling	*Chowedhury et al, 2016*	2min
N/A	Full mass scan	(+)	[M+H]+	Glycerolipids	*Brugger et al., 1997*	2min
N/A	Full mass scan	(-)	$[M-H]^-$	Free fatty acids and glycerolipids	*Brugger et al., 1997*	2min

S2 Table. MRM-profiling method in positive ion mode.

List of transitions in the MRM profiling method in positive ion mode (method 1) used to detect the relative amounts of lipids in the samples by the exploratory experiments. Each transition is represented by the *m/z* value of the parent ion, followed by the *m/z* value of the fragment released after collision at Q2.

Lipid Class	Parent	Fragment	Lipid Class	Parent	Fragment	Lipid Class	Parent	Fragment
Phosphatidylcholine (PC), alkelnyl-acyl PC (ePC), sphingomyelin (SM) and LysoPC	496.2	184.1	Phosphatidylinositol (PI)	852.5	575.5	Sphingo-sines	694.4	264.3
	520.2	184.1		854.5	577.5		873.7	264.3
	522.2	184.1		876.5	599.5		875.1	264.3
	689.8	184.1		878.5	601.5		875.6	264.3
	703.8	184.1		880.5	603.5	Dihydro-ceramides	438	266.4
	704.8	184.1		881.5	604.5		567.7	266.4
	705.8	184.1		882.5	605.5		568.6	266.4
	706.8	184.1		883.5	606.5		877.7	266.4
	719.8	184.1		904.5	627.5		900.8	266.4
	720.8	184.1		905.5	628.5		901.5	266.4
	732.8	184.1		906.5	629.5	Phytoceramides	282.1	282.4
	734.8	184.1	Phosphatydylserine (PS)	760.5	575.5		300.1	282.4
	735.8	184.1		762.5	577.5		538.2	282.4
	746.8	184.1		788.2	603.2		554.2	282.4
	758.8	184.1		789.5	604.5		564	282.4
	759.9	184.1		790.5	605.5		566.1	282.4
	760.8	184.1		791.5	606.5		650.3	282.4
	761.9	184.1		812.5	627.5	Acylcarnitines	359.25	85.1
	782.8	184.1		814.5	629.5		372.2	85.1
	784.8	184.1		816.5	631.5		376.2	85.1
	786.9	184.1		836.5	651.5		386.3	85.1
	787.9	184.1		844.5	659.5		398.3	85.1
	788.9	184.1		846.5	661.5		400.3	85.1
	815.9	184.1		872.5	687.5		401.3	85.1
Phosphatidylethanolamine (PE)	702.5	561.5		874.5	689.5		402.2	85.1
	716.5	575.5		875.5	690.5		414.3	85.1
	717.2	576.2	Sphingosines	536.1	264.3		415.25	85.1
	718.5	577.5		537.9	264.3		424.2	85.1
	719.5	578.5		538.2	264.3		426.3	85.1
	730.5	589.5		539.2	264.3		427.4	85.1
	740.5	599.5		554.2	264.3		428.3	85.1
	742.5	601.5		566.2	264.3		429.3	85.1
	743.5	602.5		622.1	264.3		442.25	85.1
	744.5	603.5		622.35	264.3		454.3	85.1
	745.5	604.5		648.4	264.3		456.3	85.1
	746.5	605.5		649.8	264.3		460.3	85.1
	747.5	606.5		650.4	264.3		484	85.1
	758.5	617.5		651.4	264.3		531.2	85.1
	766.5	625.5		666.35	264.3			
	768.5	627.5		678.4	264.3			
	769.5	628.5		679.4	264.3			
	770.5	629.5		694.15	264.3			

S3 Table. MRM-profiling method in negative ion mode.

List of single ions monitored in the MRM profiling method in negative ion mode (method 2) used to detect the relative amounts of free fatty acids in the lipid extracts from samples.

MRM	MRM	MRM
2155.2 -> 2155.2	395.4 -> 395.4	271.3 -> 271.3
2127.1 -> 2127.1	395.3 -> 395.3	256.3 -> 256.3
1864 -> 1864	393.3 -> 393.3	255.3 -> 255.3
1836.1 -> 1836.1	368.4 -> 368.4	253.3 -> 253.3
1601 -> 1601	367.4 -> 367.4	227.3 -> 227.3
1572.9 -> 1572.9	367.3 -> 367.3	225.2 -> 225.2
1544.9 -> 1544.9	365.3 -> 365.3	199.2 -> 199.2
1024.6 -> 1024.6	355.3 -> 355.3	197.2 -> 197.2
906.7 -> 906.7	353.3 -> 353.3	2181.3 -> 2181.3
904.7 -> 904.7	339.4 -> 339.4	
902.7 -> 902.7	339.3 -> 339.3	
890.7 -> 890.7	337.3 -> 337.3	
888.7 -> 888.7	331.3 -> 331.3	
886.6 -> 886.6	329.3 -> 329.3	
878.6 -> 878.6	329.3 -> 329.3	
876.6 -> 876.6	327.3 -> 327.3	
874.6 -> 874.6	327.3 -> 327.3	
864.6 -> 864.6	311.3 -> 311.3	
862.6 -> 862.6	309.3 -> 309.3	
860.6 -> 860.6	309.3 -> 309.3	
852.6 -> 852.6	305.3 -> 305.3	
850.6 -> 850.6	304.3 -> 304.3	
834.6 -> 834.6	303.3 -> 303.3	
832.6 -> 832.6	303.3 -> 303.3	
822.6 -> 822.6	301.3 -> 301.3	
806.6 -> 806.6	295.3 -> 295.3	
804.5 -> 804.5	284.3 -> 284.3	
794.7 -> 794.7	283.3 -> 283.3	
778.5 -> 778.5	283.3 -> 283.3	
507.5 -> 507.5	282.3 -> 282.3	
487.5 -> 487.5	281.3 -> 281.3	
479.4 -> 479.4	280.3 -> 280.3	
465.4 -> 465.4	279.3 -> 279.3	
451.4 -> 451.4	279.3 -> 279.3	
423.4 -> 423.4	277.3 -> 277.3	
417.4 -> 417.4	277.3 -> 277.3	
396.4 -> 396.4	275.3 -> 275.3	

S4 Table. Class prediction by ROC curve selected ceramides.

Class prediction of the validation set of samples by ROC based on potential ceramide biomarkers.

New sample name	Real class	Random Forrest		PLS-DA	
		Probability	Predicted class	Probability	Predicted class
CPDM8	CPDM	1	CPDM	0.90	CPDM
CPDM9	CPDM	1	CPDM	0.66	CPDM
CPDM10	CPDM	1	CPDM	0.79	CPDM
CPDM11	CPDM	1	CPDM	0.89	CPDM
CPDM12	CPDM	1	CPDM	0.83	CPDM
CPDM13	CPDM	1	CPDM	0.80	CPDM
CPDM14	CPDM	1	CPDM	0.78	CPDM
CPDM15	CPDM	1	CPDM	0.71	CPDM
CPDM16	CPDM	1	CPDM	0.89	CPDM
CPDM17	CPDM	1	CPDM	0.85	CPDM
WT9	WT	1	WT	0.65	WT
WT10	WT	1	WT	0.67	WT
WT11	WT	1	WT	0.64	WT
WT12	WT	1	WT	0.64	WT
WT13	WT	1	WT	0.68	WT
WT14	WT	1	WT	0.67	WT
WT15	WT	1	WT	0.66	WT
WT16	WT	1	WT	0.68	WT
WT17	WT	1	WT	0.71	WT
WT18	WT	1	WT	0.66	WT
WT19	WT	1	WT	0.69	WT

S5 Table. Class prediction by ROC curve selected FFA.

Class prediction of the validation set of samples by ROC based on potential FFA biomarkers.

New sample name	Real class	Random Forrest		PLS-DA	
		Probability	Predicted class	Probability	Predicted class
CPDM8	CPDM	1.00	CPDM	0.90	CPDM
CPDM9	CPDM	0.99	CPDM	0.71	CPDM
CPDM10	CPDM	1.00	CPDM	0.84	CPDM
CPDM11	CPDM	1.00	CPDM	0.87	CPDM
CPDM12	CPDM	1.00	CPDM	0.86	CPDM
CPDM13	CPDM	0.99	CPDM	0.87	CPDM
CPDM14	CPDM	1.00	CPDM	0.95	CPDM
CPDM15	CPDM	1.00	CPDM	0.95	CPDM
CPDM16	CPDM	1.00	CPDM	0.85	CPDM
CPDM17	CPDM	1.00	CPDM	0.88	CPDM
WT9	WT	0.68	WT	0.65	WT
WT10	WT	0.69	WT	0.62	WT
WT11	WT	0.66	WT	0.57	WT
WT12	WT	0.91	WT	0.65	WT
WT13	WT	0.65	WT	0.68	WT
WT14	WT	0.63	WT	0.67	WT
WT15	WT	0.51	WT	0.67	WT
WT16	WT	0.51	CPDM	0.57	CPDM
WT17	WT	0.67	WT	0.92	WT
WT18	WT	0.50	CPDM	0.68	WT
WT19	WT	0.58	WT	0.68	WT

CHAPTER 3. CHANGES IN EPIDERMAL LIPIDS DETECTED BY MULTIPLE-REACTION MONITORING PROFILING PREDICTS DERMATITIS PROGRESSION IN A MOUSE MODEL

3.1 Abstract

Skin is an essential organ that preserves the overall integrity of the mammalian body as it prevents water loss and penetration of pathogens, allergens, and chemicals. The maintenance of specific lipid content and composition is essential for proper epidermal barrier function. Furthermore, bioactive lipid molecules play major roles in cell signaling and activation. SHANK-associated RH domain interacting protein (SHARPIN)-deficient mice spontaneously develop chronic proliferative dermatitis (*cpdm*), a condition with similarities to atopic dermatitis in humans. To gain knowledge about changes in the epidermal lipid-content as the dermatitis develops and progresses, we tested 72 epidermis samples from three age groups corresponding to different stages of the disease of *cpdm* mice with dermatitis, and three corresponding groups of wild-type (control) animals. An agnostic (i.e. comprehensive and not dependent on database ID) mass-spectrometry strategy for biomarker discovery termed multiple-reaction monitoring (MRM)-profiling was used to detect and monitor 1030 lipid ions present in the epidermis samples. A two-tiered filter/wrapper feature-selection strategy was used to select the most relevant ions. First, we built 1030 analysis of variance (ANOVA) models linking the presence of every ion transition to disease stage information. After Benjamini-Hochberg p-value adjustment we selected only ions present in linear models connected significantly with the disease progression ($p < 0.001$), but not related to sex ($p > 0.05$). The ~50 ions selected represented η^2 effect sizes ranging from 0.724 to 0.29. In the second step, we used the reduced subset of ions to develop a predictive elastic-net (e-net) regression model linking the lipid ions identified by MRM-profiling with disease progression. The ions were ranked in terms of importance using the absolute value of the non-zero coefficients found in the tuned e-net model. The top 10 features were further compressed using parallel plot to classify individual samples into the disease stage groups. The developed model distinguished between the controls and *cpdm* mice samples. It also accurately identified the disease stages on the basis of variations in relative amounts of lipid ions corresponding to phosphatidylcholines, cholesterol esters, and glycerolipids-containing an eicosapentaenoic acid fatty acyl residue. MRM-

profiling paired with machine-learning identified predictive biomarkers of dermatitis in mice and may provide the basis for a molecular diagnostic approach to atopic dermatitis.

3.2 Introduction

Atopic dermatitis (AD) is a common chronic inflammatory skin disease associated with decreased barrier function and alterations in the lipid composition of the epidermis (1,2). Changes in ceramides with increasing hydroxylation and shorter fatty acids residues, as well as accumulating poly-unsaturated lipids are important in the impairment of the skin barrier function (3,4). Variation in ceramide structure and fatty acid chain length are usually accompanied by alterations in lipid processing enzymes involved in ceramide biosynthesis and fatty acid elongation such as β-glucocerebrosidase, acid-sphingomyelinase and ELOVL3 and 6, which are down-regulated by the type 2 cytokines IL-4 and IL-13 (5,6). Atopic dermatitis is characterized by a type 2 inflammatory response directed by Th2 CD4 T cells. The inflammation may induce or aggravate the skin barrier defect in atopic dermatitis patients. Alternatively, a primary defect in the lipid barrier may precede the dermatitis by allowing increased penetration of allergenic proteins. An immunologic basis for AD is supported by the efficacy of anti-IL4R monoclonal antibody treatment (7,8). However, changes in ceramides and fatty acids in non-affected skin from patients (9), beneficial effect of moisturizers on AD in high risk children (10), and the fact that the skin barrier abnormality returns after treatments are halted, challenge the sole immunological basis of the pathogenesis and suggest an underlying defect in lipid biosynthesis and barrier formation and maintenance (11,12).

In addition to their function as structural components of the lamellar matrix in skin, lipids perform critical roles in cell signaling, proliferation, differentiation and apoptosis (14). Glycerophospholipids in the cell membrane are reservoirs of polyunsaturated fatty acids (PUFAs) that produce lysophospholipids and bioactive long chain PUFAs after PLA_2 cleavage. Eicosanoids and specialized pro-resolution mediators are produced by cyclooxygenases (COX) and lipoxygenases (LOX) from cleaved PUFAs such as arachidonic acid (AA 20:4), eicosapentanoic acid (EPA 20:5) and docosahexaenoic acid (DHA 22:6) (15). Long chain PUFAs can interact with different cellular receptors like peroxisome proliferator-activated receptors (PPARs) which regulate lipid metabolism, promote keratinocyte terminal differentiation and antagonize pro-inflammatory transcription factors (16). Bioactive lipids can also modulate

immune cell polarization and the immune response by affecting the production of cytokines (17,18). This has been widely observed in obesity and cardiovascular disease as changes in lipid metabolism steer polarization of macrophages and T cells towards a pro-inflammatory phenotype (18). Oxidized phospholipids (oxPL) can be recognized as danger-associated molecular patterns (DAMPs) and cause inflammation (19,20). The oxPLs can be generated either by esterification of free eicosanoids or by direct oxidation of phospholipids (PL) in the cell membrane (21). Oxidized phospholipids in cell membranes can be externalized modifying the assembly of the lipid bilayer and enabling recognition by receptors like CD36 (22). Sphingomyelin (SM) can be transferred from the outer- to the inner-membrane and hydrolyzed to ceramides by the action of cellular stress activated-SMase during early apoptosis (23). Ceramides in turn contribute to apoptosis by increasing the permeability of the mitochondrial outer membrane, releasing cytochrome c and subsequently activating second mitochondria-derived activator of caspase (24). On the other hand, ceramide metabolites like ceramide-1-phosphate and sphingosine-1-phosphate inhibit inflammation and apoptosis by interfering with activation of nuclear factor kappa-light-chain-enhancer of activated B cells (NF-kB) induced by toll-like receptor (TLR)-4 or tumor necrosis factor (TNF)-α (16) illustrating how the chemical diversity of lipids accounts for an array of functional effects. As a result, dysregulation in lipid composition and metabolism has repercussions in health and disease. Sexual dimorphism in lipid metabolism may underlie differences between females and males in the clinical manifestation and incidence of cardiovascular disease, hepatic disease and obesity-related disorders (25,26). Women generally have more robust inflammatory reactions and immune responses than men and this is attributed to both sex hormones and sex-specific genetic factors (26,27). A recent study found atopic dermatitis to be more common in adult women than men (28). However, there is little information about differences between males and females in the lipid composition of the epidermis in healthy skin or dermatitis in humans or animals.

Attention towards the importance of lipids in chronic inflammation has increased in the past decade as new and improved lipidomic techniques have become available (29). Lipids are potentially valuable biomarkers as they represent the end point of metabolism and may be more representative of biological phenomena than transcriptomics and proteomics (30). In chapter 2, we identified specific changes in the ceramide and fatty acid composition in the epidermis of female SHANK-associated RH domain interacting protein (SHARPIN)-deficient mice with chronic

proliferative dermatitis (*cpdm*) using a novel accelerated lipidomics strategy, called MRM-profiling. The dermatitis in *cpdm* mice is very similar to AD in humans with pruritus, alopecia and thickening of the skin, as well as accumulation of eosinophils, mast cells, and type 2 macrophages, and increased expression of type 2 cytokines (31,32). Keratinocyte apoptosis is markedly increased in *cpdm* epidermis (33) similar to human AD (29,30). A recent report suggested that the expression of the SHARPIN protein was decreased in skin from AD patients (36). Lipidomics allows detection and identification of a large number of molecules in a high-throughput manner with possible identification of new biomarkers for diagnosis and disease progression as well as novel targets for treatment (30). However, these "-omics" approaches yield highly dimensional and complex data. This high dimensional and multicollinear data should not be analyzed solely based on univariate statistics because it may yield a high rate of possible false positive results and overfitting problems when classification and prediction is a goal. Instead, regularization should be incorporated into the analysis (37,38). Feature filtering and regularized classification and predictive algorithms, such as Elastic-net regularized regression, are useful tools for filtering the data and accurately identifying biomarkers amid the vast number of responses produced by systems biology methodologies (39–42).

In order to improve our understanding of lipid changes with disease progression in *cpdm* mice and to determine if sex had any influence on these alterations, we analyzed the lipid composition of epidermis from male and female *cpdm* mice at three disease stages and from age and sex-matched wild type (WT) littermates. These studies revealed that female and male mice had a distinct lipid profile and that sexual dimorphism was present in the lipid changes associated with disease progression. A subset of lipid ions predicted the disease stage of each of the samples independently of sex.

3.3 Materials and methods

3.3.1 Mice

72 female C57BL/KaLawRij-Sharpin^{cpdm}/Sharpin^{cpdm} RijSunJ (*cpdm*) mice and WT littermates were obtained and housed as described in Chapter 2. 18 WT males and 18 WT females and their *cpdm* littermates, were grouped into 3 different disease stages, including 6 males and 6

females per group. The disease stages corresponded to non-lesional (5 weeks of age), established (7 weeks), and advanced (10 weeks). Mice were euthanized as described (Chapter 2).

3.3.2 Sample preparation

Sample collection and lipid extraction were performed as described in Chapter 2. Briefly, skin was collected and after incubation with Thermolysin (from *Geobacillus stearothermophilus*, Sigma-Aldrich, St. Louis, MO) dissolved in HEPES buffer, the epidermis was peeled off and stored at -80°C until extraction. Tissue was weighted and homogenized in 250µL of ultra-pure water using Precellys24 tissue homogenizer (Bertin Technologies, Rockville, MD, USA). The homogenate was submitted to a Bligh and Dyer (43) liquid-liquid extraction and the organic phase was collected and dry in a concentrator. Samples were resuspended in 40µL of 3:1 (v/v) acetonitrile (ACN)/chloroform, then diluted 50X with ACN/methanol/ammonium acetate 300mM at 3:6.65:0.35 volume ratio and injected into the MS.

3.3.3 MRM-Profiling

Using our previously described methodology of MRM-profiling (chapter 2), we analyzed a composite sample of each group for the discovery experiments, directly delivering 8µL through a micro-autosampler (G1367A) into a QQQ6410 triple quadrupole mass spectrometer (Agilent Technologies, San Jose, CA) equipped with Jet Stream ESI ion source for each of the neutral loss (NL) and precursor ion (Prec) scans to profile phospholipids, acylcarnitines (AC), sulfatides, cholesterol esters (CE), ceramides, glycerolipids with diverse fatty acid acyl residues (DAG), triacylglycerides (TAG) and free fatty acids (FFA) in positive and negative ion modes. The 80 different discovery scans yielded 1811 lipid ions were collected and organized in 10 different methods of 3 minutes each. That means that each sample was flow injected 10 times to cover all the lipid ions due to the limited time (usually 1 minute) of signal generated by each flow injection.

Half of the samples from each group (n=36) were individually screened with the new 10 MRM methods and the previous methods from chapter 2, and these results will be referred as preliminary data. Normalized intensities by the total ion count were analyzed by univariate statistics to compared *cpdm* groups against WT at the different disease stages. 1030 lipid ions that resulted significantly different after t-test, volcano plots and ANOVA were selected and compiled into 6 MRM methods that were used to screen the totality of the samples. This step was performed

to remove noise and duplicate lipid ions. The raw data will be deposited at the public proteomics repository MassIVE. The tentative identification of lipid ions was performed as described in Chapter 2 through MS/MS experiments and by using reference databases.

3.3.4 Statistical analysis

The ion intensities were collected from the instrument raw data files as described in chapter 2. The *m/z* of the MRM methods were normalized by the total ion intensity to obtain relative amounts. Relative amounts were used to analyze the preliminary data organized in 6 experimental groups according to sex and disease stage using univariate statistics. Because the resulting data was heteroskedastic, data was subjected to generalized logarithm transformation and mean-centered and divided by the standard deviation of each variable to auto-scale it for univariate and multivariate statistical analysis. The significance of differences was determined at α=0.05 after false discovery rate correction for multiple comparisons.

In order to select the most predictive lipid ions, we applied a two-tiered filter/wrapper feature-selection strategy. First, 1030 ANOVA models linking the relative amounts of every lipid ion to disease stage information and sex were built. Benjamini-Hochberg p-value adjustment (44) was used to correct for false discovery and to identify the features that could predict disease progression either in sex-dependent or sex-independent manners by using $p < 0.001$ for the criteria that were included or $p > 0.05$ for the criteria that were ruled out. The lipids present in linear models connecting significantly with disease progression after Benjamini-Hochberg p-value adjustment ($p < 0.001$) and sex ($p < 0.05$) were selected as sex-dependent predictive lipids. The lipids significantly linked to disease stage but not related to sex ($p > 0.05$) were selected as sex-independent predictive lipids. About 50 ions were selected as predictive and represented η^2 effect sizes ranging from 0.724 to 0.29.

In the second step, we used an elastic-net (E-net) regression (45) as a multinomial classifier that includes a Lasso L_1 penalty term and a Ridge L_2 penalty term to reduce the high dimensionality of the data produced by the MRM-profiling.

$$\hat{\beta} = \underset{\beta}{\operatorname{argmin}}\left(\left\|y - X\beta\right\|^2 + \lambda\left((1-\alpha)\left\|\beta\right\|^2/2 + \alpha\left\|\beta\right\|_1\right)\right)$$

In the E-net formula above, the input X consists of all the pre-selected measured lipid ions and the output y describes the stage of the disease. The penalties included in the mathematical

model are on the $||\beta||_1$ term which generates a sparse model by shrinking some regression coefficients to zero and, on the $||\beta||^2$ term which removes the limitation on the number of selected variables but encourages grouping effect, allowing similar features to be selected together. The lipids with larger absolute value of β are considered to be more predictive.

The E-net introduced a second filter and ranked the lipid ions in term of importance using the absolute value of the non-zero coefficients. Subsequently, the top 10 lipid features with higher effect size were used to train the E-net regression using bootstrap and cross-validation procedures. For data visualization purposes the classification of the individual samples into the disease stages by the E-net was plotted using a parallel plot. For feature selection and e-net, the data was transformed using the hyperbolic arc-sine transformation and standardized to the female WT subgroup. Therefore, the y-axis in figures shows the difference in lipid abundance as the standard deviations away from the WT-female group.

The statistical analysis was performed using GraphPad Prism package, MetaboAnalyst 3.0 software (http://www. metaboanalyst.ca (46), JMP 13 from SAS Package, as well as the R-language for statistical computing.

3.4 Results

3.4.1 MRM-Profiling

A composite sample from each of the 12 groups (3 disease stages x 2 phenotypes x 2 sexes) was screened with 80 discovery scans. These resulted in detection of 1811 lipid ions which were organized in 10 MRM-methods and used to individually screen half of the samples (N=36; 9 males *cpdm*, 9 female *cpdm*, 9 male WT and 9 female WT). The results were analyzed by univariate statistics comparing the *cpdm* against the WT in each of the disease stage groups to select the transitions that were significantly different by t-test at $p<0.005$. In the positive ion mode, the main lipid classes represented by the altered lipids in *cpdm* were PCs, AC, sphingosine ceramides and glycerolipids containing linoleic acid. Twelve of these lipids were previously detected in the 8 week old female mice that were used for the analysis described in Chapter 2. Volcano plot analysis with $p<0.05$ and fold change of two performed on the samples separated by sex and disease stage showed that for the non-lesional stage, *cpdm* males had only one lipid ion significantly different from WT whereas females had 27. For the established stage group, six lipid ions were different in

cpdm males from WT, and eight lipid ions were different in *cpdm* females from WT, whereas 21 and 22 lipid ions were significantly different between *cpdm* and WT mice for females and males, respectively, in the advanced stage group (Figure 7).

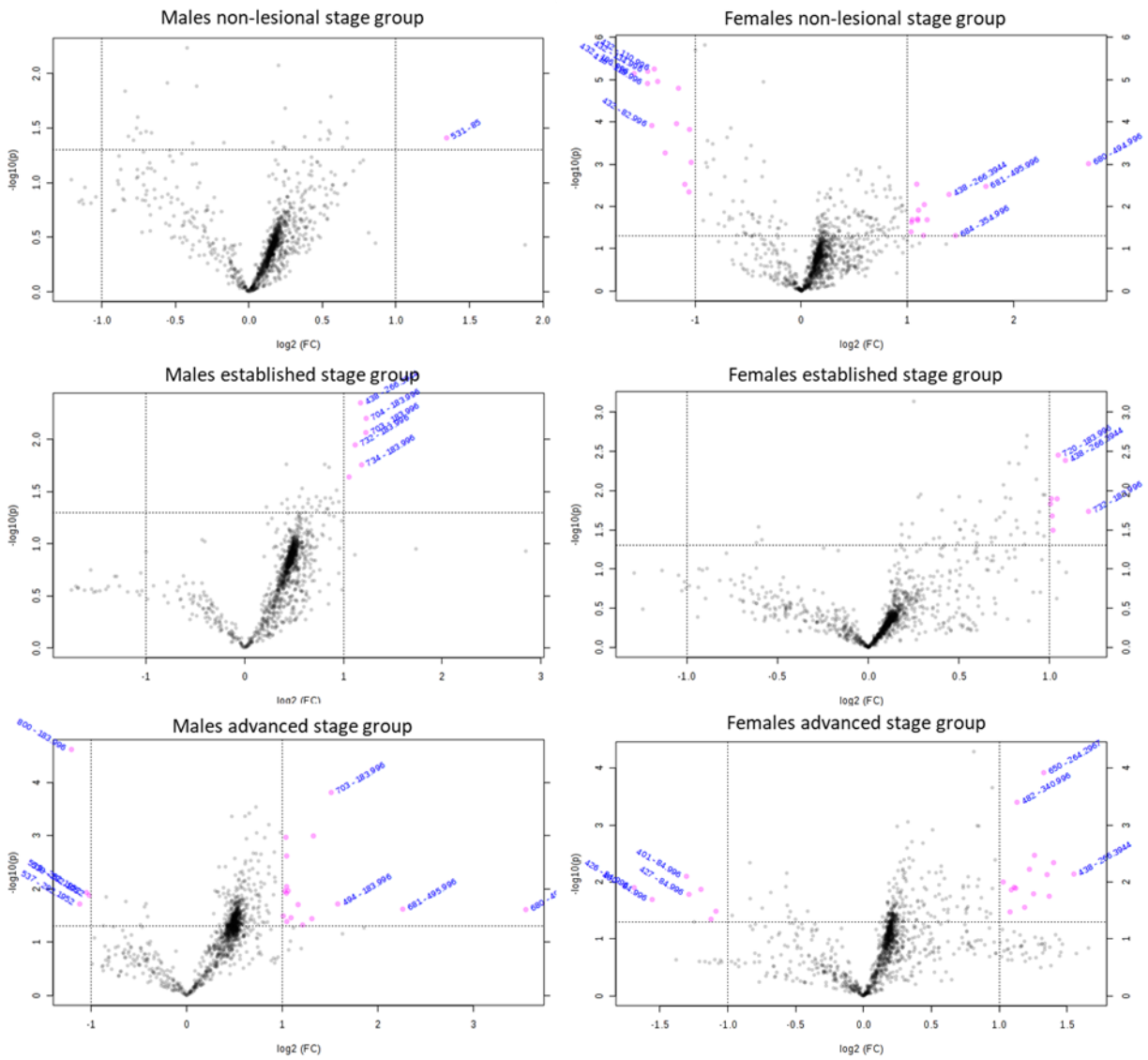

Figure 7**. Significantly different lipid ions in *cpdm* compared to WT from the preliminary analysis.** Samples were separated by sex and disease stage and analyzed by volcano plot with p<0.05 and FC=2 comparing *cpdm* vs WT. Significantly different lipid ions in the volcano plot are represented as pink circles and the most relevant ones are labeled.

The significantly different lipid ions were plotted in a Venn diagram to identify which were shared among the different experimental groups (Figure 8).

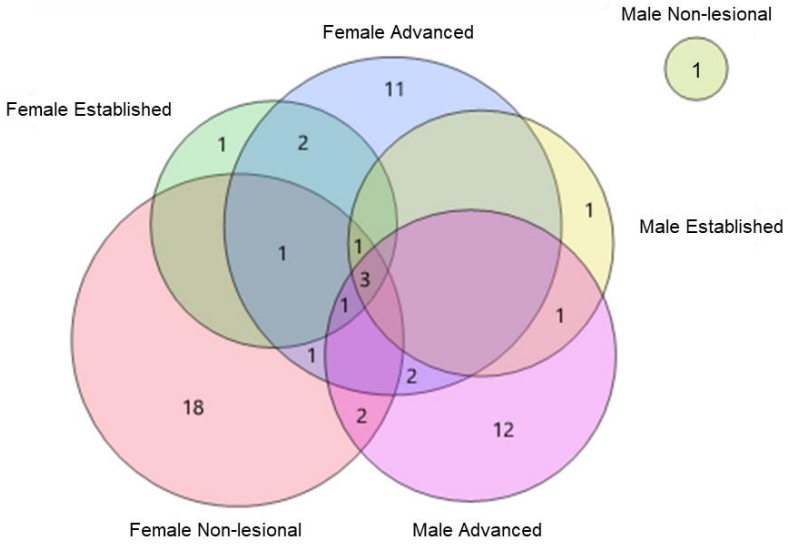

Figure 8**. Significantly different lipid ions by volcano plot in *cpdm* compared to WT from the preliminary MRM scans.** Samples were separated by sex and disease stage and analyzed by volcano plot with $p<0.05$ and FC=2 comparing *cpdm* vs WT. Significantly different lipid ions in the volcano plot were analyzed by Venn diagram to identify lipid ions that were shared by the different experimental groups. Two phosphatidylserine isomers were shared by the non-lesional female group and the advanced male group, two ceramides were shared by the advanced female and male groups, four phosphatidylcholine ions and one dihydroceramide ion were shade between most groups of males and all females. Female non-lesional: red circle; female established: green; female advanced: blue; male non-lesional: green-yellow; male established: yellow; male advanced: magenta

Six lipid ions were common to the three female groups, while four were shared among male groups of established and advanced disease. Phosphatidylcholine (PC) was the lipid class with most lipid ions changing across the experimental groups. Two phosphatidylserines were increased in the non-lesional female and in the advanced stage group of males. Interestingly, two ceramides previously detected to be increased in *cpdm* compared to WT were significantly increased only in males and females of the advanced stage groups. Individual *m/z* values of these lipids and the tentative attribution are listed in Table 2.

Table 2: List of significantly different lipid ions identified by Venn diagram to be present in males and females on the different disease stage groups.

Lipid class	MRM	Tentative attribution	Female non-lesional	Female established	Female advanced	Male non-lesional	Male established	Male advanced
Dihydroceramide	438 -> 266	Cer[DS](18:0/10:0)	X	X	X		X	X
Phosphatidylcholine	703 -> 184	SM(18:1/16:1)	X	X	X		X	X
Phosphatidylcholine	704 -> 184	PC(30:1)/ PC(P 31:0)/PKODA-PC	X	X	X		X	X
Phosphatidylcholine	732 -> 184	PC(32:1)/PC(P-33:0)/ PC(o-33:1)	X	X	X		X	
Phosphatidylcholine	494 -> 184	LCP(16:1)/PC(P-17:0)	X	X	X			X
Phosphatidylcholine	744 -> 184	PC(33:2)/ PC(O-34:2)/PC34:1)	X	X	X			
Phosphatidylcholine	733 -> 184	SM(18:0/18:0)	X		X			
Phosphatidylcholine	720 -> 184	PC(31:0)/ PC(O-32:0)/PKDdiA-PC		X	X			
Phosphatidylcholine	746 -> 184	PC(33:1)/ PC(O-34:1)/PC(P-34:0)/ OKDdiA-PC		X	X			
Phosphatidylserine	680 -> 495	PS(28:0)/ OHHdiA-PS	X					X
Phosphatidylserine	681 -> 496	Isomer of 680-495	X					X
Phosphatidylcholine	734 -> 184	PC(32:0)/PC(o-33:0)					X	X
Ceramide	538 -> 264	Cer[NS](d18:1/16:0)/ C34 Ceramide			X			X
Ceramide	650 -> 264	Cer[NS](d18:1/24:0) / C42 Ceramide			X			X

After univariate analysis, 1030 lipid ions were included in the final MRM-profiling method for individual screening of 72 samples collected and were compiled into 6 MRM-profiling methods and all samples were monitored (N=72, 36 *cpdm* and 36 WT). Samples were clearly differentiated by sex by compositional principal component (CPC) analysis, with the first component explaining 60% of the variability of the data while the disease stage explained 17% (Figure 9a). The list of lipid ions driving the separation of samples in the compositional PC score plot can be found in S6 Table of the supporting information. Cluster analysis revealed three different clusters of lipids. The first cluster had increased relative amounts of lipids in females versus males independently of the phenotype. The second cluster represents variations in the lipid content with an interaction between sex and phenotype as the decrease in lipid content in WT vs. *cpdm* was more significant in females compared to males. The opposite trend was observed in the last cluster which had increased relative amounts in *cpdm* compared to WT (Figure 9b).

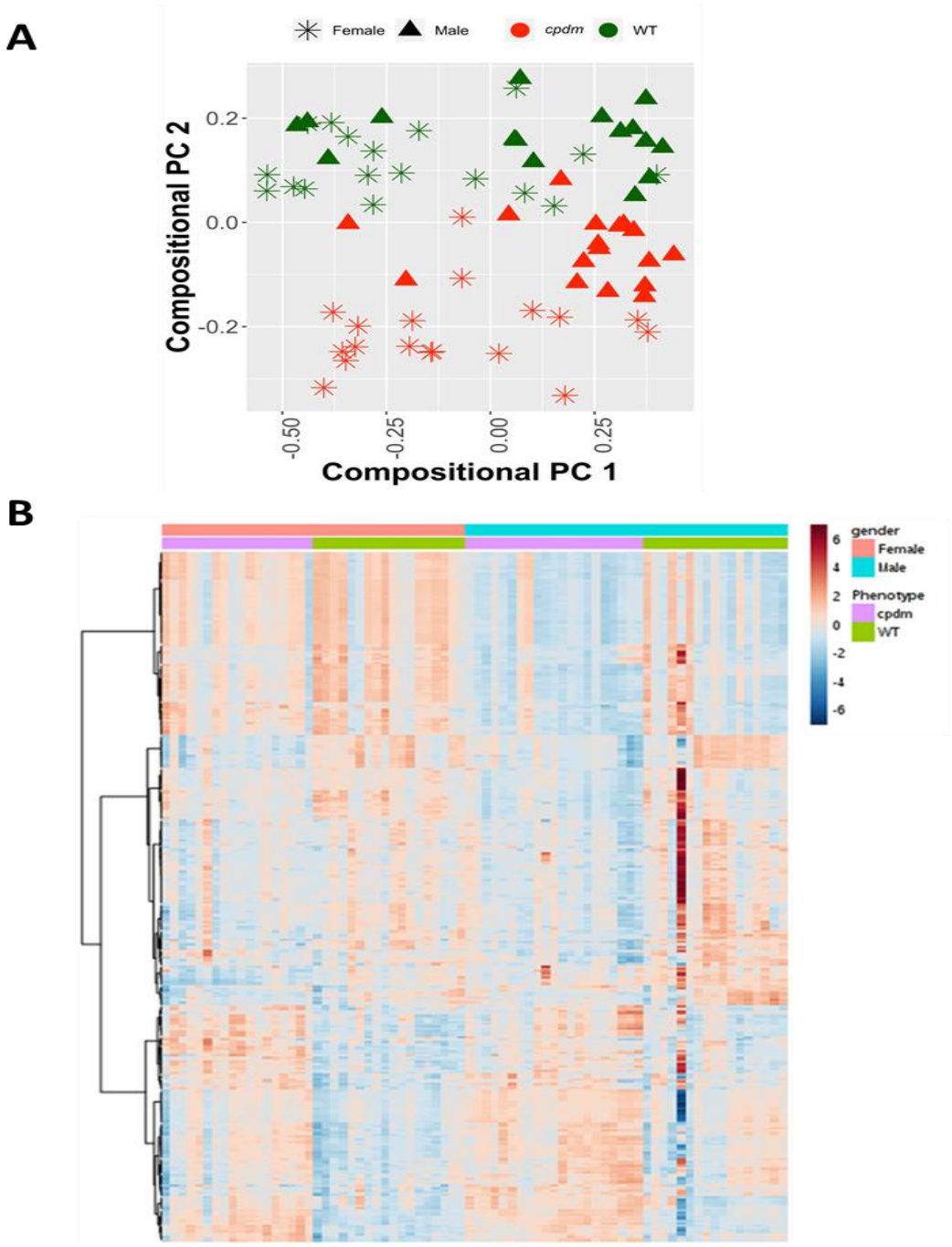

Figure 9**. Monitored lipid ions in male and female *cpdm* and WT epidermis by MRM scans in positive ion mode.** Discrimination of the sex as well as the phenotypes of WT and *cpdm* mice was observed by PCA and cluster analysis. (A) Score plot of principal component analysis (PCA). PC1 explained 60% of the variability of the data and was separating samples by sex. PC2 explained the differences of the phenotype by 16%. (B) Heat map with the distribution of lipids monitored individually in 72 samples. Color of each cell corresponds to the relative abundance of the lipid feature monitored in the sample

Fatty acids were analyzed in negative mode by single ion monitoring (SIM) as described in Chapter 2. Sex did not have a significant impact on the relative amounts of fatty acids, but disease progression was reflected in changes of certain fatty acids (Figure 10).

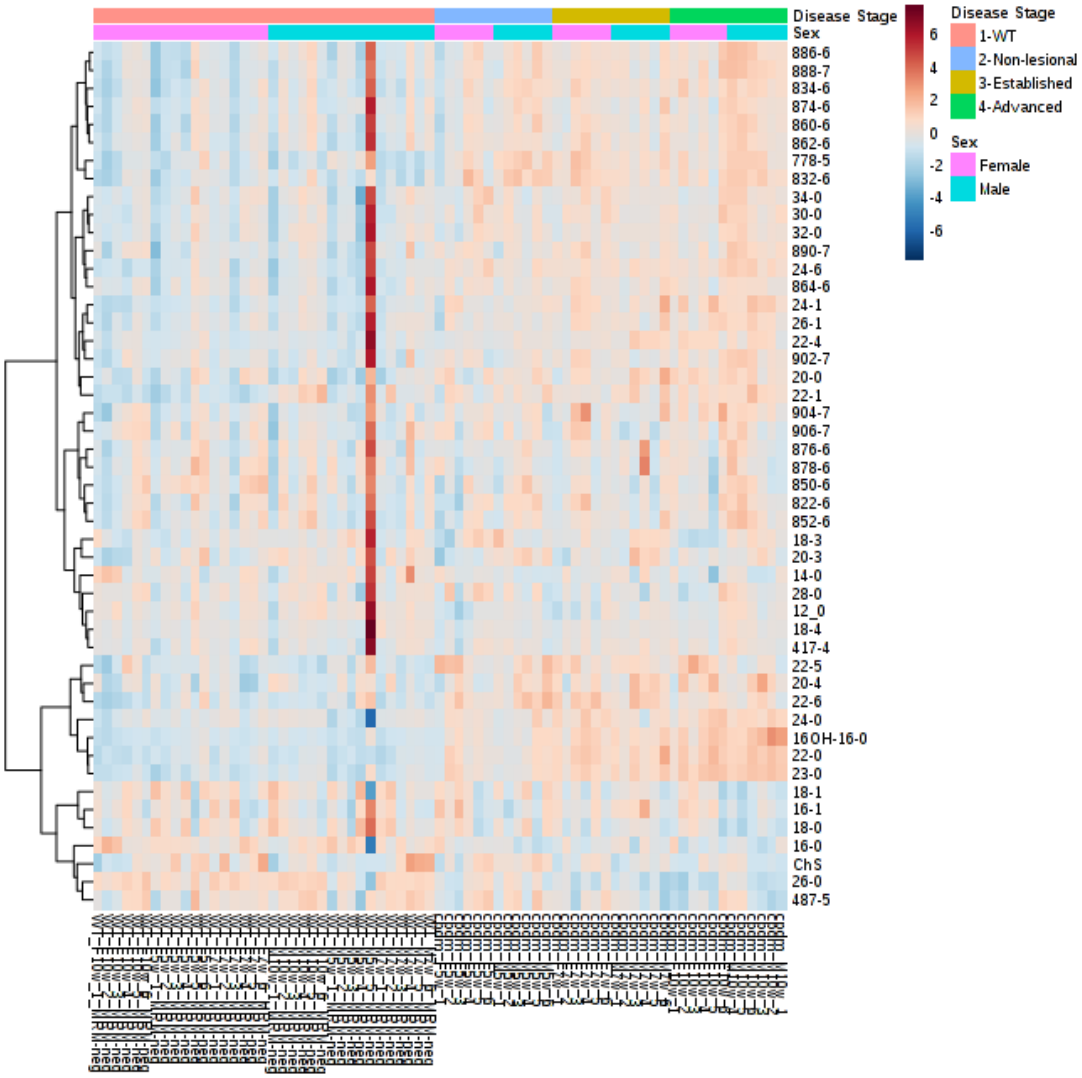

Figure 10**. Monitored lipid ions in male and female *cpdm* disease stages and WT epidermis by MRM scans in negative ion mode.** Cluster analysis did not showed discrimination of the samples by sex on free fatty acids analysis but changes over disease progression were observed. Heat map with the distribution of lipids monitored individually in negative ion mode in 72 samples. Lipids are shown with their *m/z*. Color of each cell corresponds to the relative abundance of the lipid feature monitored in the sample.

PUFAs 22:6 (DHA), 22:5 (DPA) and 24:6 were increased in *cpdm* skin compared to WT even on the non-lesional group but were not significantly different among the 3 disease stages ($p<0.05$). 20:4 (AA) seemed to be accumulating with disease progression as changes were significant only on the advanced group (Figure 11a). A similar trend was observed for saturated and mono-unsaturated fatty acids 20:0, 24:0 and 24:1 as these were significantly different from WT on the established and advanced groups but not the non-lesional group. However, this was not the case for 22:0 since the non-lesional group was significantly increased compared to WT and it was also significantly different from the advanced stage (Figure 11b). The relative amount of hydroxy-palmitic acid (16:0 OH) was increased at the early stage with further accumulation towards the advanced stage ($p<0.05$) (Figure 11c). Only a few lipid ions were reduced in epidermis of *cpdm* compared to WT. Ultra-long chain fatty 26:0 was significantly lower in *cpdm* compared to WT even in non-lesional skin ($p<0.05$). Palmitic acid 16:0 one of the most abundant fatty acids in cells decreased with disease progression as the established and the advanced groups were significantly lower than in WT (Figure 11d).

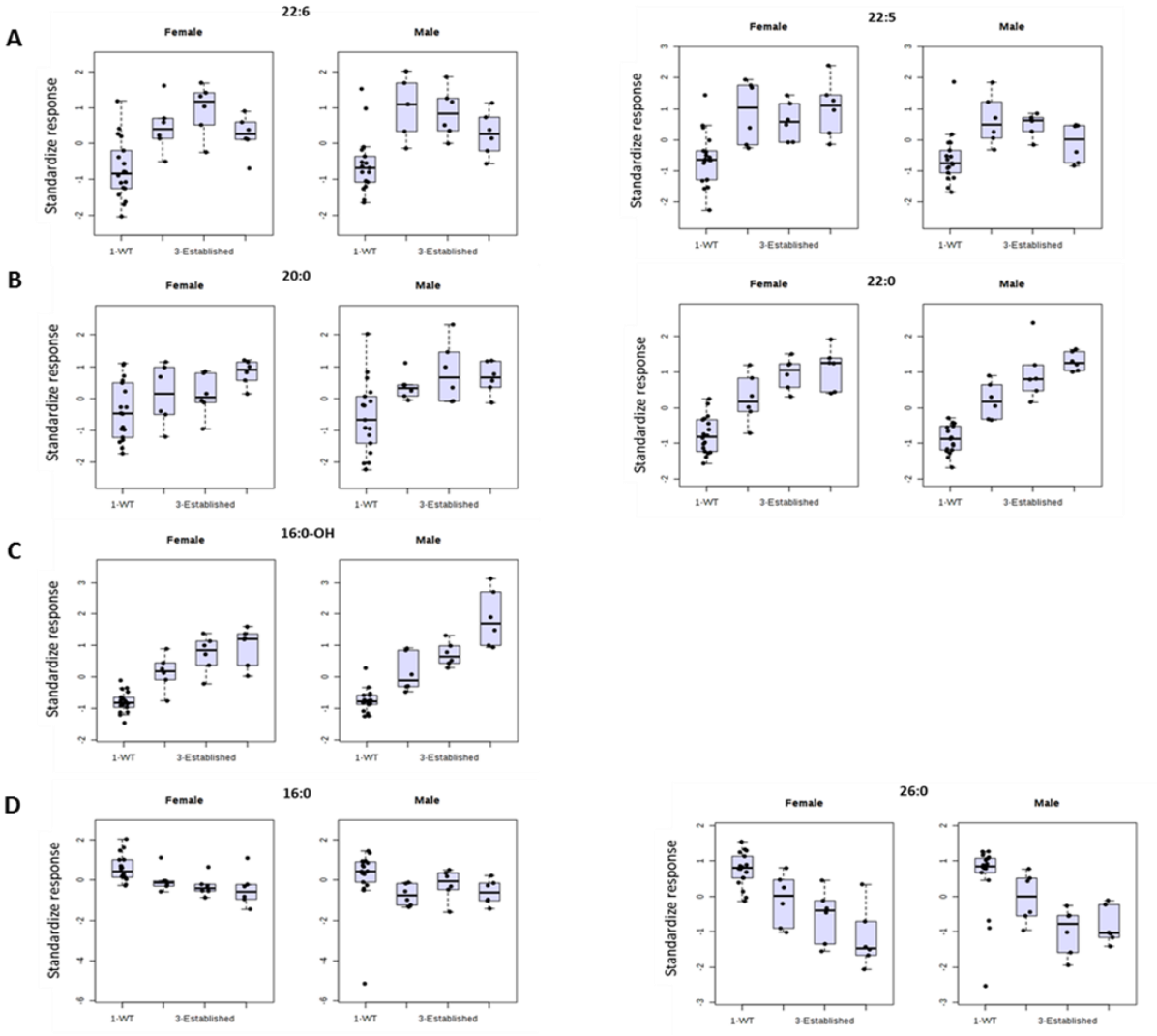

Figure 11. Relative amount of epidermal lipids significantly different in WT, non-lesional, established and advanced disease stage by ANOVA and Tukey test. Box Plots illustrates the similar trend in all females compare to males irrespective of the phenotype over disease progression. (A) Relative amounts of 22:6 and 22:5 were significantly different in non-lesional epidermis samples of cpdm mice compared to WT. Cpdm disease stages were not different from each other. (B) 20:0 relative amount was significantly different to the control on the established and advanced stages but not against non-lesional. Accumulation of 22:0 was increasing with disease severity. (C) hydroxy-palmitic acid (16:0 OH) was increased at the early stage with further accumulation towards the advanced stage (D) Ultra-long chain fatty 26:0 was significantly lower in *cpdm* compared to WT even in non-lesional skin. 16:0 was decreased in established and advanced disease stages compared to WT. The vertical axis represents the standardized relative amounts of lipids detected in the epidermis of *cpdm* and WT mice (horizontal axis). Box plots represent 72 samples from *cpdm* and WT. $p < 0.05$ based on ANOVA and Tukey posthoc with False Discovery Rate (FDR) correction for multiple comparisons. From left to right: WT, non-lesional, established and advanced groups.

3.4.2 Feature selection strategy

To further analyze the lipids in positive mode that were part of the clusters of sex influence, disease progression and their interaction, we carried out a two-step feature selection strategy where the first step was to create 1030 linear ANOVAs against sex and disease stage followed by a multinomial classifier E-net regression that incorporated a second step of feature selection.

3.4.2.1 Univariate analysis

First, we aimed to identify lipid features that were influenced by sex ($p<0.001$) but not by phenotype ($p>0.05$) after a Benjamini-Hochberg p-value adjustment by univariate analysis (S7 Table). We identified TAGs and DAGs as the main lipid classes that were significantly increased in females compared to males without being influenced by the phenotype, particularly glycerolipids containing oleic acid and palmitic acid in their aliphatic chains (Figure 12).

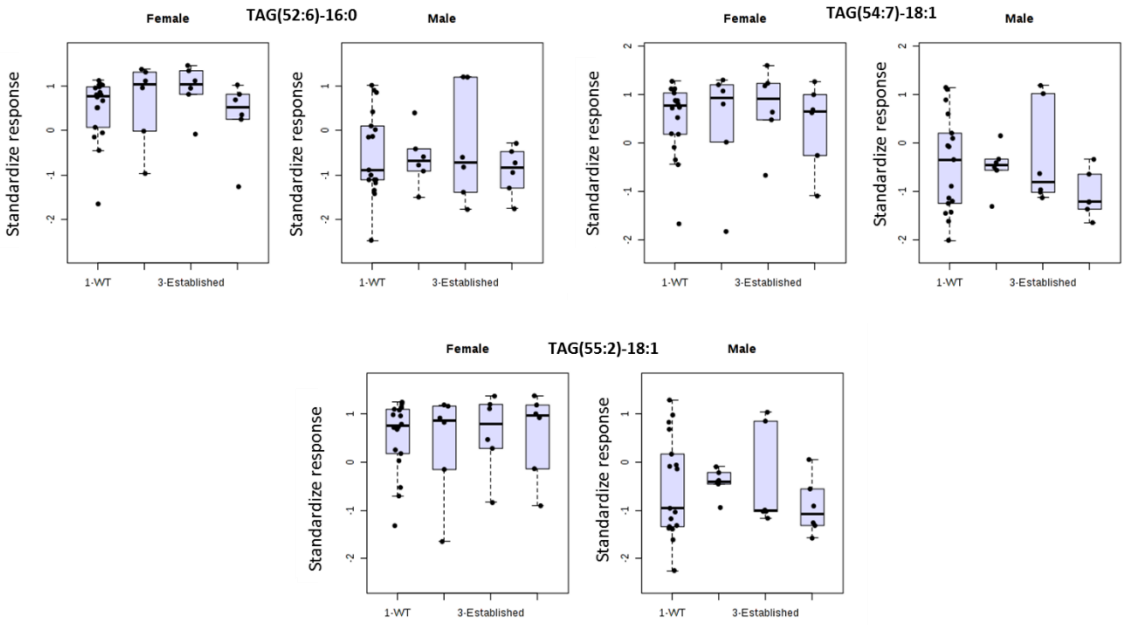

Figure 12**. Trend across disease stage of a set of three lipids influenced by sex but not phenotype.** Two-way ANOVA plot of TAGs containing oleic and palmitic acids in their aliphatic chains in the disease stages of *cpdm* and WT epidermis separated by sex ($p < 0.001$). Box Plots illustrates the similar trend in all females compare to males irrespective of the phenotype over disease progression. From left to right: WT, non-lesional, established and advanced groups.

Next, we applied a filter for sex-dependent features using $p < 0.001$ for disease stage and $p < 0.05$ for sex (S8 Table). Lipid ions were selected according to the interaction score of η^2 and the resulting top predictive lipid features belonged mostly to the sphingosine ceramide class. Female *cpdm* had increased relative amounts of sphingosine ceramides with hydroxylated acyl-chains compared to female WT, such as CerAS(d18:1/24:0)OH and CerAS(d18:1/26:0)OH, which in turn were greater compared to males (Figure 13A). On the contrary, phytosphingosine ceramides like CerNP(t18:0/16:0) were reduced in *cpdm* epidermis, replicating the findings of our previous results in females, but in males the reduction was not as striking (Figure 13B). The relative abundance of AC(20:0) was increased with a larger accumulation in the epidermis of female *cpdm* mice than males (Figure 13c).

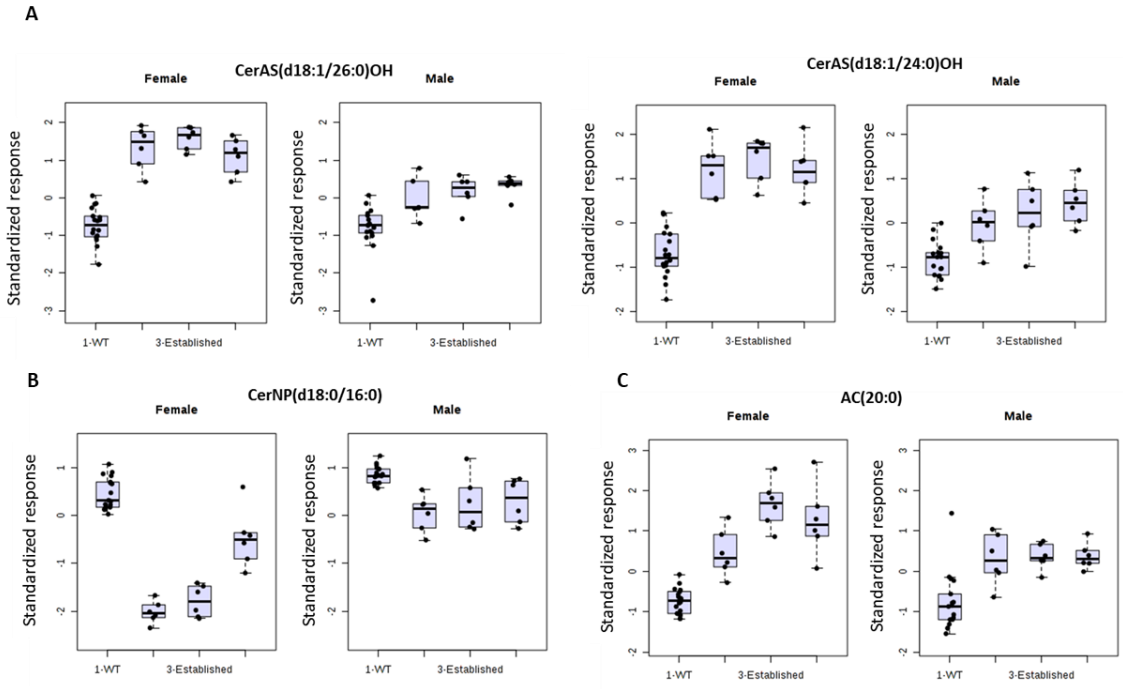

Figure 13**. Trends across disease stage of a set of three sex-dependent lipids.** Two-way ANOVA plot of ceramides and acyl-carnitine in males and females epidermis across disease stages ($p < 0.001$ for sex and $p < 0.05$ disease stage). Box plots show different behavior of the lipid trend as the disease progresses in males and females. WT males and females lipid relative amounts are comparable but in male and female *cpdm* they change differently on the 3 disease stage groups. Sphingosine ceramides in *cpdm* female mice are more increased than in the males, although for the first ones there is no evidence of variations through the progression, in the males an upward trend is observed. Conversely, the ceramides with a base of phytoshingosine are reduced in the epidermis of the *cpdm* and this reduction is more profound in the females than in the males. Acylcarnitine is more increased in *cpdm* females than in males and in the latter there is no tendency to increase with the development of the disease. From left to right: WT, non-lesional, established and advanced groups.

Subsequently, we filtered for features that were predictive of the disease progression independent of sex using $p < 0.001$ for disease stage and not significant for sex ($p>0.05$). Approximately, 50 lipid ions, mostly PCs, were selected and ranked by the η^2, which ranged from 0.7 to 0.29.

3.4.2.2 Elastic-net regression predictive model

The second filtering step included an E-NET regression to reduce dimensionality and to rank the lipids that were pre-selected as not significant for sex but with the highest η^2 for disease stage, from the most to the least predictive. The algorithm incorporated a penalty to keep the final number of selected lipids as small as possible by eliminating the β coefficients close to 0 but keeping similar features that contributed to the prediction capability of the model by encouraging a grouping effect.

The proportions of the top ten lipid features selected by the predictive E-NET are listed in Table 3 and include PC, AC and DAG-containing a 20:5 fatty acid residue. Among the PC, some were tentatively attributed as oxidized phospholipids which were accumulating in *cpdm* epidermis compared to WT (Figure 14).

The selected lipids were used to train the predictive E-NET (Table 3).

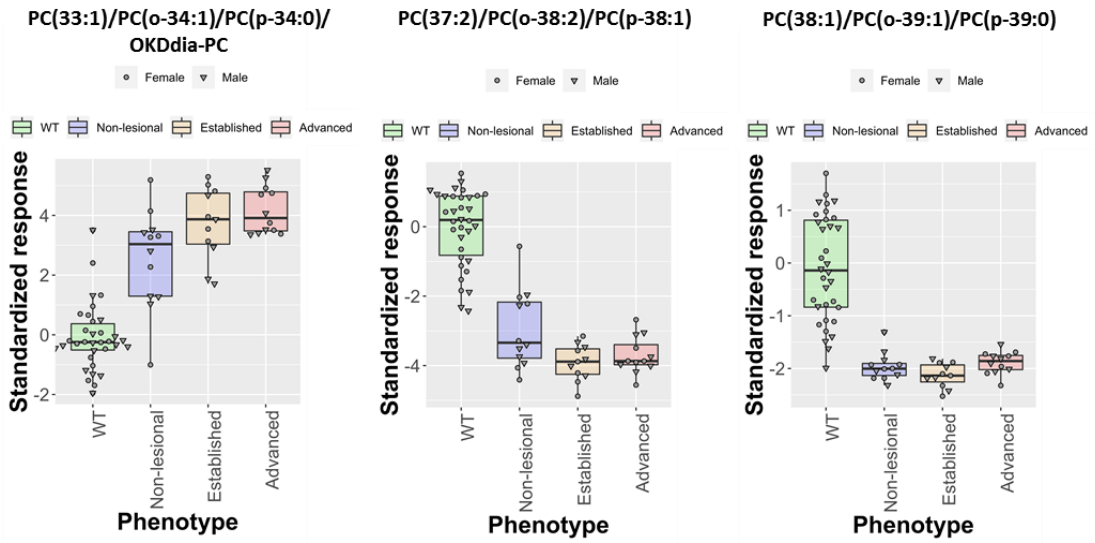

Figure 14**. Epidermal lipids predictive of disease progression in mice**. Representation of three lipids from the epidermis of WT and *cpdm* mice identified as predictive of disease stage in a sex-independent manner. Lipid features emphasize differences between controls and the diseased phenotype with medium to large effect size. Box-plots represent each of the 72 samples screened individually by the MRM-profiling method. Effect size is expressed as η^2 and represents the size of the difference between groups ($\eta^2 < 0.29$).

Table 3. List of top lipid ions identified by elastic net regression to be predictive of disease stage independent of sex.

Lipid class	MRM	Tentative attribution
Phosphatidylcholine	732 -> 184	PC(32:1)/PC(P-33:0)/PC(o-33:1)
Sphingomyelin	733 -> 184	SM(18:0/18:0) (Possible isomer of 732-184)
Sphingomyelin	745 -> 184	SM(18:1/19:0) /SM(19:0/18:1)
Phosphatidylcholine	746 -> 184	PC(33:1)/PC(O-34:1)/PC(P-34:0)/OKDdiA-PC
Phosphatidylcholine	800 -> 184	PC(37:2)/PC(O-38:2)/PC(P-38:1)
Sphingomyelin	801 -> 184	SM(16:1/25:0)/SM(18:1/23:0) (Possible isomer of 800-184)
Phosphatidylcholine	816 -> 184	PC(38:4)/PC(O-39:1)/PC(P-39:0)
Cholesterol ester	725 -> 369	CE(22:1)+NH4
glycerolipids containing 18:1 residue	627 -> 279	DAG(37:6)
Acylcarnitine	398 -> 85	AC(16:1)
Sphingomyelin	811 -> 184	SM(18:2/24:1)

These features were plotted versus the disease progression in a CPC plot showing that the model was able to delineate the controls and the three experimental groups of *cpdm* mice with 50.4% of explained variance by PC1 and 15.8% by PC2 (Figure 15). However, the discrimination was not as clear as the observed in chapter 2 for the all-female 8 weeks old mice that had an established inflammation process.

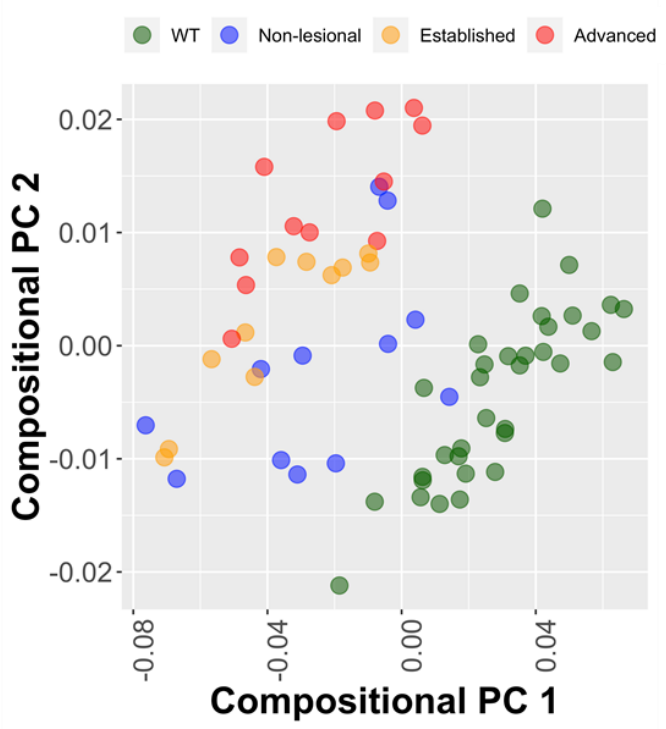

Figure 15**. E-net selected lipids delineate the disease stage groups by CPC.** The top 10 lipid features selected were compressed using compositional principal component analysis and plotted versus the disease progression. The model was able to delineate the controls and the three experimental groups of *cpdm* mice with 50.4% of explained variance by PC1 and 15.8% by PC2. Circles represent each of the 72 samples screened individually by the MRM-profiling method in relative amounts.

In order to assess the predictive capability of the selected lipid panel, we moved from unsupervised learning to a supervised learning. The proportions of the top ten lipid features selected were used to train the predictive E-NET by bootstrap and cross-validation. The composite result of the training operations is illustrated by a parallel plot where each line represents an individual sample and the highest point of the line indicates the group where would be classified

with higher probability (Figure 16). Samples were individually classified into groups including the control and the 3 disease stages with an overall accuracy of 0.90 (95% CI:0.86, 0.93) based on the proportions of the relative amounts of lipid features corresponding to PC, SM, CE, and glycerolipids-containing eicosapentaenoic acid fatty acyl residue form the epidermis of the mice.

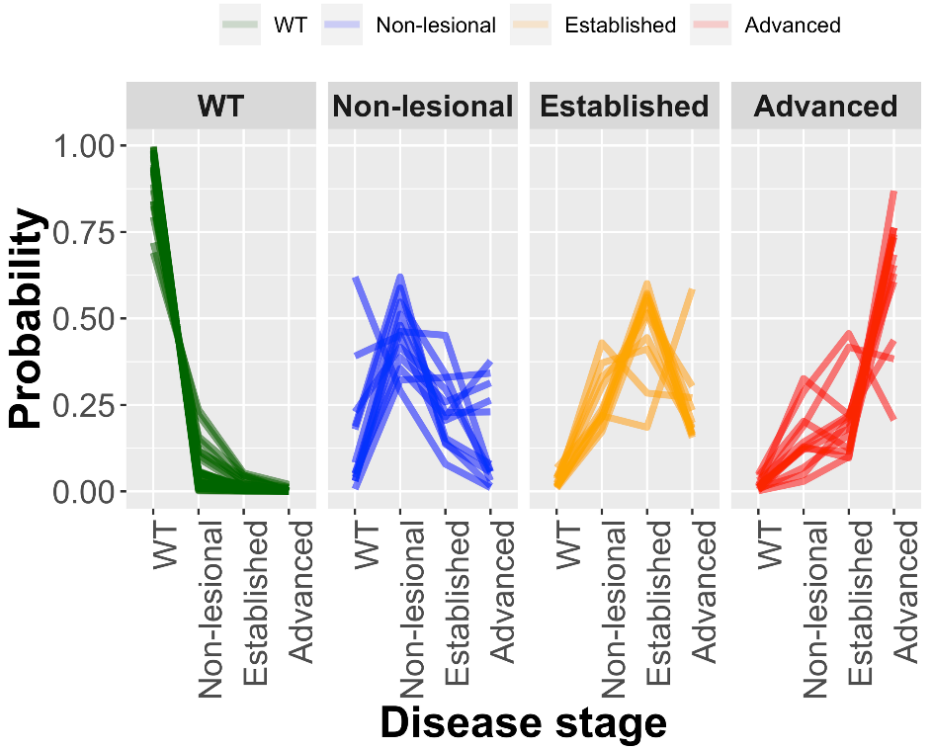

Figure 16**: Classification of samples into disease progression groups.** Parallel plot illustrating classification of individual samples by elastic net regression. Each line represents a sample and the highest point in the line corresponds to the group where the sample would be classified with higher probability. 36 *cpdm* and the 36 WT mice samples were classified into groups including the control and the 3 disease stages with an overall accuracy of 0.90 (95% CI:0.86, 0.93) on the basis of the variations in proportions of the relative amounts of lipid features corresponding to phosphatidylcholines, cholesterol esters, and glycerolipids-containing eicosapentaenoic acid fatty acyl residue.

3.5 Discussion

Lipids play an important role in the biology of the skin. The lipid fingerprint of the epidermis clearly separated male and female samples indicating a strong influence of sex on the relative amounts of lipids present in the epidermis of the mice. The sex effect was greater than the effect of the phenotype in agreement with studies of skin-surface lipid clusters in humans where samples from males and females were differentiated without observing a significant difference between atopic or healthy subjects (47,48).

Triacylglycerides dominated the cluster of lipids that delineated sex in a dermatitis-independent fashion. The epidermis from female mice had more TAGs containing oleic acid and palmitic acid compared with males. Different results were reported for human skin lipids from AD patients in which wax esters and TAGs were increased in males compare with females (48). In addition to species differences, differences in sample preparation (epidermis vs. total skin) and analytical methods may account for these disparate results.

Lipids that clustered as dermatitis- and sex-dependent included AC and ceramides. Increased relative abundance of AC (20:0) was observed with a larger accumulation in the epidermis of female *cpdm* mice than males. Sexual dimorphism of AC is organ specific and dependent on chain length and degree of saturation (49). Disruption in lipid β-oxidation and sugar metabolism with subsequent accumulation of AC takes place in AD (50,51) and, accumulation of AC can in turn interfere with insulin signaling and activate pro-inflammatory signaling pathways (52). The biological function of sphingolipids is determined by its composition, particularly the type of sphingoid base and the number of carbons and hydroxyl groups on the acyl chains. Sphingosine ceramides with hydroxylated acyl-chains of 24 (Cer[AS](d18:1/24:0)OH) and 26 (Cer[AS](d18:1/26:0)OH) carbons were increased in *cpdm* while saturated phytosphingosine ceramide with 16 (Cer[NP](t18:0/16:0) carbons was decreased in *cpdm* compared with WT. Changes in these ceramides were also influenced by sex as they were smaller, but still significant, in male mice than in females. Ceramides are increased in sebum of female atopic dermatitis patients compared with males (47) and their synthesis is affected by gonadal hormones in mice (25). These results confirm our previous findings of increased hydroxylated 16 – 24 carbon chain length ceramides in *cpdm* epidermis along with the corresponding free fatty acids necessary to acylate the sphingolipid base. This is consistent with a common synthetic pathway for ceramides and FFA (53). The relative amounts of Cer[NS](d18:1/16:0) and Cer[NS](d18:1/24:0) were

increased in both males and females, but only when the disease was advanced. Conflicting results on changes in ceramides in non-lesional skin of AD patients (54) may be due to the fact that not all ceramide species are altered at the same stage of the disease and/or by the same mechanisms. Further research is necessary to determine why some ceramides can be restored by emollients or systemic treatments (8,12). The above results show that sexual dimorphism can influence the relative amounts of a subset of epidermal lipids in mice. Sexual dimorphism in the lipid biology of AD should be further investigated as it could be related to the higher prevalence of AD in women particularly after puberty (55).

Alteration in the lipid composition of the epidermis is a hallmark of AD associated with impaired barrier function of the skin (1). However, it is still uncertain if these changes are primary or caused by the inflammatory process. Comparison of the disease stages versus the healthy control showed that, independently of sex, alterations in the lipid profile of the epidermis were present before any clinical signs and lipids predictive of disease progression could be identified by E-net regression model. These filtered predictive sex-independent lipids corresponded to PC, DAG, and CE, all of which can carry esterified fatty acids that generate lipid mediators of inflammation by undergoing fatty acyl remodeling (14). PL are important for cellular and subcellular membrane dynamics and can be secreted in the lamellar bodies of the epidermis along with the enzymes that use them as a substrate for ceramide synthesis (56). Alterations in their concentrations can affect skin barrier function, cell metabolism and inflammatory cell signaling. Alterations in lipid ratios in the cell membrane can cause externalization of PS, which is recognized by innate immune cells as an early indicator of apoptosis (57). Also, it is possible that lipids resulting of an aberrant lipid metabolism are incorporated into membranes (14,58). Oxidation of PL in cell membranes alters the bilayer conformation protruding the oxidized residues towards the aqueous compartment (59). OxPL can be recognized by macrophage pattern recognition receptors (PRRs) and promote phagocytosis (22,60). Hydroxylated fatty acids incorporated in membranes interfere with normal formation of rafts and function of membrane receptor activity (58). They are linked to induction of apoptosis in a caspase-dependent manner (61) that is responsive to the concentration and time of exposure of cells (62). However, the appropriate balance of lipids can inhibit the pro-apoptotic effect of hydroxylated fatty acids (63). Hydroxylated ceramides can also induce apoptosis, and they accumulate after the onset and sustain the apoptotic process (23). The changes in the lipid composition of the *cpdm* epidermis with an increased relative amount of hydroxylated palmitic

acid (16:0-OH) in *cpdm* mice could contribute to the increased apoptotic rate of *cpdm* keratinocytes (33).

Impaired beta-oxidation may occur in AD and cause increasing concentrations of 16:0-OH, as well as saturated and unsaturated very long fatty acids (50,51). Saturated and polyunsaturated very-long chain fatty acids (VLCFA), as well as products of CYP4A ω-hydroxylases and plasmalogens can undergo peroxisomal β-oxidation as very-long chain acyl-CoA synthase and acyl-CoA oxidase (ACOX1), the rate limiting enzymes required for these type of lipids, are only present in peroxisomes (64). In flaky tail mice, a model for AD, the number of peroxisomes was increased in the epidermis and mRNA levels of epidermal fatty acid binding protein 5 (FABP5) and acyl-CoA oxidase 1 (ACOX1) were increased compared to control mice resulting in increased concentration of VLCFA in epidermis (65). FABP5 is an intracellular lipid chaperone that can promote the production of IL-1β and IL-18 from macrophages in response to high levels of saturated fatty acids by coupling Nucleotide-Binding Oligomerization Domain, Leucine Rich Repeat And Pyrin Domain Containing 3 (NLRP3)- apoptosis-associated speck-like protein containing C-terminal caspase recruitment domain/caspase-1 (ASC) with lipid droplets inside these cells (66). In preliminary proteomics studies of *cpdm* epidermis, FABP5 was considerably increased compared to WT, suggesting a possible role in the *cpdm* dermatitis.

The fact that the lipid profile from the *cpdm* epidermis was altered before clinical signs and that the lipid variations reflected the disease stages allowed us to identify potential biomarkers for diagnosis and disease progression using E-net. The classification algorithm trained with the selected predictive lipids was able to discriminate the samples with a high accuracy and confidence. The reproducibility of the results between these analyses and those reported in Chapter 2, along with the capacity to detect subtle changes in the relative amounts of epidermal lipids from non-lesional skin, support the use of MRM-profiling as a fast and robust analytical method to determine the lipid fingerprint of dermatitis. Furthermore, pairing the high-throughput MS analysis with the feature selection strategy provided us with a potential tool to classify epidermal samples in dermatitis with a high confidence level.

In summary, changes in epidermal lipids in SHARPIN-deficient *cpdm* mice, a mouse model of intrinsic AD (31,32), are similar to those observed in human AD patients. Here, we show that alterations in the epidermal lipid composition of *cpdm* mice are detectable before the onset of clinical and histological inflammation and that clusters of lipids changed with progression of the

dermatitis. Sex-specific differences were identified in the lipid fingerprint of the epidermis and sexual dimorphism was evident in the lipid alterations in *cpdm* dermatitis. MRM-profiling paired with machine learning identified sex-dependent and –independent changes in the lipid profile associated with increasing severity of the dermatitis and accurately classified the epidermal samples into disease stages categories.

3.6 References

1. Elias PM. Lipid abnormalities and lipid-based repair strategies in atopic dermatitis. Biochim Biophys Acta - Mol Cell Biol Lipids. 2014;1841(3):323–30.
2. De Benedetto A, Kubo A, Beck LA. Skin barrier disruption: A requirement for allergen sensitization. J Invest Dermatol. 2012;132(3 PART 2):949–63.
3. Janssens M, van Smeden J, Gooris GS, Bras W, Portale G, Caspers PJ, et al. Increase in short-chain ceramides correlates with an altered lipid organization and decreased barrier function in atopic eczema patients. J Lipid Res. 2012;53(12):2755–66.
4. van Smeden J, Janssens M, Gooris GS, Bouwstra JA. The important role of stratum corneum lipids for the cutaneous barrier function. Biochim Biophys Acta - Mol Cell Biol Lipids. 2014;1841(3):295–313.
5. Danso MMO, Boiten W, van Drongelen V, Gmelig KM, Gooris G, El Ghalbzouri A, et al. Altered expression of epidermal lipid bio-synthesis enzymes in atopic dermatitis skin is accompanied by changes in stratum corneum lipid composition. J Dermatol Sci. 2017;88(1):57–66.
6. Berdyshev E, Goleva E, Bronova I, Dyjack N, Rios C, Jung J, et al. Lipid abnormalities in atopic skin are driven by type 2 cytokines. JCI insight. 2018;3(4):1–15.
7. Brunner PM, Guttman-Yassky E, Leung DYM. The immunology of atopic dermatitis and its reversibility with broad-spectrum and targeted therapies. J Allergy Clin Immunol. 2017;139(4):S65–76.
8. Hamilton JD, Suárez-Fariñas M, Dhingra N, Cardinale I, Li X, Kostic A, et al. Dupilumab improves the molecular signature in skin of patients with moderate-to-severe atopic dermatitis. J Allergy Clin Immunol. 2014;134(6):1293–300.

9. Joo K-M, Hwang J-H, Bae S, Nahm D-H, Park H-S, Ye Y-M, et al. Relationship of ceramide–, and free fatty acid–cholesterol ratios in the stratum corneum with skin barrier function of normal, atopic dermatitis lesional and non-lesional skins. J Dermatol Sci. 2015;77(1):71–4.

10. Simpson EL, Chalmers JR, Hanifin JM, Thomas KS, Cork MJ, McLean WHI, et al. Emollient enhancement of the skin barrier from birth offers effective atopic dermatitis prevention. J Allergy Clin Immunol. 2014;134(4):818–23.

11. Holm JG, Agner T, Clausen M-L, Thomsen SF. Determinants of disease severity among patients with atopic dermatitis: association with components of the atopic march. Arch Dermatol Res. 2019;0(0):0.

12. Elias PM. Primary role of barrier dysfunction in the pathogenesis of atopic dermatitis. Exp Dermatol. 2018;27(8):847–51.

13. Ardern-Jones MR. Characterisation of atopic dermatitis (AD) endotypes and novel treatment targets: towards a molecular classification. Exp Dermatol. 2018;27(4):433–4.

14. Han X. Lipidomics for studying metabolism. Nat Rev Endocrinol. 2016;12(11):668–79.

15. Ilic D, Bollinger JM, Gelb M, Mauro TM. SPLA2 and the epidermal barrier. Biochim Biophys Acta - Mol Cell Biol Lipids. 2014;1841(3):416–21.

16. Jia Y, Gan Y, He C, Chen Z, Zhou C. The mechanism of skin lipids influencing skin status. J Dermatol Sci. 2018;89(2):112–9.

17. Tetsuya H, Kenji K. Prostanoids and leukotrienes in the pathophysiology of atopic dermatitis and psoriasis. Int Immunol. 2019:1–7.

18. Hubler MJ, Kennedy AJ. Role of lipids in the metabolism and activation of immune cells. J Nutr Biochem. 2016;34(3):1–7.

19. Weismann D, Binder CJ. The innate immune response to products of phospholipid peroxidation. Biochim Biophys Acta - Biomembr. 2012;1818(10):2465–75.

20. O'Donnell VB, Murphy RC. New families of bioactive oxidized phospholipids generated by immune cells: Identification and signaling actions. Blood. 2012;120(10):1985–92.

21. Hammond VJ, O'Donnell VB. Esterified eicosanoids: Generation, characterization and function. Biochim Biophys Acta - Biomembr. 2012;1818(10):2403–12.

22. Hazen SL. Oxidized Phospholipids as Endogenous Pattern Recognition Ligands in Innate Immunity. J Biol Chem. 2008;283(23):15527–31.

23. Andrieu-Abadie N, Levade T. Sphingomyelin hydrolysis during apoptosis. Biochim Biophys Acta - Mol Cell Biol Lipids. 2002;1585(2–3):126–34.

24. Lizardo DY, Parisi LR, Li N, Atilla-Gokcumen GE. Noncanonical Roles of Lipids in Different Cellular Fates. Biochemistry. 2018;57(1):22–9.

25. Norheim F, Bjellaas T, Hui ST, Chella Krishnan K, Lee J, Gupta S, et al. Genetic, dietary, and sex-specific regulation of hepatic ceramides and the relationship between hepatic ceramides and IR. J Lipid Res. 2018;59(7):1164–74.

26. Zore T, Palafox M, Reue K. Sex differences in obesity, lipid metabolism, and inflammation—A role for the sex chromosomes? Mol Metab. 2018;15:35–44.

27. Klein SL, Flanagan KL. Sex differences in immune responses. Nat Rev Immunol. 2016;16(10):626–38.

28. Barbarot S, Auziere S, Gadkari A, Girolomoni G, Puig L, Simpson EL, et al. Epidemiology of atopic dermatitis in adults: Results from an international survey. Allergy Eur J Allergy Clin Immunol. 2018;73(6):1284–93.

29. Lam SM, Shui G. Lipidomics as a Principal Tool for Advancing Biomedical Research. J Genet Genomics. 2013;40(8):375–90.

30. Stephenson DJ, Hoeferlin LA, Chalfant CE. Lipidomics in translational research and the clinical significance of lipid-based biomarkers. Transl Res. 2017;189:13–29.

31. HogenEsch H, Torregrosa SE, Boggess D, Sundberg BA, Carroll J, Sundberg JP. Increased expression of type 2 cytokines in chronic proliferative dermatitis (cpdm) mutant mice and resolution of inflammation following treatment with IL-12. Eur J Immunol. 2001;31(3):734–42.

32. HogenEsch H, Dunham A, Seymour R, Renninger M, Sundberg JP. Expression of chitinase-like proteins in the skin of chronic proliferative dermatitis (cpdm/cpdm) mice. Exp Dermatol. 2006;15(10):808–14.

33. Liang Y, Sundberg JP. SHARPIN regulates mitochondria-dependent apoptosis in keratinocytes. J Dermatol Sci. 2011;63(3):148–53.

34. Rebane A, Zimmermann M, Aab A, Baurecht H, Koreck A, Karelson M, et al. Mechanisms of IFN-γ–induced apoptosis of human skin keratinocytes in patients with atopic dermatitis. J Allergy Clin Immunol. 2012;129(5):1297–306.

35. Trautmann A, Akdis M, Klunker S, Blaser K, Akdis CA. Role of apoptosis in atopic dermatitis. Int Arch Allergy Immunol. 2001;124(1–3):230–2.

36. Tang L, Wang J, Zhu J, Liang Y. Down-regulated SHARPIN may accelerate the development of atopic dermatitis through activating interleukin-33/ST2 signalling. Experimental Dermatology. 2018;1328–35.

37. Majd TM, Kalantari S, Shahraki HR, Nafar M, Almasi A, Samavat S, et al. Application of sparse linear discriminant analysis and elastic net for diagnosis of IgA nephropathy: Statistical and biological viewpoints. Iran Biomed J. 2018;22(6):374–84.

38. Newman JRB, Kirpich A, McIntyre LM, Ainsworth EA, Wedow JM, Michailidis G. Variable selection in omics data: A practical evaluation of small sample sizes. PLoS One. 2018;13(6):e0197910.

39. Basu A, Mitra R, Liu H, Schreiber SL, Clemons PA. RWEN: Response-weighted elastic net for prediction of chemosensitivity of cancer cell lines. Bioinformatics. 2018;34(19):3332–9.

40. Gonzales GB, De Saeger S. Elastic net regularized regression for time-series analysis of plasma metabolome stability under sub-optimal freezing condition. Sci Rep. 2018;8(1):1–10.

41. Bujak R, Daghir-Wojtkowiak E, Kaliszan R, Markuszewski MJ. PLS-Based and Regularization-Based Methods for the Selection of Relevant Variables in Non-targeted Metabolomics Data. Front Mol Biosci. 2016;3:1–10.

42. Furman D, Davis MM. New approaches to understanding the immune response to vaccination and infection. Vaccine. 2015;33(40):5271–81.

43. Bligh EG, Dyer WJ. A rapid method of total lipid extraction and purification. Can J Biochem Physiol. 1959;37(8):911–7.

44. Benjamini Y, Hochberg Y. Controlling the False Discovery Rate: A Practical and Powerful Approach to Multiple Testing. J R Stat Soc Ser B. 1995 Jan;57(1):289–300.

45. Zou H, Hastie T. Regularization and variable selection via the elastic net. J R Stat Soc B. 2005;67(2):301–20.

46. Xia J, Sinelnikov I V., Han B, Wishart DS. MetaboAnalyst 3.0--making metabolomics more meaningful. Nucleic Acids Res. 2015;43(W1):W251-7.

47. Agrawal K, Hassoun LA, Foolad N, Borkowski K, Pedersen TL, Sivamani RK, et al. Effects of atopic dermatitis and gender on sebum lipid mediator and fatty acid profiles. Prostaglandins Leukot Essent Fat Acids. 2018 ;134:7–16.

48. Cotterill JA, Cunliffe WJ, Williamson B, Bulusu L. Age and sex variation in skin surface lipid composition and sebum excretion rate. Br J Dermatol. 1972;87(4):333–40.

49. Ruoppolo M, Caterino M, Albano L, Pecce R, Di Girolamo MG, Crisci D, et al. Targeted metabolomic profiling in rat tissues reveals sex differences. Sci Rep. 2018;8(1):1–12.

50. Ottas A, Fishman D, Okas T-L, Püssa T, Toomik P, Märtson A, et al. Blood serum metabolome of atopic dermatitis: Altered energy cycle and the markers of systemic inflammation. Motta A, editor. PLoS One. 2017;12(11):e0188580.

51. Seino S, Tanaka Y, Honma T, Yanaka M, Sato K, Shinohara N, et al. Atopic dermatitis causes lipid accumulation in the liver of NC/Nga mouse. J Clin Biochem Nutr. 2012;50(2):152–7.

52. Rutkowsky JM, Knotts T a, Ono-Moore KD, McCoin CS, Huang S, Schneider D, et al. Acylcarnitines activate proinflammatory signaling pathways. Am J Physiol Endocrinol Metab. 2014;306(12):E1378-87.

53. van Smeden J, Janssens M, Kaye ECJ, Caspers PJ, Lavrijsen AP, Vreeken RJ, et al. The importance of free fatty acid chain length for the skin barrier function in atopic eczema patients. Exp Dermatol. 2014;23(1):45–52.

54. Borodzicz S, Rudnicka L, Mirowska-Guzel D, Cudnoch-Jedrzejewska A. The role of epidermal sphingolipids in dermatologic diseases. Lipids Health Dis. 2016;15(1):1–9.

55. Sacotte R, Silverberg JI. Epidemiology of adult atopic dermatitis. Clin Dermatol. 2018;36(5):595–605.

56. Radner FPW, Fischer J. The important role of epidermal triacylglycerol metabolism for maintenance of the skin permeability barrier function. Biochim Biophys Acta - Mol Cell Biol Lipids. 2014;1841(3):409–15.

57. Maciel E, Nunes R, Simões C, Domingues P, Domingues MRM. Structural Characterization of Oxidized Glycerophosphatidylserine : Evidence of Polar Head Oxidation. 2011;1804–14.

58. Piotto S, Trapani A, Bianchino E, Ibarguren M, López DJ, Busquets X, et al. The effect of hydroxylated fatty acid-containing phospholipids in the remodeling of lipid membranes. Biochim Biophys Acta - Biomembr. 2014;1838(6):1509–17.

59. Catalá Á. Lipid peroxidation modifies the assembly of biological membranes "The Lipid Whisker Model." Front Physiol. 2015;6:1–4.

60. Serbulea V, DeWeese D, Leitinger N. The effect of oxidized phospholipids on phenotypic polarization and function of macrophages. Free Radic Biol Med. 2017;111:156–68.

61. Tsuboi K. 2-Hydroxylated fatty acids as candidates of novel drugs to promote chemosensitivity of gastric cancer. EBioMedicine. 2019;2–3.

62. Abe A, Yamane M, Yamada H, Sugawara I. The ω-hydroxy palmitic acid induced apoptosis in human lung carcinoma cell lines H596 and A549. J Biochem Mol Biol Biophys. 2002;

63. Beeharry N, Chambers JA, Green IC. Fatty acid protection from palmitic acid-induced apoptosis is lost following PI3-kinase inhibition. Apoptosis. 2004;9(5):599–607.

64. Reddy JK, Hashimoto T. Peroxisomal beta-oxidation and peroxisome proliferator-activated receptor alpha: an adaptive metabolic system. Annu Rev Nutr. 2001;21(1):193–230.

65. Pavel P, Leman G, Hermann M, Rühl R, Schmuth M, Dubrac S. Peroxisomes contribute to inflammation in atopic dermatitis. J Invest Dermatol. 2018;138(5):S111.

66. Zhang Y, Li Q, Rao E, Sun Y, Grossmann ME, Morris RJ, et al. Epidermal Fatty Acid Binding Protein Promotes Skin Inflammation Induced by High-Fat Diet. Immunity. 2015;42(5):953–64.

3.7 Supporting information

S6 Table: Lipid ions diving the separation of samples by of compositional principal component analysis. CPC-1 contributes to separation of male and female in positive ion mode. The CPC-2 contributes to separation of samples by phenotype.

MRM	contribution to CPC-1	MRM	contribution to CPC-2
851_84.996	0.244620514	427.39_84.996	0.314948532
876_84.996	0.243260247	426.29_84.996	0.312457034
476_195.996	0.241313307	434_84.996	0.310778192
775_501.996	0.24012582	404_84.996	0.308739893
458_136.996	0.239652645	426_80.996	0.306622303
903_625.996	0.239177777	432_84.996	0.300859655
414_94.996	0.239175473	433_84.996	0.300353122
422_100.996	0.238719442	620_84.996	0.295594499
685_427.996	0.238707988	415_84.996	0.29317244
474_152.996	0.238660783	376_84.996	0.292836405
877.7_266.3	0.238532592	335_84.996	0.292278195
653_467.996	0.238445945	464_84.996	0.291185789
417_117.996	0.238356572	398_84.996	0.289468582
729_549.996	0.23835276	305_84.996	0.288134204
417_97.996	0.238196428	538_84.996	0.285871913
553_295.996	0.238089886	281_84.996	0.284067777
683_425.996	0.238060086	697.44_369.09	0.281359773
599_413.996	0.238038179	813_399.996	0.281152282
454_274.996	0.237984335	757_427.996	0.280445729
812.5_627.996	0.237969558	301_84.996	0.27874416
418_118.996	0.23792977	353_84.996	0.277998838
631_335.996	0.237850303	470_84.996	0.277285376
882.5_605.996	0.237837341	1157_743.996	0.27701919
480_154.996	0.237796416	482_84.996	0.275741886
643_457.996	0.237782924	699.40_369.09	0.275557967
421_235.996	0.237690844	701_353.996	0.275421928
637_451.996	0.237635125	727.40_369.09	0.275118117
493_235.996	0.237514106	1009_595.996	0.275043932
660_360.996	0.237415836	1131_717.996	0.274743777
816.5_631.996	0.237400866	359_84.996	0.274519572
463_291.996	0.237303362	283_84.996	0.27399934
459_195.996	0.237285512	408_84.996	0.273921282
629_443.996	0.237215873	1068_654.996	0.273668545
607_281.996	0.237094696	785_371.996	0.273458082
431_105.996	0.237065745	1133_719.996	0.273262513
679_493.996	0.237058451	966_552.996	0.273179971
431_245.996	0.236976058	431_55.996	0.272824042
789.5_604.996	0.236842155	256_84.996	0.272223043
701_427.996	0.236825511	580_84.996	0.271887387
844.5_659.996	0.236760388	563_84.996	0.270941084
875.5_264.212	0.236555545	366_84.996	0.270817934
477_335.996	0.236513741	1171_757.996	0.270278171
906.5_629.996	0.236508869	1021_607.996	0.27002068
424_98.996	0.236482359	325_84.996	0.269955576
450_195.996	0.236461777	699_353.996	0.269566361
790.5_605.996	0.236340398	472_84.996	0.2693588
814.5_629.996	0.23633665	537_195.996	0.268611291
762.5_577.996	0.23633591	1119_705.996	0.268477786
760.5_575.996	0.236304461	493_84.996	0.266784564
479_205.996	0.236280074	683_353.996	0.266529467

S7 Table: List of selected sex predictive lipid ions that are not dependent of phenotype after Benjamini-Hochberg p-value adjustment by univariate analysis.

Sex related lipid features independent of phenotype	
MRM	**Tentative attribution**
851 -> 577.996	TAG(50:2)_FA 16:0
878.5 -> 579.996	TAG(52:1)_FA 18:1
902.5999756 -> 603.996	TAG(54:3)_FA 18:1
903.5999756 -> 604.996	N/A
877.5 -> 578.996	N/A
876.5 -> 577.996	TAG(52:2)_FA 18:1
903 -> 603.996	N/A
850.5 -> 551.996	TAG(50:2)_FA 18:1

S8 Table: List of selected sex-dependent predictive lipid ions after Benjamini-Hochberg p-value adjustment by univariate analysis.

Sex-dependent predictive lipid features	
MRM	**Tentative attribution**
694.4 -> 264.29	Cer(d18:1/26:0(2 -OH)
666 -> 264.29	Cer(d18:0/24:1)
456 -> 84.996	AC(20:0)
678.40 -> 264.29	Cer(d18:1/26:0)
714 -> 282.1952187	HexCer(d18:1/16:1(2 -OH)
680 -> 264.2967812	Cer(d18:0/26:0)
484 -> 84.996	AC(22:0)
554.200 -> 282.19	Cer(t18:0/16:1)
704.798 -> 183.99	PC (30:1)
650.40 -> 264.29	Cer(d18:1/24:0)
300.10 -> 282.19	Sphinganine
703.799 -> 183.99	SM(16:0)
538 -> 282.195	Cer(d18:1/16:0)
540 -> 282.195	Cer(d18:0/16:0)
556 -> 264.296	Cer(d18:0/16:0(2OH)

CHAPTER 4. LIPID BIOMARKERS FOR DIAGNOSIS AND DISEASE PROGRESSION OF CANINE ATOPIC DERMATITIS

4.1 Abstract

Atopic dermatitis is an allergic inflammatory skin disease that is common in humans and dogs. Altered lipid composition of the epidermis is a prominent feature of the disease, however, it remains to be determined if these changes underlie a primary skin barrier defect or are the result of the inflammation. The diagnosis of canine atopic dermatitis (CAD) is based on exclusion of causes of pruritus which is a time consuming and expensive process. Since alterations in the lipid composition of the skin plays a key role in the pathogenesis of the disease, we used a mass spectrometry-based lipidomics strategy aimed at identifying a lipid fingerprint that could be useful for its diagnosis. Skin punch biopsies were collected from 14 client owned CAD patients and 11 healthy controls and the clinical disease extend and severity index (CADESI-4) was recorded. The lipid composition of the epidermis substantially distinguished samples of healthy dogs from atopic dogs. A feature selection strategy found oleic acid containing triacylglycerides, long-chain acylcarnitines and sphingolipids as predictive lipids that highly correlated (R^2=0.89) with the disease severity score of patients. Changes in the lipid composition of the skin were identified in atopic dogs even when the skin appeared clinically healthy and selected lipids predicted the progression of the disease. The lipid biomarkers identified here are potentially useful for the diagnosis and monitoring of atopic dermatitis.

4.2 Introduction

Atopic dermatitis (AD) is a chronic inflammatory skin disease caused by an aberrant immune response to percutaneously absorbed proteins, such as house dust mite antigens and pollen (1,2). It commonly affects people and dogs worldwide (3,4). As progress has been made in the knowledge of canine atopic dermatitis (CAD), it is clear that the clinical manifestations and pathophysiologic mechanisms of the disease in dogs is very similar to human AD, including the possibilities of multiple endotypes (5–7). The diagnosis in CAD is based on the evaluation of clinical characteristics grouped under a set of criteria (8) and the exclusion of other causes of pruritic dermatitis such as ectoparasites, microorganisms and food allergy. This makes CAD

diagnosis a long, costly and sometimes frustrating process for both the clinician and the patient's owners. Over the years, the diagnosis and evaluation of the severity of AD has been based on subjective clinical criteria with large inter-observer variation (9,10).

Efforts have been made to discover a biomarker that can convert subjective observational evaluation to objective and quantifiable criteria that can be compared easily in cross-sectional studies (9,11,12). However, this goal has not been easy to achieve since AD is highly complex with very heterogeneous presentations among individuals. Accurate classification of patients by a single biomarker, such as mutations in filaggrin gene or elevated concentrations of allergen-specific IgE in serum, is restricted to a limited group of human patients (13). In CAD, heterogeneous subtypes with normal or elevated serum IgE suggest that CAD is a syndrome rather than a specific skin disease (5,14). Disease severity assessment in people has been correlated with measurements such as transepidermal water loss (TEWL) and pH, and with determinations of serum proteins such as eosinophil cationic protein (ECP), total immunoglobulin (Ig)-E, IL-22 and thymus and activation-regulated chemokine (TARC) which suggests that a panel of biomarkers could have a better correlation than a single one (10,15). The few studies that have sought to correlate the severity of CAD with serum biomarkers or TEWL, pH and skin hydration have had limited results due to variability among observer, site to site measurement and environmental conditions (16–19). Recently, the repeatability of non-invasive tools to assess the skin barrier integrity in dogs was investigated and even though high repeatability was observed among instruments, differences between groups were not significant and there was a low correlation between the barrier assessment and the clinical CADESI-04 score (20). Nevertheless, the increased values of TEWL in atopic dog skin provided an assessment of the epidermal barrier function showing that its alteration is involved in the development of the disease (21).

Healthy skin forms a physical barrier that prevents water-loss and percutaneous penetration of allergens and is formed by corneocytes embedded in a lamellar lipid matrix (22). The composition of the lipid matrix is essential to the barrier function of the skin (23,24). The main classes of lipids that make up the epidermal lipid matrix are free fatty acids (FFAs), cholesterol esters (CE), and ceramides (23,25). The overall content of epidermal lipids is reduced in skin of human AD patients with alterations in ceramides and fatty acids (26). Whether the changes in the lipid barrier in atopic dermatitis are primary or secondary to the inflammation is unclear, but cytokines released during the inflammatory process induce changes in lipid production that

weaken the barrier function and exacerbate the disease (27). A few studies have investigated the lipid composition of the stratum corneum and epidermis in dogs with CAD. The overall number of ceramides was decreased in dogs with CAD compared with normal dogs (28–31) whereas variable results have been reported for FFA and cholesterol esters (29,32). Unfortunately, these lipid analyses did not correlate disease severity with lipid content. Considering the important role of lipids in cell biology (33) and cell signaling (34), in chronic inflammation (35) and in antimicrobial activity by enhancing the effect of antimicrobial peptides (36), analysis beyond the main lipid components of the epidermis should be performed.

Recent advances in lipidomics have provided tools to perform high-throughput analysis of lipids in an untargeted and more efficient fashion (37,38). Techniques traditionally used to quantify the lipid composition in skin and other tissues for specific ceramides and fatty acids (39) like thin-layer chromatography (TLC) and LC tandem mass spectrometry (LC-MS/MS) are highly demanding in sample preparation and instrument time and can only screen for a limited number of lipid features at a time. Untargeted metabolomics emerged recently as a useful tool for biomarker discovery and drug discovery safety, but it usually requires expensive high-resolution MS instruments that have lower sensitivity compared to triple quadrupole mass spectrometers and the identification of detected ions is time-consuming, requiring accurate mass databases and specialized software (40).

We developed a novel mass spectrometry analytical strategy, multiple reaction monitoring (MRM)-profiling, that can rapidly identify discriminant lipids by flow injection with minimal sample preparation (41). Multiple reaction monitoring-profiling is a small molecule accelerated discovery workflow performed in two phases. Briefly, the first phase consists of discovery experiments based on neutral loss (NL) and precursor ion (Prec) scan experiments to detect lipids and metabolites in the samples by targeting class-specific chemical motifs (or chemical functional groups) such as polar heads of phospholipids or sphingoid bases of ceramides. The second phase of the MRM-profiling is the screening of a larger set of samples for the transitions detected in the discovery phase (42–44). The main advantages of this technique are reduced time for sample preparation, the capability to screen thousands of lipids at the speed of over 200 lipid ions in three minutes, and the straightforward data processing workflow resulting in fast identification of the lipid fingerprint present in each sample in a high throughput manner. Identification of a molecular fingerprint of lipids in the skin would allow clinicians to make a better-informed and faster

diagnosis as it may result in new diagnostic biomarkers and could eventually provide an objective assessment tool for disease severity that could be potentially used to compare treatment response across studies.

4.3 Materials and methods

4.3.1 Animals

14 CAD patients and 11 healthy control dogs were recruited at the Dermatology service of the Small Animal Hospital of the Purdue College of Veterinary Medicine. All recruited CAD patients were client owned, at least 12 months old, and in overall good health. They had a documented history of non-seasonal pruritus responsive to steroids but had not received any immunosuppressive or anti-inflammatory treatment for at least two weeks prior to the sample collection. The healthy control dogs were owned by staff and students affiliated with the small animal hospital and dogs from a local shelter. Punch biopsies of 8mm were collected from each dog. Two biopsies from affected skin and one from unaffected skin was collected from CAD patients, and two biopsies from healthy skin were collected from control dogs. The CADESI-04 score (range 0 – 180) was recorded on the day of sample collection along with the signalment of each dog (breed, color, age, sex, and reproductive status), site of sampling and swab culture test results (S9 and S10 Tables). Samples were collected from standardized areas of the abdomen and flank. The protocol was approved by the Purdue University Animal Care and Use Committee (PACUC protocol 1510001312) and owners provided informed consent.

4.3.2 Sample preparation

The epidermis was separated from the dermis by floating the skin biopsies in Thermolysin (from *Geobacillus stearothermophilus*, Sigma-Aldrich, St. Louis, MO) diluted in HEPES, weighed, homogenized and extracted in the same manner as the mouse epidermis as described in Chapter 2. During homogenization in Precellys, two samples were lost due to breakage of the tube, one from the non-affected atopic group and one from control.

4.3.3 MRM-profiling

The limited sample from dog epidermis only permitted extraction of the total sample and a discovery step was therefore not performed. Instead, the two methods described in Chapter 2 for

the mouse epidermis were applied to all samples so that each sample was individually screened in a high-throughput manner (approx. 3 min/sample) by injecting 8 µL of lipid extract through the micro-autosampler (G1367A) into a QQQ6410 triple quadrupole mass spectrometer (Agilent Technologies, San Jose, CA) equipped with Jet Stream ESI ion source. Conditions of the MS and tentative identification of lipid ions were performed as previously described in Chapter 2. The raw data will be deposited at the public proteomics repository MassIVE.

4.3.4 Statistical analysis

The mass spectrometry raw files were converted, and data was collected as previously described (Chapter 2). Samples were normalized by the total ion count to obtain relative amounts of lipid in the sample which are used for statistical analysis.

For univariate and multivariate statistical analysis, the normalized relative amount of each lipid ion was transformed by generalized logarithm transformation and mean-centered and divided by the standard deviation of each variable to auto-scale the data. The significance of differences was determined at (α=0.05) after false discovery rate correction for multiple comparisons. For feature selection and E-net regression, the data was transformed using log-ratio transformation to correct for heteroskedasticity and spurious correlations. The statistical model of disease progression was developed by feature extraction of the epidermal lipid composition data as described in chapter 3. Briefly, a set of linear models using CADESI-4 score and sex were built for each lipid ion and the high-performing univariate models were selected. Subsequently, an E-net model automatically selected the most relevant features, zeroing out all the unnecessary model components. Linear discriminant analysis and receiver operator characteristic curve analysis were used to evaluate classification accuracy of the lipid features selected and an E-net regression predictor model was trained using a bootstrap procedure to determine correlation with CADESI-4. The statistical analysis was performed using GraphPad Prism package, MetaboAnalyst 3.0 software (http://www. metaboanalyst.ca (45), JMP 13 from SAS Package, as well as the R-language for statistical computing.

4.4 Results

4.4.1 Lipid profile of epidermis in atopic dermatitis

4.4.1.1 Epidermal lipid fingerprint of healthy and atopic skin

Univariate analysis of the data collected by MRM-profiling of the average of two epidermis samples from 11 healthy control dogs and the average of two affected epidermal samples from 14 clinically diagnosed atopic dogs was performed. Unsupervised exploratory analysis of the lipid content by PCA separated the samples into atopic and control by the second component, explaining just 23.2% of the variance (Figure 17a). However, visualization of the data by heat map showed two clusters of lipids that clearly differentiated the profiles of atopic from healthy dogs (Figure 17b).

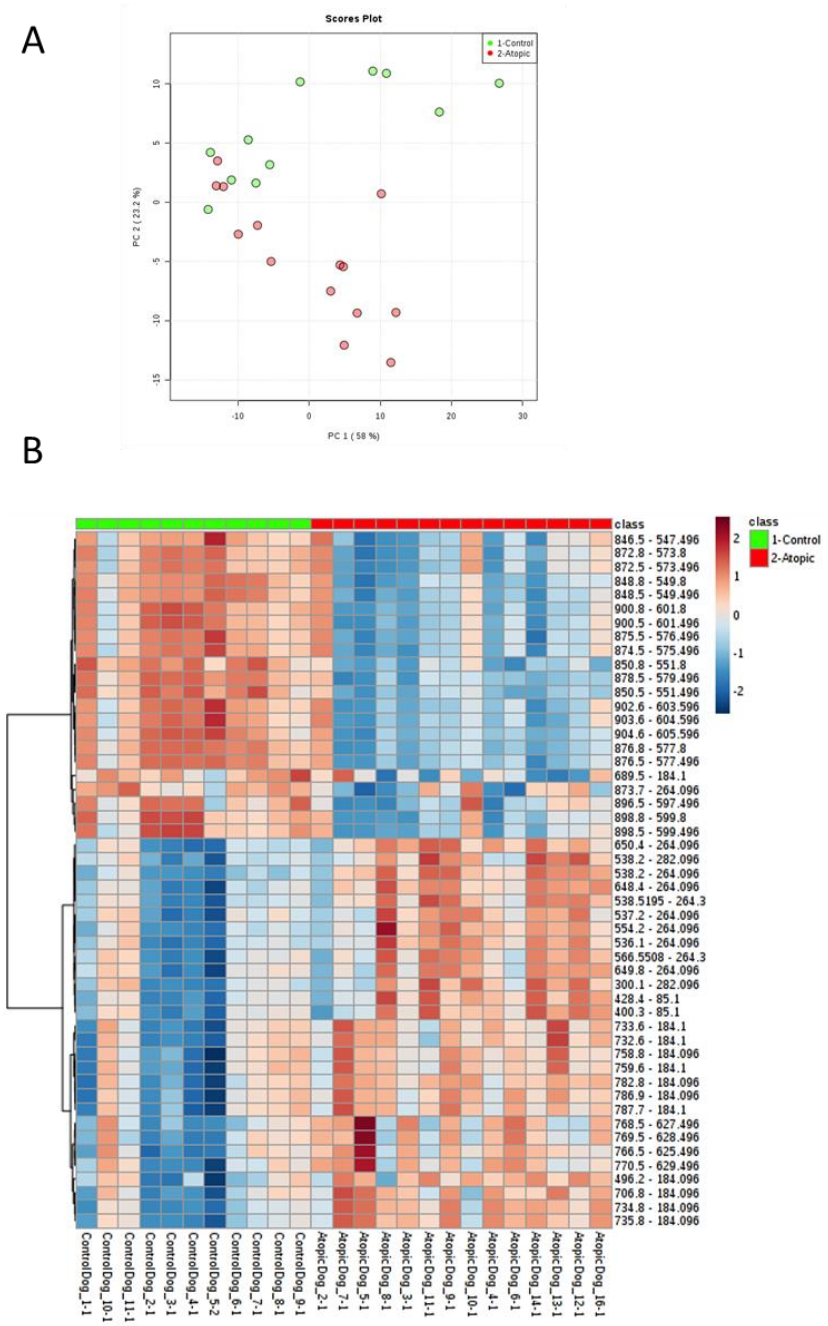

Figure 17**. Unsupervised analysis of lipid ions monitored in CAD patients and healthy controls**. Discrimination of atopic and healthy epidermis was observed by PCA and cluster analysis. (A) Score plot of principal component analysis (PCA). PC1 explained 58% of the variability of the data. PC2 explained the variance by 23.26%. (B) Values are means of two epidermal samples for each atopic dogs (n=14) and two samples from each control dog (n=11). Lipids are shown with their *m/z* and corresponding lipid class characteristic fragment. Color of each cell corresponds to the relative abundance of the lipid feature monitored in the sample.

The first cluster, driven by triacylglycerides (TAGs) containing an oleic acid residue, had decreased relative amounts in atopic skin compared to healthy skin (Figure 18a), while the second cluster had the opposite trend and comprised increased palmitic acid containing ceramides, AC (18:0) and PCs (Figure 18b). Among the fatty acids monitored, 26:0 and 28:0 ultra-long chain fatty acids were decreased and oleic acid (18:1) and arachidonic acid (20:4) were increased in atopic compared to healthy epidermis (Figure 18c). Lipids monitored from the epidermis of control and atopic groups revealed a lipid fingerprint of dermatitis.

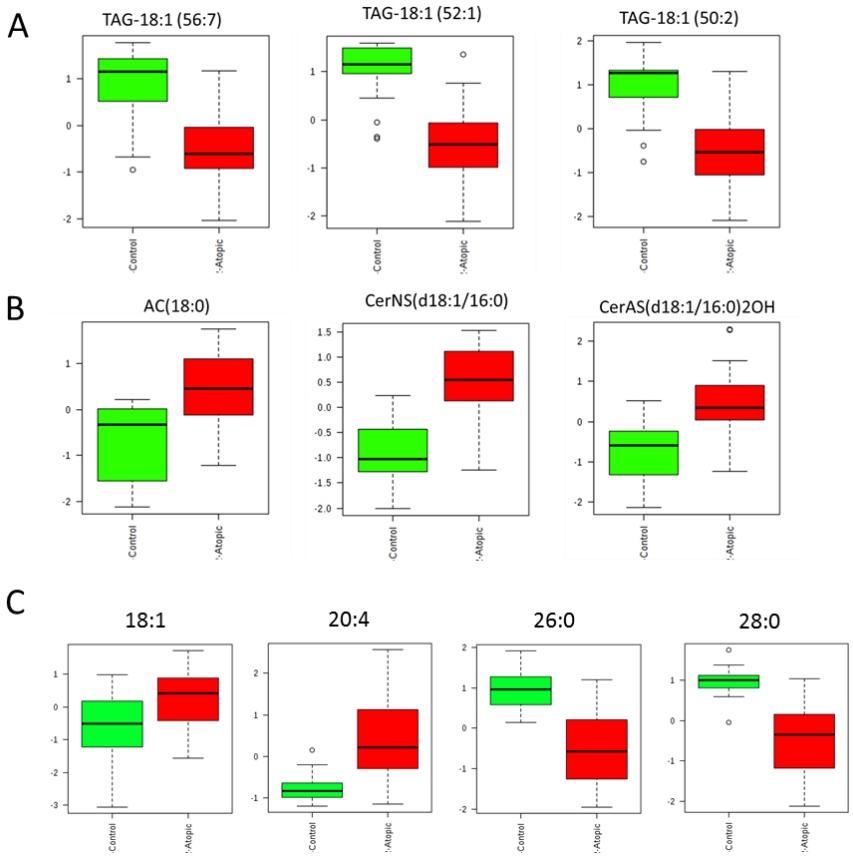

Figure 18**. Relative amount of representative lipids clustering in atopic versus healthy epidermis from dogs by MRM-profiling**. (A) TAGs containing an oleic acid residue had decrease relative amounts in atopic skin compared to healthy. (B) The relative amount of stearic acylcarnitine and ceramides with 16 carbon fatty acid residues was larger in atopic dogs compared to controls. (C) Ultra-long chain fatty acids were decreased and oleic acid (18:1) and arachidonic acid (20:4) were increased in atopic compared to healthy epidermis. The vertical axis represents standardized the relative amounts of lipids detected in the epidermis of atopic and healthy dogs (horizontal axis). Box plots represent mean values of two epidermal samples for each atopic dogs (n=14) and two samples from each control (n=11). $p < 0.05$ based on unpaired t-test with False Discovery Rate (FDR) correction for multiple comparisons for all the plots represented.

4.4.1.2 Differences in lipid content of non-affected and affected epidermis

Since samples were collected from affected and non-affected skin areas of CAD patients, we separated the samples by skin condition at the time of biopsy. Non-affected (n=13), affected (n=14) and healthy control (n=11) were compared by multivariate analysis. Localization of the samples in the unsupervised PCA space indicated that the lipid content of non-affected samples was in a transitional stage between healthy and affected samples (Figure 19a). Visualization of the relative amounts of lipids by heat map showed that a cluster of the lipids monitored by MRM-profiling was increased in affected epidermis compared to healthy and these lipids corresponded to AC, long chain ceramides and PCs. A second lipid cluster was decreased in affected skin compared to control skin, mostly driven by TAGs and ultra-long ceramides (Figure 19b).

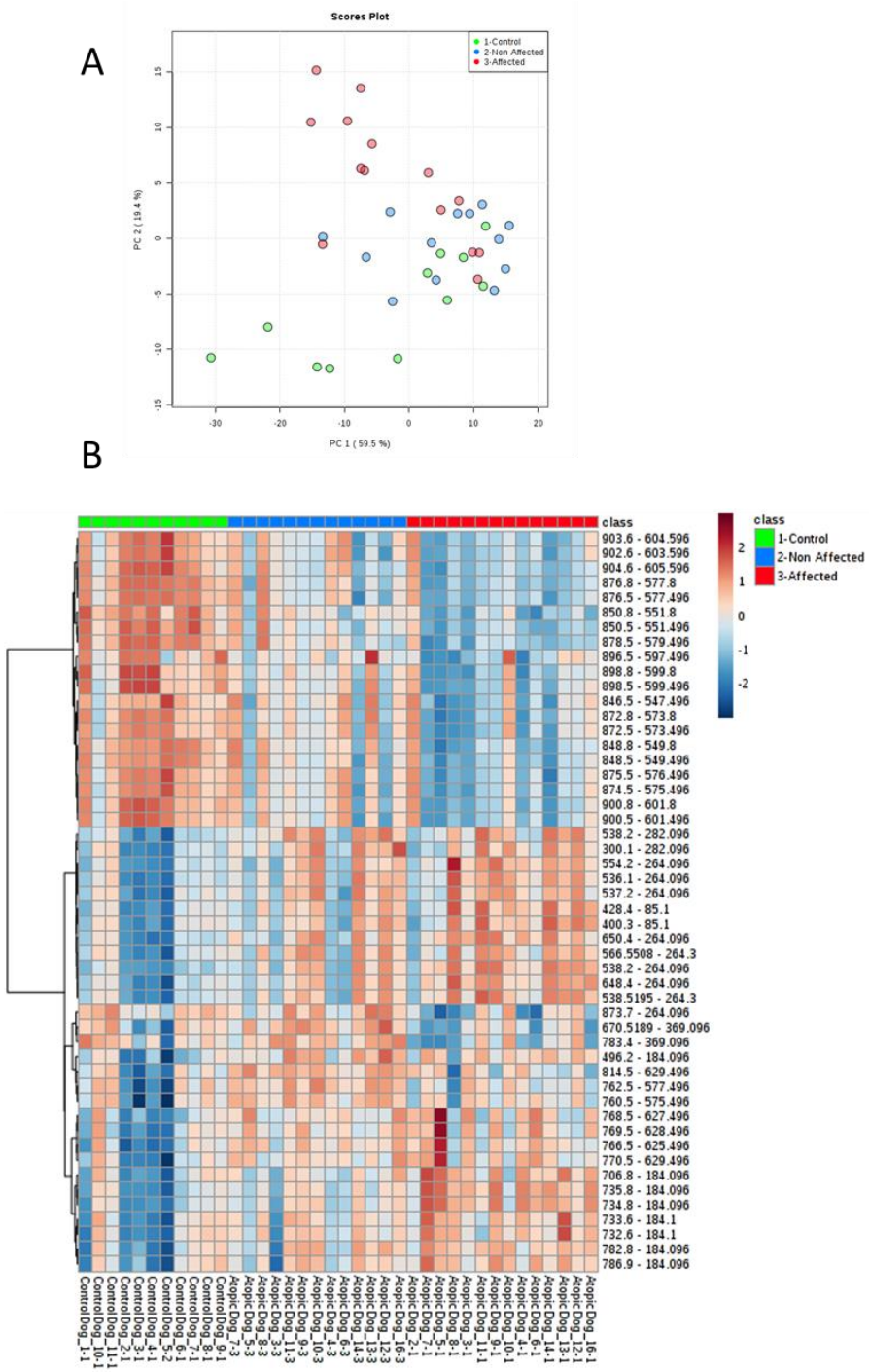

Figure 19**. Unsupervised analysis of lipid ions monitored in CAD patients and healthy controls by skin condition at the time of biopsy**. Discrimination of healthy, non-affected and affected epidermis was observed by PCA and cluster analysis. (A) Score plot of principal component analysis (PCA). PC1 explained 59.5% of the variability of the data. PC2 explained the variance by 19.4%. (B) Values are means of two affected epidermal samples for each atopic dog (n=14), 13 samples from atopic non affected skin and means of two samples from each control (n=11). Lipids are shown with their *m/z* and corresponding lipid class characteristic fragment.

In both cases, samples from non-affected skin of CAD patients showed an ambivalence that was reflected in the posthoc results. Samples from the two atopic groups were significantly reduced compared with the healthy control for TAG (50:2) containing oleic acid, 26:0 and 28:0 FFA (Figure 20a). Lipids that were significantly different from the healthy control but not among non-affected and affected group included TAG (52:1) containing oleic acid that was decreased and lyso-phosphatidylcholine LPC(16:0) and Cer[NP](t18:0/16:0) that were both increased (Figure 20b). On the other hand, hydroxy-oleic acid and linoleic acid were not different between healthy and non-affected but the affected group was significantly increased compared to the previously mentioned groups (Figure 20c). Finally, arachidonic acid and sphingosine ceramides with 16, 18 and 24 carbon chains residues were only significantly increased compared to healthy control group (Figure 20d). Variations in lipid composition of the epidermal lipids were present even though the skin area from which the sample was collected was clinically normal.

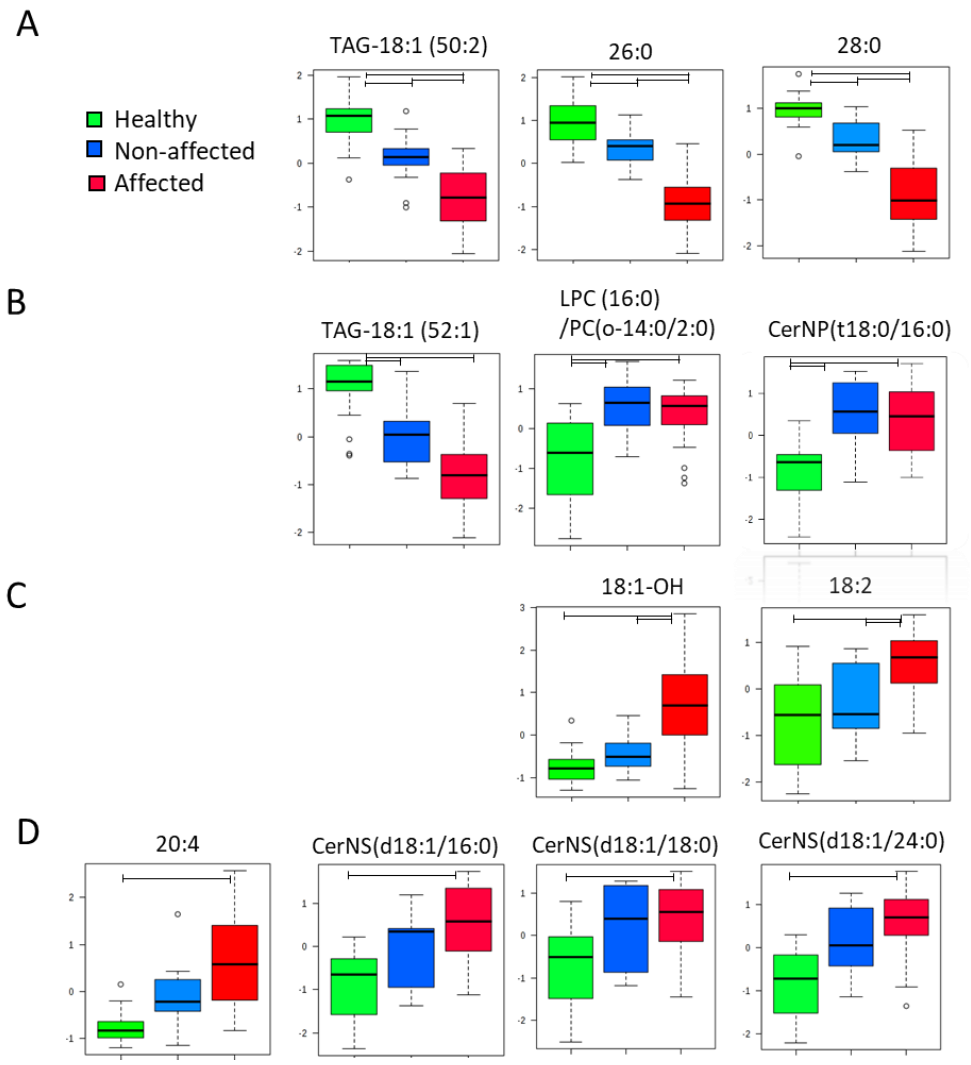

Figure 20**. Relative amount of lipids significantly different in healthy, non-affected and affected epidermis by ANOVA and Tukey test**. (A) Relative amounts of TAG (50:2) containing oleic acid, 26:0 and 28:0 FFA were significantly different among the three groups, separating healthy from non-affected epidermal samples of atopic dogs. (B) TAG (52:1) containing oleic acid lyso-phosphatidylcholine (16:0) and Cer[NP](t18:0/16:0) were significantly different to the healthy control but not among non-affected and affected group. (C) Hydroxy-oleic acid and linoleic acid relative amounts were significantly increased in affected epidermis compared to non-affected and healthy, which were not significantly different from each other. (D) Arachidonic acid and sphingosine ceramides with 16, 18 and 24 carbon chains residues were only significantly increased compared to healthy control group, and non-affected samples were no having difference from either of the other two groups. The vertical axis represents the standardized relative amounts of lipids detected in the epidermis of atopic and healthy dogs (horizontal axis). Box plots represent mean values of two affected epidermal samples for each atopic dog (n=14), 13 samples from atopic non affected skin and means of two samples from each control (n=11). $p < 0.05$ based on ANOVA and Tukey posthoc with False Discovery Rate (FDR) correction for multiple comparisons.

4.4.1.3 Discriminant capability of epidermal lipids for healthy, non-affected and affected epidermis.

To test the capability of the lipid composition to discriminate between healthy, non-affected and affected epidermis, data collected by MRM-profiling was subjected to linear discriminant analysis (LDA). Classification of the samples into the three groups of skin condition at the time of biopsy was highly accurate with correct classification of all samples. The LDA distinguished the affected epidermis from healthy skin, as well as atopic non-affected epidermis from control skin samples. Seven samples were misclassified between affected and non-affected (Figure 21). However, the LDA model used the 220 lipids monitored by MRM-profiling which makes this prediction less robust and more likely to be overfitted.

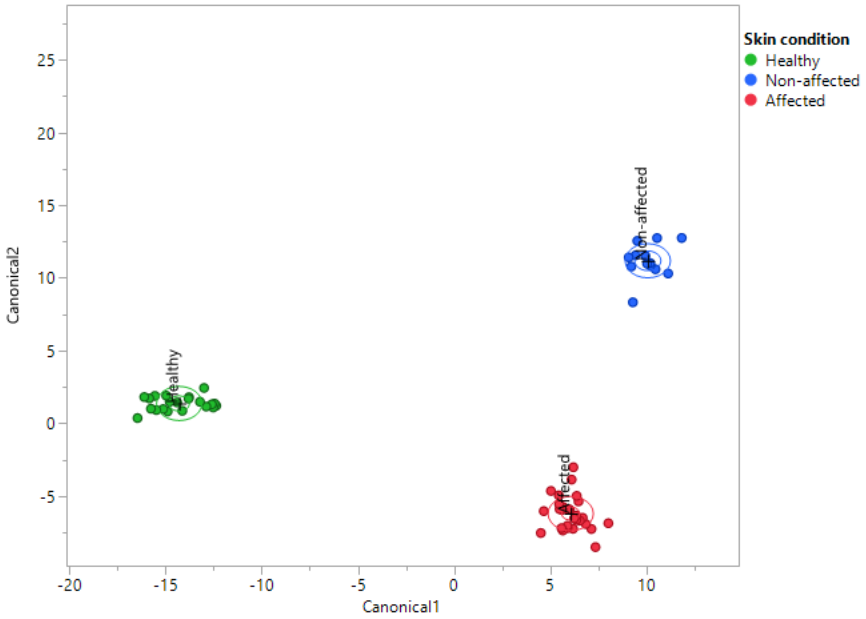

Figure 21**. Classification of samples based on the lipid content of the epidermis**. Linear discrimination analysis of the samples in to the healthy, non-affected and affected categories using all lipids monitored. Epidermal samples from healthy dogs not only differed substantially from CAD skin but could also be easily distinguished from the seemingly unaffected epidermis of the same CAD patients. Circles represent each of the 62 samples analyzed (Healthy n=21; Non-affected n=13, Affected n=28). (Entropy R^2=0.96, -2LogLikelihood=4.15; Percent misclassified=0)

4.4.2 Dependency of epidermal lipid composition, disease severity and sex.

Disease severity was evaluated by CADESI-4 and was recorded for each patient at the day of biopsy. Healthy patients were scored as 0 and atopic patients scores ranged from 30 to 121. All lipids monitored were compressed using PCA and plotted versus CADESI-4. The position of the samples in the PCA space reflected that the lipid composition of the epidermis is dependent of the disease severity, including affected and non-affected samples (Figure 22).

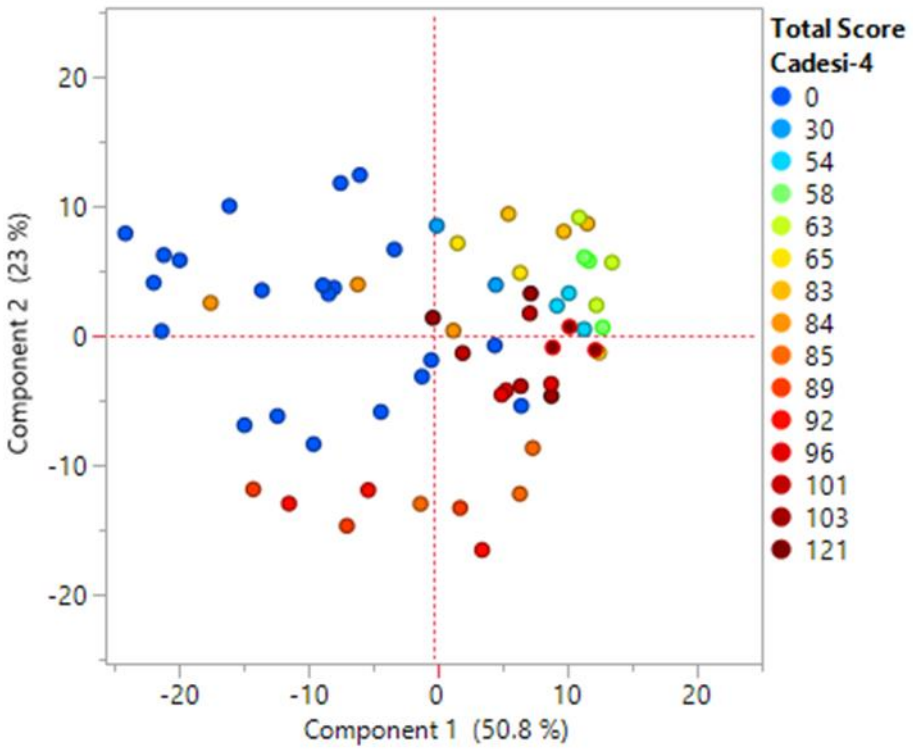

Figure 22**: Dependency of lipid content and disease severity**. All lipids were compressed using a principal component analysis (PCA) and plotted versus the disease severity. The added explained variance of components 1 and 2 is 73.8%. The PCA score plot of the lipid profile shows that the lipid composition is dependent of the disease severity. Circles represent all samples including affected and non-affected skin areas and healthy controls. Color represent increasing severity of the disease from blue for healthy to red for high severity.

4.4.2.1 Lipid profile reflects CADESI-4 score cohorts.

CADESI cohorts were created in order to standardize the CADESI-4 scores. Scores between 30 and 85 were grouped as low-score and all above were labeled as high-score. Samples collected from healthy dogs was labeled as healthy. Analysis of the samples using the cohort classification, showed that the first component of the CPC obtained from the relative amount of all epidermal lipids collected was able to significantly differentiate the healthy population from the atopic, but there was significant difference between low or high score (Figure 23).

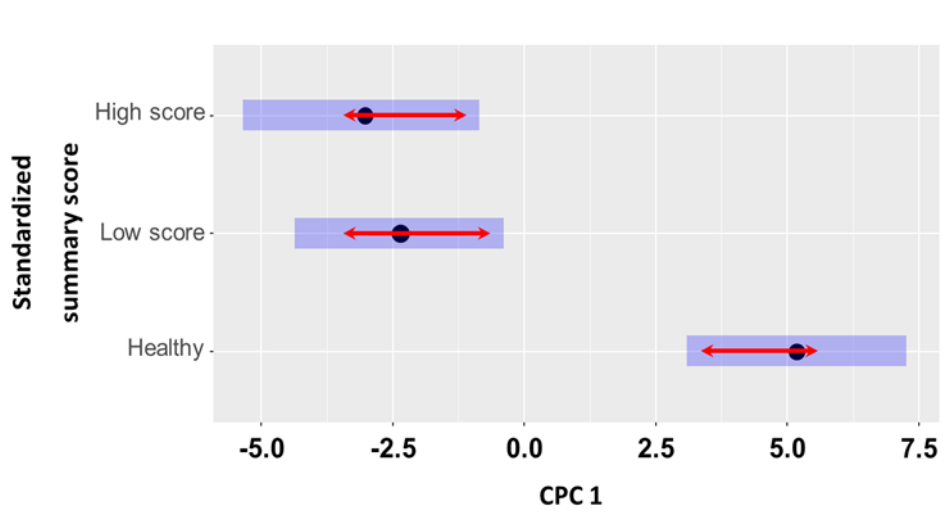

Figure 23**. Differentiation of healthy controls and atopic dogs by the lipid content**. All lipids were compressed using a CPC analysis and plotted versus 3 cohorts of the disease severity score (healthy, low-score and high-score). First PC differentiated the control population from low-score and high-score; however, the difference between low-score and the high-score cohorts was not statistically significant at $P < 0.05$. Blue bars: confidence intervals; Red arrows: Sidak-adjusted post-hoc pairwise comparisons between groups.

4.4.2.2 Interaction of sex and disease severity in epidermal lipid content

Considering that we have previously observed an impact of sex on the lipid profile of the epidermis in chapter 3, we separated the samples by sex of the dog, independently of their reproductive status. The results after this separation showed that an interaction between sex and

disease severity is reflected on the lipid fingerprint of the epidermis. Female cohorts for disease progression were all significantly different, while male cohorts were not (Figure 24).

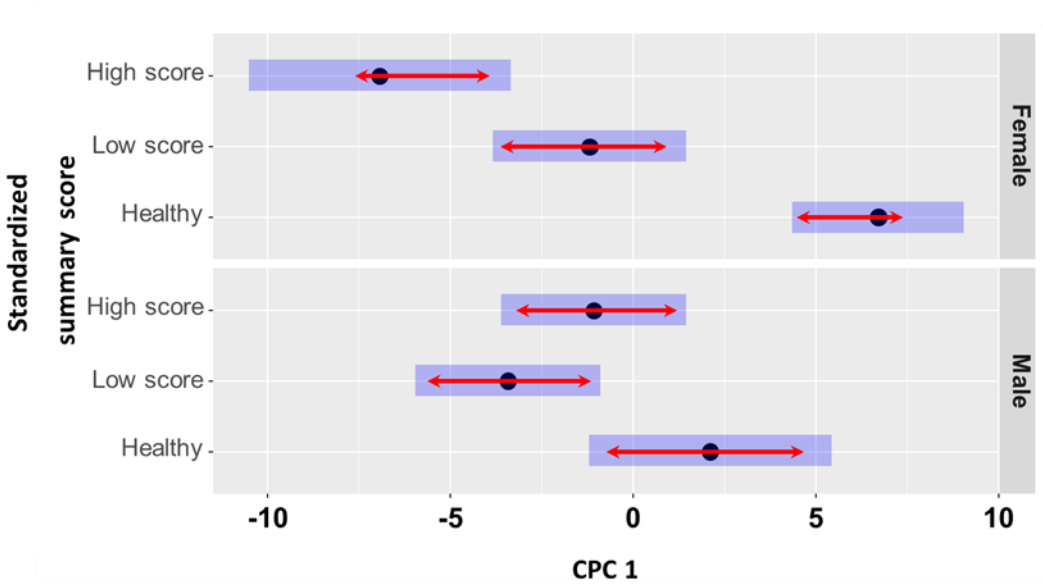

Figure 24**. Interaction of sex and disease severity reflected by lipid composition**. All lipids were compressed using a CPC analysis and plotted versus 3 cohorts of the disease severity score (healthy, low-score and high-score) by sex of the dog. For females the 3 cohorts were significantly different, but for males the mid and high scores of disease severity were not significantly different among them at $P < 0.05$. Blue bars: confidence intervals; Red arrows: Sidak-adjusted post-hoc pairwise comparisons between groups.

Two-way ANOVA analysis of the data separated by CADESI cohorts and sex found no significantly different features for sex. However, the interaction had p-values < 0.05 for key lipids with different trends for each sex. In females, ceramides with a palmitic acid residue and sphingosine accumulated with increasing disease severity, while in males, these lipids were increased in the low-score group compared to healthy but decreased on the high-score cohort. On the other hand, AC (20:0), had a complete opposite trend in females and males, as its relative concentration increased in females and decreased in males with increasing disease severity (S8 Figure).

4.4.3 Effect of *Staphylococcus intermedius* on epidermal lipid profile

Secondary infection by *Staphylococcus pseudintermedius* present in the skin of CAD patients at the time of biopsy was determined by swab culture (Infected n=8; non-infected n=6) (S9 Table). Unsupervised analysis of lipids in epidermis of patients separated by the presence or absence of infection was performed to assess the effect of bacteria on the lipid composition. Two-way ANOVAs were performed using skin condition and CADESI score cohort versus *S. pseudintermedius* infection status, labeled as non-infected or infected (Figure 25). In the presence of *S. pseudintermedius* infection SM and PC were significantly changed, particularly SM(d36:0), SM(d37:1), PC(33:1) and PC(34:1). In the absence of infection, these lipids were increased in the affected skin compared to the non-affected skin of the atopic dogs, but no change was observed when there was infection. A similar trend was observed after analyzing the infection versus the CADESI cohorts. Low-score cohort had increased relative amounts of PC and SM than high-score cohort when no infection was observed. But under infected conditions, the lipids were equally reduced for both disease severity cohorts compared to non-infected skin.

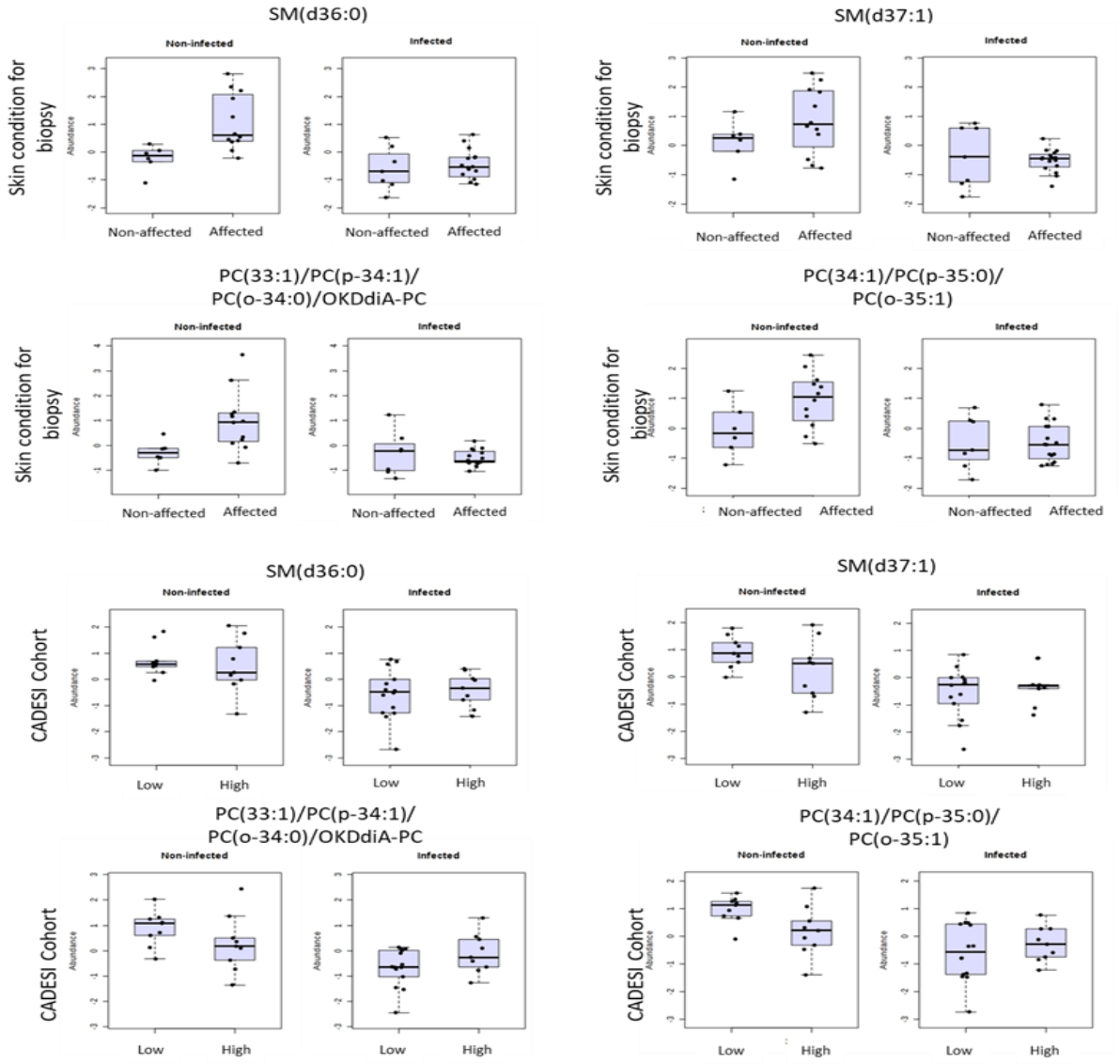

Figure 25**. Effect of *Staphylococcus pseudintermedius* on relative amounts of phospatidylcholine and sphingomyelin**. Relative amounts of SM(d36:0), SM(d37:1), PC(33:1) and PC(34:1) were identified to change when infection by *Staphylococcus pseudintermedius* is present in the epidermis of atopic dogs. (A) SM(d36:0), SM(d37:1), PC(33:1) and PC(34:1) accumulate in affected skin of atopic dogs compared to non-affected in absence of *S. pseudintermedius* infection, but there is no there is no difference between the two skin conditions when there is colonization by the bacteria. (B) In atopic dogs with high CADESI score, SM(d36:0), SM(d37:1), PC(33:1) and PC(34:1) tend to reduce compared to low CADESI score in absence of *S. pseudintermedius* infection. However, both CADESI score cohorts were reduced in epidermis infected with *S. pseudintermedius.* Results for CADESI cohorts versus infection includes affected and non-affected skin samples. The vertical axis represents standardized the relative amounts of lipids. Box plots represent each of the samples obtained from 14 atopic dogs (Infected n=8; non-infected n=6). $p < 0.05$ based on two-way ANOVA of skin condition versus swab culture result for *S. pseudintermedius* after False Discovery Rate (FDR) correction for multiple comparisons.

4.4.4 Potential lipid biomarkers for atopic dermatitis and disease progression

To identify potential lipid biomarkers to be used for predictive analysis, we performed a two-step feature selection strategy to select only the lipids with high accuracy prediction capability. Step one consisted of selection of features associated with a significant univariate effect size separating the CADESI cohorts, computed via ANOVA, and not associated with a significant effect size regarding sex differences. In step two an elastic net regression was used to reduce the number of features by eliminating the unnecessary ones. The features selected during elastic net regression were ranked by the effect size and the top 10 were used in further analysis. The lipids with a high predictive capability are listed in Table 4 along with their tentative attribution and relative importance. Selected lipids included one TAG with an oleic acid as one of the acyl residues that was reduced in atopic samples compared to healthy. All other lipids selected, namely sphingosine, C24-sphingosine ceramide, C16-phytoceramide, C18:1-phytoceramide, one hydroxyladed phytoceramide, two long chain acylcarnitine and a lysophosphatidylcholine, were increased in atopic compared with healthy epidermis. Since the lipid features selected by E-NET did not include the lipids influenced by *S. pseudintermedius* infection, its presence or absence did not interfere with the predictive capability of the lipid biomarkers.

Two types of predictions were performed; one for diagnosis and one for disease progression. A binary classification into atopic or healthy epidermis was performed to evaluate the selected lipids as diagnosis biomarkers, and the correlation of relative amounts of lipids with standardize CADESI-4 score was performed to evaluate the lipids as biomarkers of disease progression.

Table 4: Top lipid features selected by higher η^2 effect size

Transition	Relative importance, scaled [0,100]	Interpretation Tentative Attribution
850.8->551.8	100	TAG(50:2)_FA 18:1
538.2->282.096	99.444	CerNP(t18:0/16:0)
456.4->85.1	69.378	Arachidyl carnitine
300.1->282.096	66.866	Sphingosine
386.3->85.096	31.633	O-hydroxytetradecenoyl-L-carnitine
281.3->281.3	29.299	N/A
650.6447->264.3	24.669	CerNS(d18:1/24:0)
650.3->282.096	8.049	CerAP(t18:1/22:0)OH
566.1->282.096	4.302	CerNP(t18:0/18:1)
496.2->184.096	0.29	16:0 LYSO-PC/PC(O-14:0/2:0)

4.4.4.1 Evaluation of potential biomarkers for diagnosis by Receiver Operator Characteristic (ROC) curves analysis.

ROC curve plots sensitivity versus specificity of a single or panel of features to classify the samples based on an optimal cut-off. In order to evaluate the performance of the selected lipids as diagnosis biomarkers, we performed ROC curve analysis using a subset of atopic (n=26) and control (n=11) samples which were used as a training set. The remaining samples, called "new samples" (atopic n=15; control n=10) were left un-labeled so the model calculated the probability of each sample for each class. The area under the curve (AUC) of the multivariate model based on the average performance of the cross-validation operation was 0.98 with an 95% CI:0.888-1 and, the empirical p-value of the permutations test was $p < 0.001$ (S8 Figures).

All samples, including samples from non-affected skin, were used for the evaluation of the selected lipids. Individual assessment of lipids by univariate ROC curve can be found in S9 Figure of the supporting information. The confusion matrix of the model training showed that 3 samples were misclassified into control (Figure 26). One sample was from affected skin of a dog with a low CADESI-4 of 30, the other two samples were from non-affected skin areas which may account for the misclassification.

Next, we used the trained model by cross-validation to classify the "new samples". The probability results of the "new samples" are listed in Table 5. A control sample was misclassified into the atopic group with a probability of 0.59 out of 1. All samples from atopic dogs were accurately classified, even the ones from non-affected skin areas with an average probability of 0.96. The evaluation results of the lipid features as diagnosis biomarkers for CAD suggest that, this panel of lipids can provide high predictive accuracy.

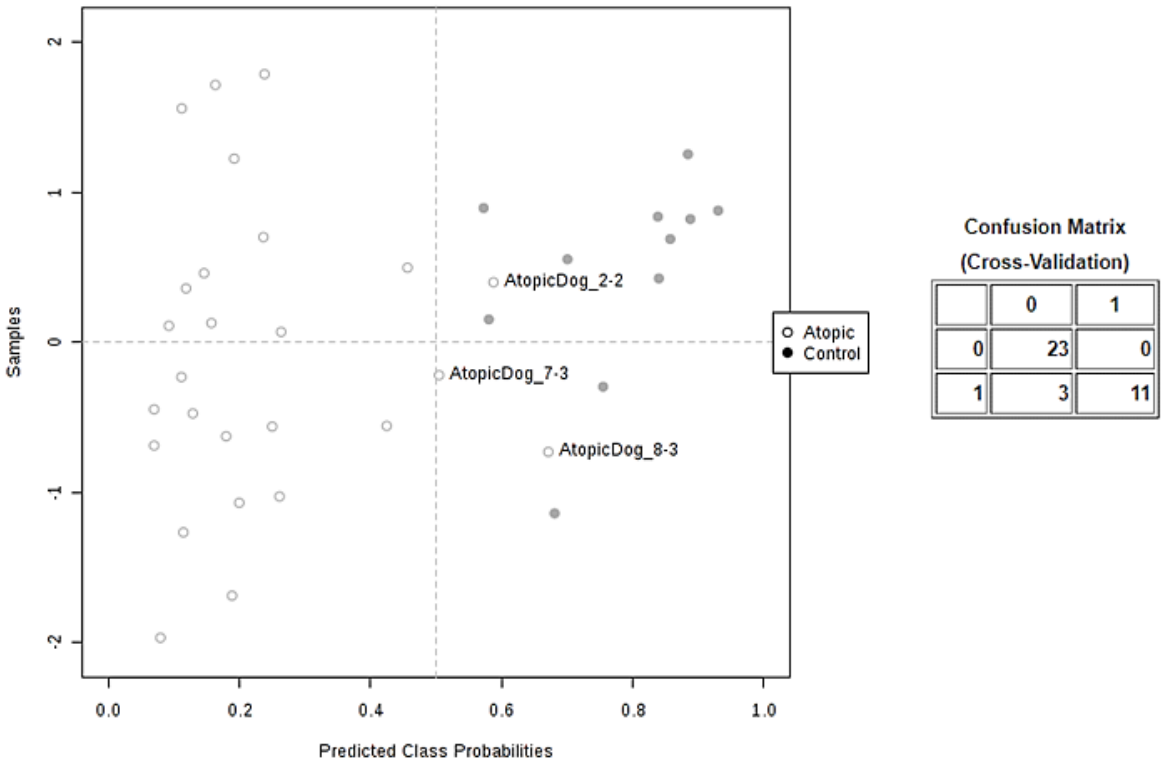

Figure 26**. ROC curve prediction for training set using selected features**. Prediction of samples used to build the ROC curve. Out of a subset of atopic (n=26) and control (n=11) dog samples, three were misclassified. These corresponded to non-affected skin and an atopic dog with the lower CADESI-4 Score.

Table 5: Classification probability of non-label samples by ROC curve using the selected lipid features.

Sample Name	Skin condition	Probability	Predicted	Actual
AtopicDog_10-2	Affected	0.98	Atopic	Atopic
AtopicDog_11-2	Affected	1.00	Atopic	Atopic
AtopicDog_12-2	Affected	0.99	Atopic	Atopic
AtopicDog_13-3	Non-affected	0.96	Atopic	Atopic
AtopicDog_14-3	Non-affected	1.00	Atopic	Atopic
AtopicDog_16-2	Affected	1.00	Atopic	Atopic
AtopicDog_2-1	Affected	0.89	Atopic	Atopic
AtopicDog_3-1	Affected	0.99	Atopic	Atopic
AtopicDog_4-1	Affected	0.95	Atopic	Atopic
AtopicDog_5-1	Affected	0.99	Atopic	Atopic
AtopicDog_6-1	Affected	1.00	Atopic	Atopic
AtopicDog_6-3	Non-affected	0.98	Atopic	Atopic
AtopicDog_7-2	Affected	1.00	Atopic	Atopic
AtopicDog_8-2	Affected	0.88	Atopic	Atopic
AtopicDog_9-2	Affected	0.99	Atopic	Atopic
ControlDog_10-2	Healthy	0.82	Control	Control
ControlDog_11-1	Healthy	0.59	Atopic	Control
ControlDog_1-2	Healthy	0.83	Control	Control
ControlDog_2-2	Healthy	0.96	Control	Control
ControlDog_3-2	Healthy	0.82	Control	Control
ControlDog_4-2	Healthy	0.93	Control	Control
ControlDog_6-1	Healthy	0.98	Control	Control
ControlDog_7-1	Healthy	0.97	Control	Control
ControlDog_8-1	Healthy	0.94	Control	Control
ControlDog_9-1	Healthy	0.60	Control	Control

4.4.4.2 Discriminant capability of selected lipid features for CADESI score cohorts by sex.

Next, we evaluated the performance of the E-NET selected lipid features to classify the samples into CADESI-04 cohorts by LDA. Low and high-score CADESI cohorts were not significantly different when analyzing the entire sample population. We therefore separated the samples by sex and performed individual LDA for males and females. Also, we subdivided the original cohorts to get closer to the array of possibilities of the observational scoring index. Information about the distribution of the samples used for the LDA can be found in S10 Table of the supporting information.

Samples obtained from female dogs, including affected and non-affected, were easily differentiated among the cohorts in the canonical plot after LDA using the selected ceramides, acylcarnitines and glycerolipids. The classification of the samples was highly accurate, with an entropy R^2 of 0.96 and no samples misclassified. The probabilities for all samples for the corresponding class were above 0.8 (Figure 27).

Analysis of samples obtained from males had an acceptable accuracy. In the canonical plot, samples from healthy dogs were easily differentiated from atopic but the different cohorts of CADESI-04 score were clustering too close to each other. Four samples from the atopic dogs were misclassified to the adjacent classes. Two samples were from non-lesional skin and two were from affected skin areas. The probabilities of the samples to each class are represented on the parallel plots (Figure 28).

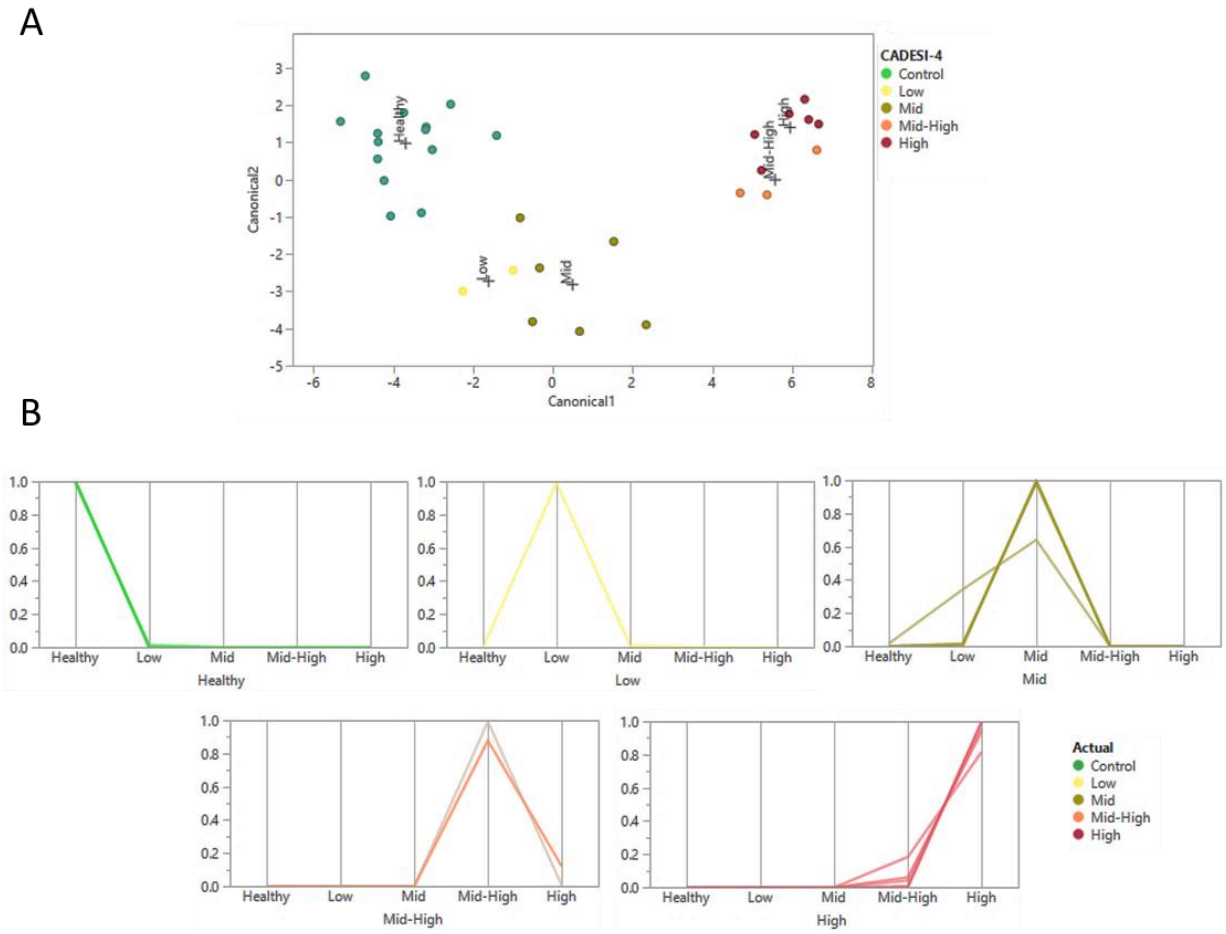

Figure 27**. Linear discriminant analysis for females using the selected lipid features**. (A) Discriminant score plot for CADESI cohort for females (B) Parallel plot illustrating the classification of the samples from females in to the healthy, low, mid, mid-high and high score cohorts by linear discriminant analysis classifier using selected lipids. Each of the 31 samples obtained from 7 healthy and 7 atopic female dogs were accurately classified. Each line represents a sample and is draw according to the probability to each group. (Entropy R^2=0.97, -2LogLikelihood=2.00137; Percent misclassified=3.22581).

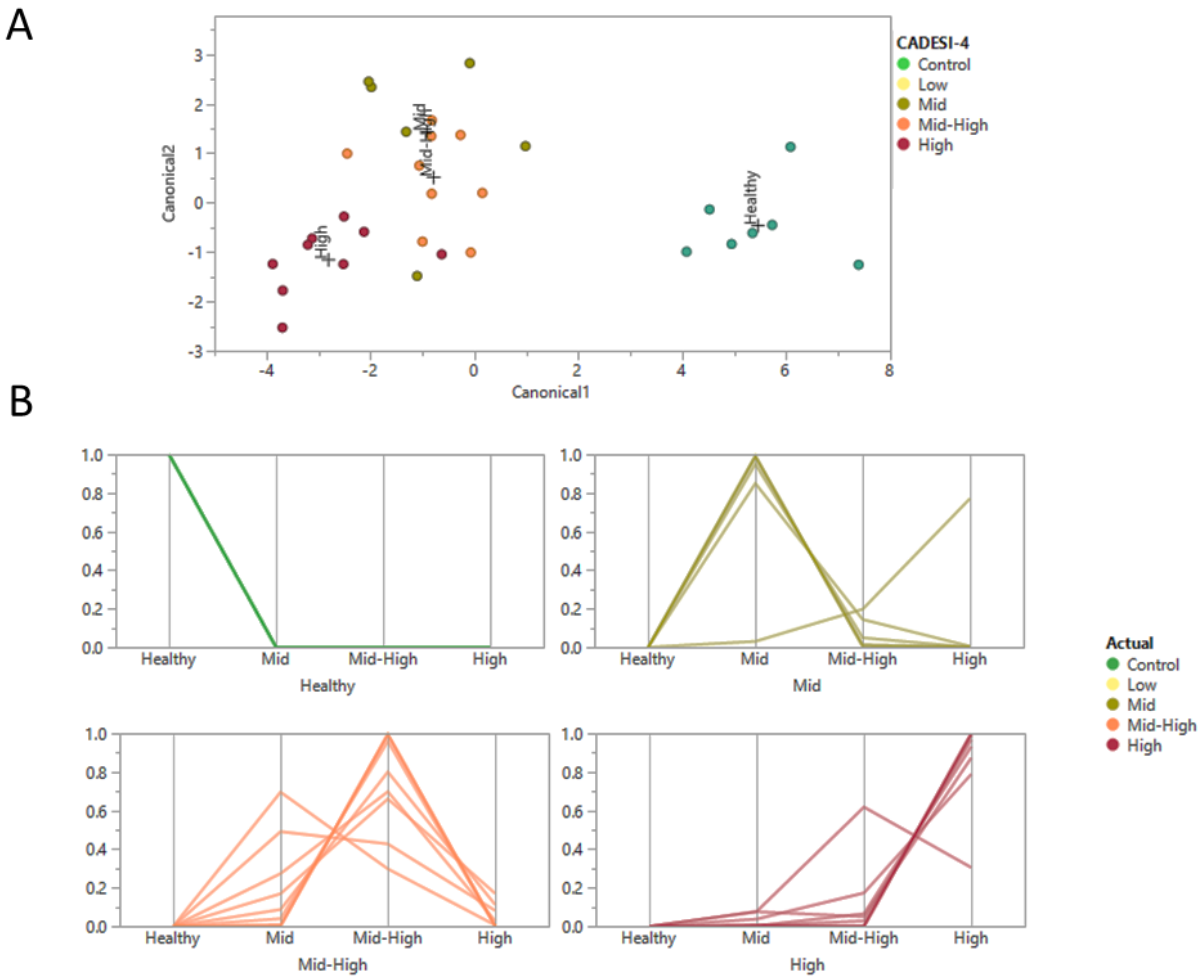

Figure 28**: Linear discriminant analysis for males using the selected lipid features**. (A) Discriminant score plot for CADESI cohort for males (B) Parallel plot illustrating the classification of the samples from males in to the healthy, low, mid, mid-high and high score cohorts by linear discriminant analysis classifier using all selected lipids. Out of 31 samples obtained from 4 healthy and 10 atopic male dogs, 4 were misclassified. Samples misclassified were put in adjacent categories. The actual groups are illustrated separately. Each line represents a sample and is drawn according to the probability to be classified into other group, being the highest point of the line the most probable category. (Entropy R^2=0.79979, -2LogLikelihood=17.0308; Percent misclassified=12.9032).

4.4.4.3 Correlation of predictive Elastic-net regression model with CADESI-4 score cohorts.

A predictive E-net regression model was constructed using the lipid features selected by the two-step feature selection strategy against the standardized CADESI-4. The predictive model was trained by bootstrap using all the samples collected from the recruited dogs independently of the sex or the skin condition at the site of biopsy. The compiled result of all the bootstrap operations is represented in the linear regression plot in Figure 29. The prediction of the standardized CADESI-4 highly correlated with the relative amounts of ceramides, acylcarnitines and glycerolipids with and R^2 of 0.89. The result of the predictive regression model showed that the strategy developed in this study provided a very high prediction rate and simultaneously selected the essential molecular features very precisely to avoid noise and overfit.

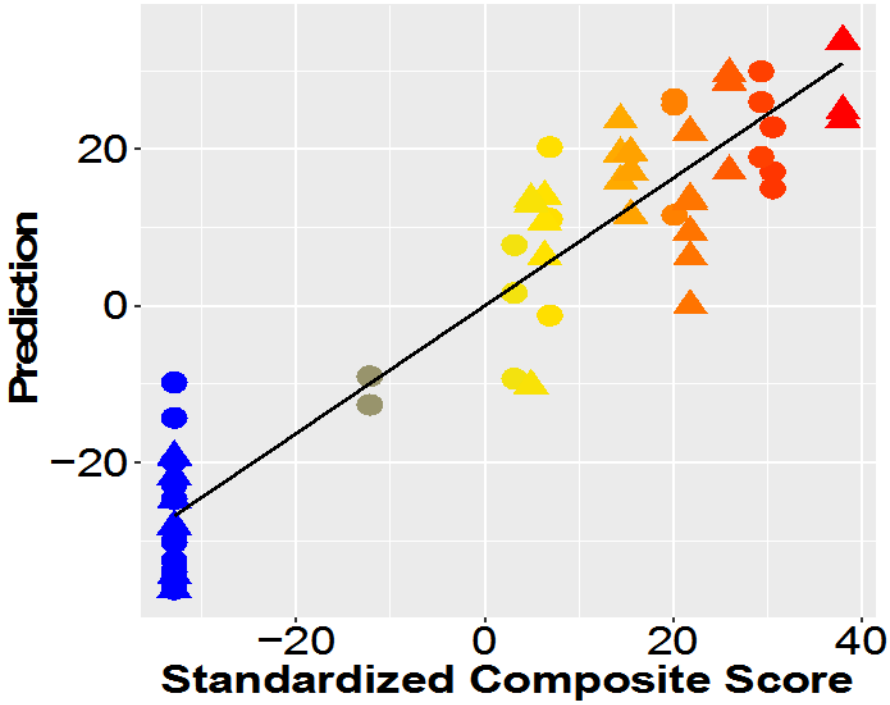

Figure 29**. Relative amounts of selected lipids can predict disease progression**. The model built with the features selected highly correlated (R^2=0.89) the lipid fingerprint with the classification of the standardized clinical severity score, on the basis of the variations in relative amounts TAG containing oleic acid, ceramides, long chain acylcarnitines and lyso-phosphatidylcholine.

4.5 Discussion

Lipidomics analysis are powerful sources of information in metabolism research and biomarker discovery (33,46). Clinically diagnosed atopic dogs presented an altered lipid profile compared to healthy controls. Individual lipid analysis showed that TAGs containing oleic acid (TAG_18:1) were decreased and free oleic acid was increased in CAD compared to healthy. In non-affected skin, TAG_18:1 (50:2) was significantly reduced compared to control and was further reduced in affected skin. Bee venom and house dust mite (HDM) are able to drive the expression of cytosolic phospholipase A_2 ($cPLA_2$) in antigen-presenting cells (APC), which cleaves fatty acids from their own PC and TAGs to generate self-antigens such as oleic acid (47–50). These cleaved fatty acids can be presented directly to autoreactive T cells by CD1a-expresing innate lymphoid cells (ILC), Langerhans cells or plasmacytoid dendritic cells in the skin triggering a rapid production of IL-5, IL-13, and IL-22 (50–52). Cluster of differentiation (CD)1a is express by APC's in dogs (53) and the early response to HDM in canine AD models is characterized by increase in IL-5, IL-13 and IL-22 (54). In a conceptual synergy, it could be proposed that TAGs with oleic acid in the fatty acid residues could be being consumed by $cPLA_2$ with the subsequent release and increased levels of oleic acid in CAD patient's epidermis. Oleic acid accumulation intensifies as the skin gets affected and under a lipid surveillance of APCs in the skin is presented to autoreactive T cells (51). HDM sensitized dogs have up-regulated expression of IL-22 6 hours after exposure which can cause epidermal hyperplasia (55). The proliferation of cells in the epidermis could account for some of the changes observed in the lipid profile as more lipids are produced to meet the need to form more plasma membranes and organelles (56). Additional early responses to HDM exposure included down-regulation of ELOVL1, required for elongation of VLCFA, such as 26:0 and 28:0 that we found reduced even in non-lesional skin of CAD patients. VLCFA are essential for the formation and maintenance of the lipid matrix (57,58) and their reduction can directly impair the barrier function of the skin, as does the inhibitory effect of IL-22 in epidermal differentiation-mediated proteins (55).

Lipid homeostasis is a tightly regulated process (56,59–61). Alteration in lipid ratios can trigger a chain reaction of lipid dysregulations, leading to disorganization of plasma and organelle bilayers generating cell stress or accumulation of bioactive lipids. These can be read as loss of cellular homeostasis by innate immune cells and mount a response to it (60,62,63). The advantage of a lipid profile compared to the analysis of targeted molecules is that it provides a biological

read-out of the epidermis status, based on relative amounts of lipids present in plasma membranes, organelles, cytosol, and extracellular spaces (64) representing all the possible molecular and cellular scenarios taking place at the sampling moment. Seen from a systems biology approach, lipidomics is useful for identification of biomarkers in diseases as heterogeneous as AD, as the majority of alterations, independent of their cause, will be represented as close to the phenotype as possible (59,65,66).

Profiling of 222 lipids from the epidermis of CAD patients allowed the classification of the samples as atopic affected, atopic non-affected or healthy with an overall good accuracy. The clear separation of healthy and non-affected samples confirms that lipids in atopic skin are altered even though the skin appears clinically healthy. These results are supported by previous findings of ultrastructural alterations of the *stratum corneum* and changes in ceramides in non-affected skin from atopic dogs (29,67,68). This suggests that it is not necessary to collect samples from affected areas that are more sensitive and delicate than non-affected ones. Therefore, the possibility to screen for CAD in dogs, using lipid profiling, before the clinical onset of the disease exists should be further investigated. Furthermore, changes in epidermal lipids reflect the disease severity of the patients evaluated by CADESI-4. Few studies have investigated the correlation of parameters with CADESI evaluated disease severity. Correlation of TEWL as a measure of barrier dysfunction with disease severity scores had variable results as the TEWL measurement is inconsistent across instruments and body sites (18–20).

To the best of our knowledge, this is the first report of the influence of sex in the epidermal lipid response to disease severity in CAD patients. Female dogs had a stronger change in their lipid profile as the disease progressed compared with males in which the lipid profile did not reflect the increase in disease severity. This observation was independent of the reproductive status, since the groups included intact animals and animals that were neutered and spayed. This fact suggests that the observed sex dimorphism is not under direct influence of steroid hormones as has been proposed for people (69).

The feature selection strategy employed in this study allowed us to filter out lipids that were responsive to other factors, like sex or changes due to infection by *S. aureus*, selecting only the lipids that were related to AD disease. The panel of biomarkers proposed here includes lipids that could be involved in several processes considered to play important roles in the development and progression of AD: TAG_18:1 and LPC as results of $cPLA_2$ action (47,51), ceramides that are

involved in envelope corneocyte and lipid matrix formation (70,71), long chain acylcarnitine that can trigger apoptosis of cells (72), sphingosines that are involved in cell signaling and proliferation of cells (73). An unattributed *m/z* value was included in this panel but considering the importance of recently discovered lipids such as special pro-resolution mediators (74,75) and the still massive size of undiscover lipidome (57), we decided to include it as it passed all the filter steps. The E-net strategy ensures that the lipid biomarkers selected provided a robust response that allows analysis of samples in different batches or different instruments and obtain accurate classification based on disease and no other practical variabilities (66,76–78).

A panel of biomarkers was suggested to be better suited for diagnosis and disease severity of AD in humans due to its heterogenicity (15). The lipid biomarker panel proposed here could predict the clinical diagnosis of the dogs, as atopic or healthy, from epidermal samples that included non-affected and affected skin areas, with high accuracy, sensitivity and specificity measured by ROC curve analysis. Further research is necessary to investigate its utility as a diagnostic test for CAD. The strong correlation of the selected lipids with disease severity indicated by the CADESI-4 score indicates that this lipid panel could be used as a molecular read-out of disease severity in atopic dogs and could provide an objective assessment of response therapy. This is urgently needed in AD research to unravel its pathogenesis and to identify and evaluate new courses of treatment.

4.6 References

1. Marsella R, Sousa CA, Gonzales AJ, Fadok VA. Current understanding of the pathophysiologic mechanisms of canine atopic dermatitis. J Am Vet Med Assoc. 2012;241(2):194–207.
2. Weidinger S, Novak N. Atopic dermatitis. Lancet (London, England). 2016 Mar 12;387(10023):1109–22.
3. Barbarot S, Auziere S, Gadkari A, Girolomoni G, Puig L, Simpson EL, et al. Epidemiology of atopic dermatitis in adults: Results from an international survey. Allergy Eur J Allergy Clin Immunol. 2018;73(6):1284–93.
4. Hillier a, Griffin CE. The ACVD task force on canine atopic dermatitis (X): is there a relationship between canine atopic dermatitis and cutaneous adverse food reactions? Vet Immunol Immunopathol. 2001;81(3–4):227–31.

5. Marsella R, De Benedetto A. Atopic Dermatitis in Animals and People: An Update and Comparative Review. Vet Sci. 2017;4(3):37.

6. Marsella R, Girolomoni G. Canine models of atopic dermatitis: a useful tool with untapped potential. J Invest Dermatol. 2009;129(10):2351–7.

7. Martel BC, Lovato P, Bäumer W, Olivry T. Translational Animal Models of Atopic Dermatitis for Preclinical Studies. Yale J Biol Med. 2017;90(3):389–402.

8. Favrot C, Steffan J, Seewald W, Picco F. A prospective study on the clinical features of chronic canine atopic dermatitis and its diagnosis. Vet Dermatol. 2010;21(1):23–31.

9. Krause L, Mourantchanian V, Brockow K, Theis FJ, Schmidt-Weber CB, Knapp B, et al. A computational model to predict severity of atopic eczema from 30 serum proteins. J Allergy Clin Immunol. 2016;138(4):1207–1210.e2.

10. Thijs JL, de Bruin-Weller MS, Hijnen DJ. Current and Future Biomarkers in Atopic Dermatitis. Immunol Allergy Clin North Am. 2017;37(1):51–61.

11. Thijs JL, Strickland I, Bruijnzeel-Koomen CAFM, Nierkens S, Giovannone B, Knol EF, et al. Serum biomarker profiles suggest that atopic dermatitis is a systemic disease. J Allergy Clin Immunol. 2018;141(4):1523–6.

12. Thijs J, van Seggelen W, Bruijnzeel-Koomen C, de Bruin-Weller M, Hijnen D. New Developments in Biomarkers for Atopic Dermatitis. J Clin Med. 2015;4(3):479–87.

13. Thijs JL, Strickland I, Bruijnzeel-Koomen CAFM, Nierkens S, Giovannone B, Csomor E, et al. Moving toward endotypes in atopic dermatitis: Identification of patient clusters based on serum biomarker analysis. J Allergy Clin Immunol. 2017;140(3):730–7.

14. Santoro D. Therapies in Canine Atopic Dermatitis. Vet Clin North Am Small Anim Pract. 2019;49(1):9–26.

15. Thijs JL, Nierkens S, Herath A, Bruijnzeel-Koomen CAF, Knol EF, Giovannone B, et al. A panel of biomarkers for disease severity in atopic dermatitis. Clin Exp Allergy. 2015;45(3):698–701.

16. Almela RM, Rubio CP, Cerón JJ, Ansón A, Tichy A, Mayer U. Selected serum oxidative stress biomarkers in dogs with non-food-induced and food-induced atopic dermatitis. Vet Dermatol. 2018;29(3):229-e82.

17. Zając M, Szczepanik MP, Wilkołek PM, Adamek ŁR, Pomorski ZJH, Sitkowski W, et al. Assessment of a correlation between Canine Atopic Dermatitis Extent and Severity Index (CADESI-03) and selected biophysical skin measures (skin hydration, pH, and erythema intensity) in dogs with naturally occurring atopic dermatitis. Can J Vet Res. 2015;79(2):136–40.
18. Zając M, Szczepanik MP, Wilkołek PM, Adamek ŁR, Pomorski ZJH, Sitkowski W, et al. Assessment of the relationship between transepidermal water loss (TEWL) and severity of clinical signs (CADESI-03) in atopic dogs. Vet Dermatol. 2014;25(6):503-e83.
19. Marsella R. Are transepidermal water loss and clinical signs correlated in canine atopic dermatitis? A compilation of studies. Vet Dermatol. 2012;23(3).
20. Cobiella D, Archer L, Bohannon M, Santoro D. Pilot study using five methods to evaluate skin barrier function in healthy dogs and in dogs with atopic dermatitis. Vet Dermatol. 2019;20–2.
21. Cornegliani L, Vercelli A, Sala E, Marsella R. Transepidermal water loss in healthy and atopic dogs, treated and untreated: a comparative preliminary study. Vet Dermatol. 2012;23(1):41-e10.
22. van Smeden J, Janssens M, Boiten WA, van Drongelen V, Furio L, Vreeken RJ, et al. Intercellular skin barrier lipid composition and organization in Netherton syndrome patients. J Invest Dermatol. 2014;134(5):1238–45.
23. Feingold KR, Elias PM. Role of lipids in the formation and maintenance of the cutaneous permeability barrier. Biochim Biophys Acta - Mol Cell Biol Lipids. 2014;1841(3):280–94.
24. van Smeden J, Janssens M, Gooris GS, Bouwstra JA. The important role of stratum corneum lipids for the cutaneous barrier function. Biochim Biophys Acta - Mol Cell Biol Lipids. 2014 Mar;1841(3):295–313.
25. van Smeden J, Janssens M, Kaye ECJ, Caspers PJ, Lavrijsen AP, Vreeken RJ, et al. The importance of free fatty acid chain length for the skin barrier function in atopic eczema patients. Exp Dermatol. 2014 Jan;23(1):45–52.
26. Janssens M, van Smeden J, Gooris GS, Bras W, Portale G, Caspers PJ, et al. Increase in short-chain ceramides correlates with an altered lipid organization and decreased barrier function in atopic eczema patients. J Lipid Res. 2012;53(12):2755–66.

27. Danso MO, van Drongelen V, Mulder A, van Esch J, Scott H, van Smeden J, et al. TNF-α and Th2 cytokines induce atopic dermatitis-like features on epidermal differentiation proteins and stratum corneum lipids in human skin equivalents. J Invest Dermatol. 2014;134(7):1941–50.

28. Reiter L V, Torres SMF, Wertz PW. Characterization and quantification of ceramides in the nonlesional skin of canine patients with atopic dermatitis compared with controls. Vet Dermatol. 2009;20(4):260–6.

29. Shimada K, Yoon J-S, Yoshihara T, Iwasaki T, Nishifuji K. Increased transepidermal water loss and decreased ceramide content in lesional and non-lesional skin of dogs with atopic dermatitis. Vet Dermatol. 2009;20(5–6):541–6.

30. Chermprapai S, Broere F, Gooris G, Schlotter YM, Rutten VPMG, Bouwstra JA. Altered lipid properties of the stratum corneum in Canine Atopic Dermatitis. Biochim Biophys Acta - Biomembr. 2018;1860(2):526–33.

31. Popa I, Pin D, Remoué N, Remoué N, Osta B, Callejon S, et al. Analysis of epidermal lipids in normal and atopic dogs, before and after administration of an oral omega-6/omega-3 fatty acid feed supplement. A pilot study. Vet Res Commun. 2011;35(8):501–9.

32. Angelbeck-Schulze M, Mischke R, Rohn K, Hewicker-Trautwein M, Naim HY, Bäumer W. Canine epidermal lipid sampling by skin scrub revealed variations between different body sites and normal and atopic dogs. BMC Vet Res. 2014;10(1):152.

33. Han X. Lipidomics for studying metabolism. Nat Rev Endocrinol. 2016;12(11):668–79.

34. Tetsuya H, Kenji K. Prostanoids and leukotrienes in the pathophysiology of atopic dermatitis and psoriasis. Int Immunol. 2019;1–7.

35. Lizardo DY, Parisi LR, Li N, Atilla-Gokcumen GE. Noncanonical Roles of Lipids in Different Cellular Fates. Biochemistry. 2018;57(1):22–9.

36. Fischer CL, Blanchette DR, Brogden K a., Dawson D V., Drake DR, Hill JR, et al. The roles of cutaneous lipids in host defense. Biochim Biophys Acta - Mol Cell Biol Lipids. 2014;1841(3):319–22.

37. Li S, Ganguli-Indra G, Indra AK. Lipidomic analysis of epidermal lipids: a tool to predict progression of inflammatory skin disease in humans. Expert Rev Proteomics. 2016;13(5):451–6.

38. Sadowski T, Klose C, Gerl MJ, Wójcik-Maciejewicz A, Herzog R, Simons K, et al. Large-scale human skin lipidomics by quantitative, high-throughput shotgun mass spectrometry. Sci Rep. 2017;7:43761.

39. Merrill AH, Sullards MC, Allegood JC, Kelly S, Wang E. Sphingolipidomics: high-throughput, structure-specific, and quantitative analysis of sphingolipids by liquid chromatography tandem mass spectrometry. Methods. 2005;36(2):207–24.

40. Li K, Naviaux JC, Bright AT, Wang L, Naviaux RK. A robust, single-injection method for targeted, broad-spectrum plasma metabolomics. Metabolomics. 2017;13(10):1–12.

41. Franco J, Ferreira C, Paschoal Sobreira TJ, Sundberg JP, HogenEsch H. Profiling of epidermal lipids in a mouse model of dermatitis: Identification of potential biomarkers. Witt SN, editor. PLoS One. 2018;13(4):e0196595.

42. Wang M, Wang C, Han RH, Han X. Novel advances in shotgun lipidomics for biology and medicine. Prog Lipid Res. 2016;61:83–108.

43. Schwudke D, Schuhmann K, Herzog R, Bornstein SR, Shevchenko A. Shotgun lipidomics on high resolution mass spectrometers. Cold Spring Harb Perspect Biol. 2011 ;3(9):a004614

44. Ferreira CR, Yannell KE, Mollenhauer B, Espy RD, Cordeiro FB, Ouyang Z, et al. Chemical profiling of cerebrospinal fluid by multiple reaction monitoring mass spectrometry. Analyst. 2016;141(18):5252–5.

45. Xia J, Sinelnikov I V., Han B, Wishart DS. MetaboAnalyst 3.0--making metabolomics more meaningful. Nucleic Acids Res. 2015;43(W1):W251-7.

46. Kendall AC, Koszyczarek MM, Jones EA, Hart PJ, Towers M, Griffiths CEM, et al. Lipidomics for translational skin research: A primer for the uninitiated. Exp Dermatol. 2018;4:1–8.

47. Bourgeois EA, Subramaniam S, Cheng T-Y, De Jong A, Layre E, Ly D, et al. Bee venom processes human skin lipids for presentation by CD1a. J Exp Med. 2015;212(2):149–63.

48. de Jong A, Cheng T, Huang S, Gras S, Birkinshaw RW, Kasmar AG, et al. CD1a-autoreactive T cells recognize natural skin oils that function as headless antigens. Nat Immunol. 2014;15(2):177–85.

49. De Jong A, Peña-Cruz V, Cheng TY, Clark RA, Van Rhijn I, Moody DB. CD1a-autoreactive T cells are a normal component of the human αβ T cell repertoire. Nat Immunol. 2010;11(12):1102–9.

50. Hardman CS, Chen YL, Salimi M, Jarrett R, Johnson D, Järvinen VJ, et al. CD1a presentation of endogenous antigens by group 2 innate lymphoid cells. Sci Immunol. 2017;2(18):1–13.

51. De Jong A, Cheng TY, Huang S, Gras S, Birkinshaw RW, Kasmar AG, et al. CD1a-autoreactive T cells recognize natural skin oils that function as headless antigens. Nat Immunol. 2014;15(2):177–85.

52. Colonna M. Skin function for human CD1a-reactive T cells. Nat Immunol. 2010;11(12):1079–80.

53. Looringh Van Beeck FA, Zajonc DM, Moore PF, Schlotter YM, Broere F, Rutten VPMG, et al. Two canine CD1a proteins are differentially expressed in skin. Immunogenetics. 2008;60(6):315–24.

54. Olivry T, Mayhew D, Paps JS, Linder KE, Peredo C, Rajpal D, et al. Early Activation of Th2/Th22 Inflammatory and Pruritogenic Pathways in Acute Canine Atopic Dermatitis Skin Lesions. J Invest Dermatol. 2016;136(10):1961–9.

55. Olivry T, Mayhew D, Paps JS, Linder KE, Peredo C, Rajpal D, et al. Early Activation of Th2/Th22 Inflammatory and Pruritogenic Pathways in Acute Canine Atopic Dermatitis Skin Lesions. J Invest Dermatol. 2016;136(10):1961–9.

56. Holthuis JCM, Menon AK. Lipid landscapes and pipelines in membrane homeostasis. Nature. 2014 Jun 5;510(7503):48–57.

57. Jia Y, Gan Y, He C, Chen Z, Zhou C. The mechanism of skin lipids influencing skin status. J Dermatol Sci. 2018;89(2):112–9.

58. Danso MMO, Boiten W, van Drongelen V, Gmelig KM, Gooris G, El Ghalbzouri A, et al. Altered expression of epidermal lipid bio-synthesis enzymes in atopic dermatitis skin is accompanied by changes in stratum corneum lipid composition. J Dermatol Sci. 2017 May;88(1):57–66.

59. Hyötyläinen T, Orešič M. Systems biology strategies to study lipidomes in health and disease. Prog Lipid Res. 2014;55(1):43–60.

60. Wymann MP, Schneiter R. Lipid signalling in disease. Nat Rev Mol Cell Biol. 2008;9(2):162–76.

61. Young MM, Kester M, Wang H-G. Sphingolipids: regulators of crosstalk between apoptosis and autophagy. J Lipid Res. 2013;54(1):5–19.

62. Liston A, Masters SL. Homeostasis-altering molecular processes as mechanisms of inflammasome activation. Nat Rev Immunol. 2017;17(3):208–14.

63. Köberlin MS, Snijder B, Heinz LX, Baumann CL, Fauster A, Vladimer GI, et al. A Conserved Circular Network of Coregulated Lipids Modulates Innate Immune Responses. Cell. 2015;162(1):170–83.

64. Ghosh D, Bernstein JA, Khurana Hershey GK, Rothenberg ME, Mersha TB. Leveraging Multilayered "Omics" Data for Atopic Dermatitis: A Road Map to Precision Medicine. Front Immunol. 2018 Dec 12;9:1–22.

65. Stephenson DJ, Hoeferlin LA, Chalfant CE. Lipidomics in translational research and the clinical significance of lipid-based biomarkers. Transl Res. 2017;189:13–29.

66. Zhao Y, Cheng X, Lin R. Lipidomics Applications for Discovering Biomarkers of Diseases in Clinical Chemistry. Vol. 313, International Review of Cell and Molecular Biology. Elsevier Inc.; 2018. 1-26 p.

67. Santoro D, Marsella R, Pucheu-Haston CM, Eisenschenk MNCC, Nuttall T, Bizikova P. Review: Pathogenesis of canine atopic dermatitis: skin barrier and host-micro-organism interaction. Vet Dermatol. 2015;26(2):84-e25.

68. Inman a. O, Olivry T, Dunston SM, Monteiro-Riviere N a., Gatto H. Electron microscopic observations of stratum corneum intercellular lipids in normal and atopic dogs. Vet Pathol. 2001;38(6):720–3.

69. Sacotte R, Silverberg JI. Epidemiology of adult atopic dermatitis. Clin Dermatol. 2018;36(5):595–605.

70. Mojumdar EH, Kariman Z, van Kerckhove L, Gooris GS, Bouwstra J a. The role of ceramide chain length distribution on the barrier properties of the skin lipid membranes. Biochim Biophys Acta. 2014;1838(10):2473–83.

71. Rabionet M, Gorgas K, Sandhoff R. Ceramide synthesis in the epidermis. Biochim Biophys Acta - Mol Cell Biol Lipids. 2014;1841(3):422–34.

72. Rutkowsky JM, Knotts T a, Ono-Moore KD, McCoin CS, Huang S, Schneider D, et al. Acylcarnitines activate proinflammatory signaling pathways. Am J Physiol Endocrinol Metab. 2014;306(12):E1378-87.

73. Uchida Y. Ceramide signaling in mammalian epidermis. Biochim Biophys Acta - Mol Cell Biol Lipids. 2014;1841(3):453–62.

74. Spite M, Clària J, Serhan CN. Resolvins, specialized proresolving lipid mediators, and their potential roles in metabolic diseases. Cell Metab. 2014;19(1):21–36.

75. Serhan CN, Yacoubian S, Yang R. Anti-Inflammatory and Proresolving Lipid Mediators. Annu Rev Pathol Mech Dis. 2008;3(1):279–312.

76. Majd TM, Kalantari S, Shahraki HR, Nafar M, Almasi A, Samavat S, et al. Application of sparse linear discriminant analysis and elastic net for diagnosis of IgA nephropathy: Statistical and biological viewpoints. Iran Biomed J. 2018;22(6):374–84.

77. Alexandrov T, Kesz O, Lorenz D a, Schiffler S, Steinhorst K. An active set approach to the elastic-net and its applications in mass spectrometry. Signal Process with Adapt Sparse Struct Represent. 2009;1:1–4.

78. Zou H, Hastie T. Regularization and variable selection via the elastic net. J R Stat Soc B. 2005;67(2):301–20.

4.7 Supporting information

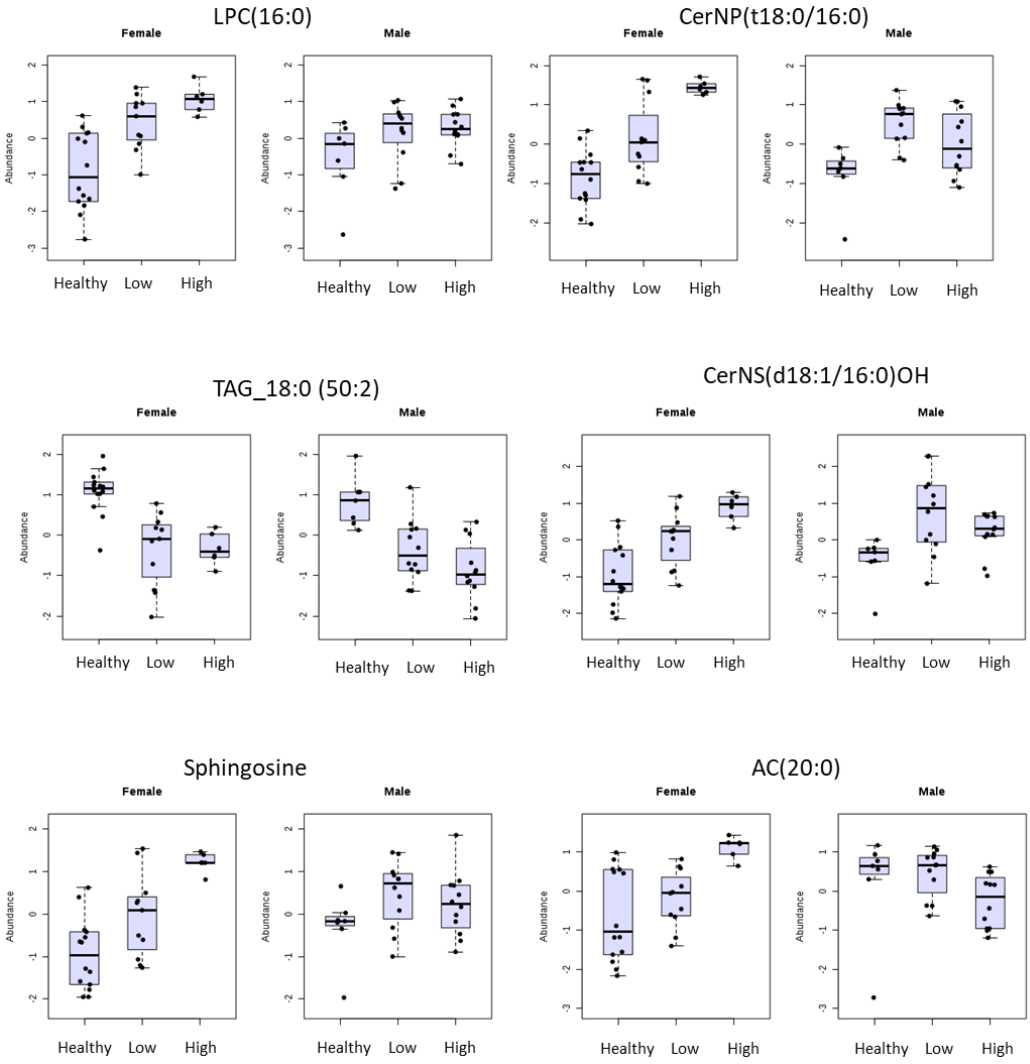

S8 Figure: Boxplots CADESI cohort by sex.

Significant lipid features for CADESI but not sex ($p<0.05$) after two-way ANOVA of CADESI cohort by sex. Although not significant, the differences in trend between male and female is sufficient to turn the lipid profile unable to discriminate between low and high-scores.

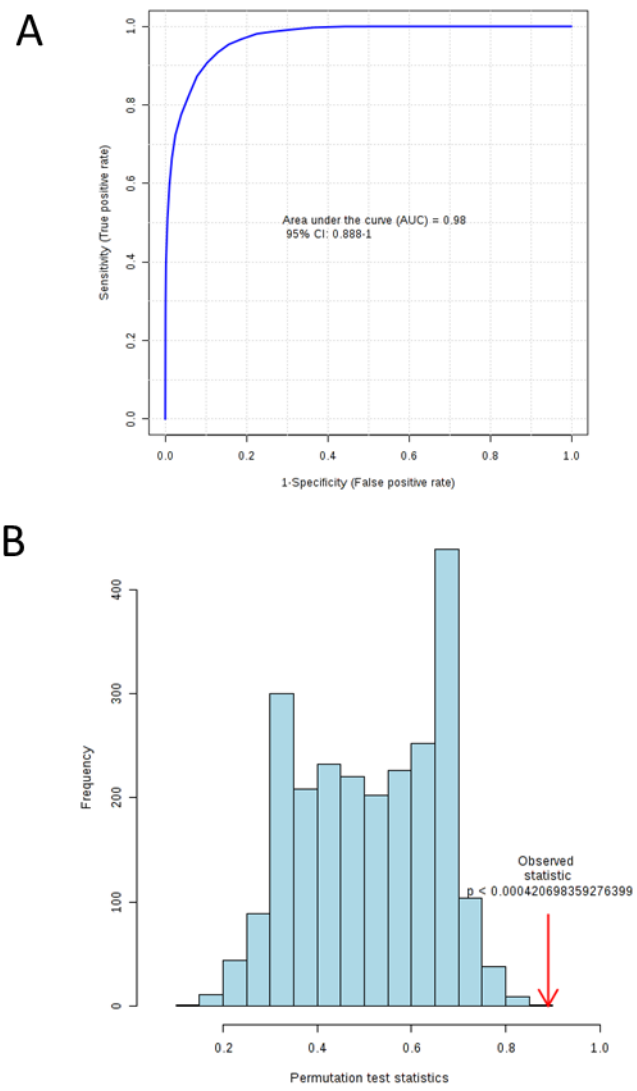

S9 Figure: Multivariate ROC curve accuracy evaluation

(A) Area under the curve of the ROC multivariate model. (B) Permutation test of the ROC model.

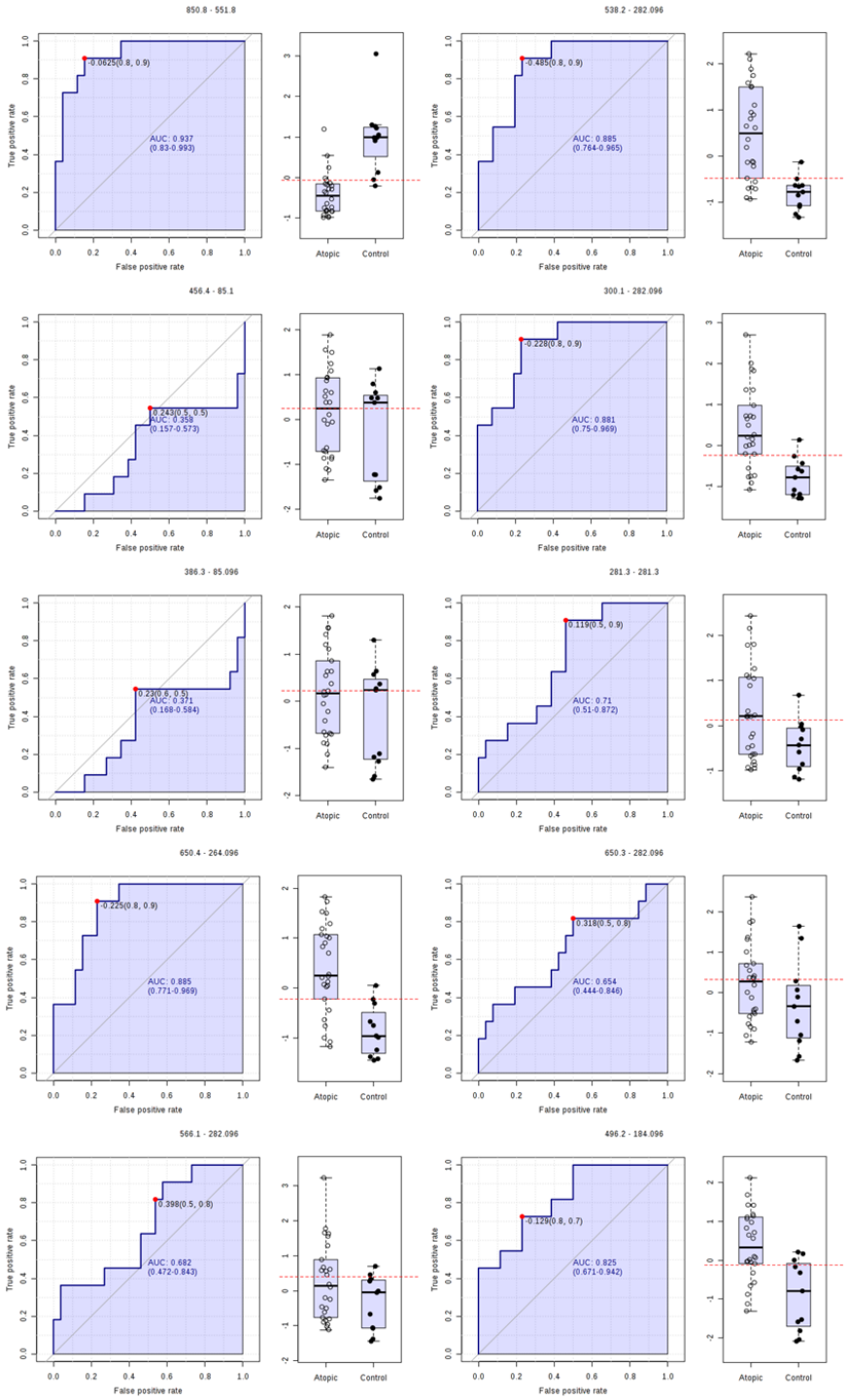

S10 Figure: Individual ROC curves of the lipid features selected by E-net.

S9 Table: Swab culture results

Atopic patients	*Staphylococcus pseudintermedius*	*Malassezia*	*Streptococcus*	Positive MecA
Infected	8	2	3	2
Non-infected	6	12	11	12

S10 Table: CADESI-4 cohort sample information

CADESI Cohort	Detailed CADESI Cohort	Total Score Cadesi-4	Samples from females	Samples from males	Total samples obtained from dogs*	Number of recruited dogs		Clinical diagnosis
						Females	Males	
Healthy	Healthy	0	14	7	21	7	4	Control
Low	Low	30	2	0	41	7	7	Atopic
	Mid	60	6	6				
High	Mid-High	85.25	3	9				
	High	102.6	6	9				

*Two samples were lost in sample preparation

CHAPTER 5. GENERAL CONCLUSIONS AND FUTURE DIRECTIONS

The advancement of lipidomics has increased the understanding of lipid functions in cell biology (1–4). The identification of lipids at their molecular level revealed the link between lipid profiles in health and disease beyond traditional analysis of cholesterol LDL or HDL (5–7). The understanding that lipids are more than structural components and rather are molecules that actively participate in cell metabolism and cell signaling and that are surveilled by immune cells, has led to the growing interest in monitoring their changes and to associate these with immune responses (8–13).

High-throughput analysis developed in recent years enabled investigatigation of a large number of molecules at a time accelerating the discovery of lipid alterations in diseases (14,15). Improvements in mass spectrometry technologies have simplified sample preparation allowing the analysis of many molecules from one extraction process instead of having to perform extensive and complicated procedures to recover just a few molecules from one lipid class (16–18).

The lipids of the stratum corneum are essential for the proper formation and maintenance of the barrier function of the skin and changes in the composition have been related to increased penetration of xenobiotics that can trigger exaggerated immune responses (19–23). In atopic dermatitis (AD), changes in the *stratum corneum* species of ceramides and increase of polyunsaturated fatty acids are responsible for a less organized and dense lipid matrix that creates gaps between corneocytes allowing increased penetration of antigens, irritants or allergens (24–26). Immune cells from atopic patients have a type-2 skewed immune response that leads to chronic inflammation (27). Recent findings have shown that changes that take place beyond the *stratum corneum* of the epidermis involving lipids in plasma membranes and organelles can activate the immune system and generate inflammation (6,7,28).

Here, we showed that the lipid profile of the epidermis is altered in dermatitis, and that these changes were not limited to ceramides and fatty acids. On the contrary, the changes encompassed most classes of lipids involved in homeostasis of cell membranes, and normal metabolism of organelles including the mitochondria (5,6,28,29). These alterations could represent a disturbance of the lipid metabolism beyond what has been considered until now and based on the new findings of how immune cells monitor lipid changes, might account for the heterogenicity

of AD immunological manifestations (11,30). Future studies should investigate if different lipid environments can trigger immune cells to respond with different polarizations and cytokine production that could explain the endotypes observed in AD patients.

The lipidomics methodology developed for this research proved to be useful for accelerated discovery of biomarkers in dermatitis as changes in the lipid profile were observed in analysis that takes up to 3 minutes per sample. These changes discriminated between samples of dermatitis or healthy skin for both the mouse model and the atopic dogs. In addition, the methodology was sensitive enough to detect changes in the lipid fingerprint of the epidermis before the onset of the clinical manifestations of the disease. We suggest that our newly developed lipidomics strategy could be useful for the screening of individuals at risk of developing AD based on their epidemiological data allowing for early intervention of this disease (31–33).

The lipidomics methodology allowed classification of samples into categories of disease severity with high accuracy after selecting the lipids with a higher effect size and more predictive of disease progression. Interestingly, and perhaps because of the heterogeneity of AD, these lipids corresponded to different classes and are linked to different routes of cell signaling and inflammation (34,35). This suggests that the lipid dysregulation becomes more severe as the disease progresses. The fact that this panel of lipid biomarkers correlated with the clinical severity index indicates its possible utility as a tool to evaluate treatment response in an objective way, free of inter- or intra observer variability, that can help in the evaluation and development of future therapeutics (36,37).

The combination of the lipidomics method and the statistical analysis developed here yield a panel of biomarkers that are simple to monitor and interpret and that could be implemented as a diagnostic tool that is not time consuming nor more expensive than routine clinical practice analysis. The ratios of lipids selected here as biomarkers provide a robust measurement that is not easily influenced by artifacts of analysis. The development of a kit that integrates the lipidomic method and the Elastic-net algorithm would allow the convenient use of this objective lipid biomarker panel as molecular diagnostic for canine atopic dermatitis.

Suggestions for future studies

1. Evaluate the lipid biomarker panel proposed here in a larger cohort of patients including ones with dermatitis that are differential diagnoses of AD to determine if different types of dermatitis can be discriminated based on their lipid profiles.
2. Investigate immune cell responses under different lipid environments to determine if the composition of lipids can affect the polarization of immune cells and cytokine production.
3. Screen susceptible individuals based on epidemiological data before age of onset of AD to determine if the lipid biomarker panel is predictive of the disease.
4. Follow the patients before and after treatment to evaluate if the lipid profile changes reflect the response to treatment and can be used as a treatment response measurement that helps in therapeutics development.

5.1 References

1. Ferraz EG, Henrique-Araújo R, Fernandez LG, Rolim AEH, de Araújo Alves Dultra FK. Lipidomics in the study of lipid metabolism: Current perspectives in the omic sciences. Gene. 2014;554(2):131–9.
2. Han X. Lipidomics for precision medicine and metabolism: A personal view. Biochim Biophys Acta - Mol Cell Biol Lipids. 2017;1862(8).
3. Stephenson DJ, Hoeferlin LA, Chalfant CE. Lipidomics in translational research and the clinical significance of lipid-based biomarkers. Transl Res. 2017;189:13–29.
4. Kendall AC, Koszyczarek MM, Jones EA, Hart PJ, Towers M, Griffiths CEM, et al. Lipidomics for translational skin research: A primer for the uninitiated. Exp Dermatol. 2018;1–8.
5. Crimi M, Esposti MD. Apoptosis-induced changes in mitochondrial lipids. Biochim Biophys Acta - Mol Cell Res. 2011;1813(4):551–7.
6. McIntyre TM. Bioactive oxidatively truncated phospholipids in inflammation and apoptosis: Formation, targets, and inactivation. Biochim Biophys Acta - Biomembr. 2012;1818(10):2456–64.
7. Holthuis JCM, Menon AK. Lipid landscapes and pipelines in membrane homeostasis. Nature. 2014 5;510(7503):48–57.
8. del Moral MG, Martínez-Naves E. The Role of Lipids in Development of Allergic Responses. Immune Netw. 2017;17(3):133.

9. Han J, Kaufman RJ. The role of ER stress in lipid metabolism and lipotoxicity. J Lipid Res. 2016;57(8):1329–38.

10. Oliphant CJ, Hwang YY, Walker JA, Salimi M, Wong SH, Brewer JM, et al. MHCII-mediated dialog between group 2 innate lymphoid cells and CD4 + T cells potentiates type 2 immunity and promotes parasitic helminth expulsion. Immunity. 2014;41(2):283–95.

11. Bourgeois EA, Subramaniam S, Cheng T-Y, De Jong A, Layre E, Ly D, et al. Bee venom processes human skin lipids for presentation by CD1a. J Exp Med. 2015;212(2):149–63.

12. de Jong AJ, Kloppenburg M, Toes REM, Ioan-Facsinay A. Fatty acids, lipid mediators, and T-cell function. Front Immunol. 2014;5:3–9.

13. Jia Y, Gan Y, He C, Chen Z, Zhou C. The mechanism of skin lipids influencing skin status. J Dermatol Sci. 2018;89(2):112–9.

14. Wang C, Han X, Liu F, Patterson TA, Hanig JP, Paule MG, et al. Lipid profiling as an effective approach for identifying biomarkers/adverse events associated with pediatric anesthesia. Toxicol Appl Pharmacol. 2018;354:191-195.

15. Haslam RP, Feussner I. Green light for lipid fingerprinting. Biochim Biophys Acta - Mol Cell Biol Lipids. 2017;1862(8):782–5.

16. Merrill AH, Sullards MC, Allegood JC, Kelly S, Wang E. Sphingolipidomics: high-throughput, structure-specific, and quantitative analysis of sphingolipids by liquid chromatography tandem mass spectrometry. Methods. 2005;36(2):207–24.

17. Wang M, Wang C, Han RH, Han X. Novel advances in shotgun lipidomics for biology and medicine. Prog Lipid Res. 2016;61:83–108.

18. Han X, Gross RW. Shotgun lipidomics: Electrospray ionization mass spectrometric analysis and quantitation of cellular lipidomes directly from crude extracts of biological samples. Mass Spectrom Rev. 2005;24(3):367–412.

19. Boncheva M. The physical chemistry of the stratum corneum lipids. Int J Cosmet Sci. 2014;36(6):505–15.

20. Breiden B, Sandhoff K. The role of sphingolipid metabolism in cutaneous permeability barrier formation. Biochim Biophys Acta. 2014 Mar;1841(3):441–52.

21. Janssens M, van Smeden J, Gooris GS, Bras W, Portale G, Caspers PJ, et al. Increase in short-chain ceramides correlates with an altered lipid organization and decreased barrier function in atopic eczema patients. J Lipid Res. 2012;53(12):2755–66.

22. Behne M, Uchida Y, Seki T, de Montellano PO, Elias PM, Holleran WM. Omega-Hydroxyceramides are Required for Corneocyte Lipid Envelope (CLE) Formation and Normal Epidermal Permeability Barrier Function. J Invest Dermatol. 2000;114(1):185–92.

23. Rabionet M, Gorgas K, Sandhoff R. Ceramide synthesis in the epidermis. Biochim Biophys Acta - Mol Cell Biol Lipids. 2014;1841(3):422–34.

24.Weidinger S, Novak N. Atopic dermatitis. Lancet (London, England). 2016;387(10023):1109–22.

25. Elias PM, Wakefield JS. Mechanisms of abnormal lamellar body secretion and the dysfunctional skin barrier in patients with atopic dermatitis. J Allergy Clin Immunol. 2014;134(4):781–791.e1.

26. Gittler JK, Krueger JG, Guttman-Yassky E. Atopic dermatitis results in intrinsic barrier and immune abnormalities: Implications for contact dermatitis. J Allergy Clin Immunol. 2013;131(2):300–13.

27. Furue M, Chiba T, Tsuji G, Ulzii D, Kido-Nakahara M, Nakahara T, et al. Atopic dermatitis: immune deviation, barrier dysfunction, IgE autoreactivity and new therapies. Allergol Int. 2017;66(3):398–403.

28. Lizardo DY, Parisi LR, Li N, Atilla-Gokcumen GE. Noncanonical Roles of Lipids in Different Cellular Fates. Biochemistry. 2018;57(1):22–9.

29. Jacquemyn J, Cascalho A, Goodchild RE. The ins and outs of endoplasmic reticulum-controlled lipid biosynthesis. EMBO Rep. 2017;18(11):1905–21.

30. Hardman CS, Chen YL, Salimi M, Jarrett R, Johnson D, Järvinen VJ, et al. CD1a presentation of endogenous antigens by group 2 innate lymphoid cells. Sci Immunol. 2017;2(18):1–13.

31. Marsella R, De Benedetto A. Atopic Dermatitis in Animals and People: An Update and Comparative Review. Vet Sci. 2017;4(3):37.

32. Olivry T, DeBoer DJ, Favrot C, Jackson HA, Mueller RS, Nuttall T, et al. Treatment of canine atopic dermatitis: 2015 updated guidelines from the International Committee on Allergic Diseases of Animals (ICADA). BMC Vet Res. 2015;11(1):1–15.

33. Paller AS, Kabashima K, Bieber T. Therapeutic pipeline for atopic dermatitis: End of the drought? J Allergy Clin Immunol. 2017;140(3):633–43.

34. Wymann MP, Schneiter R. Lipid signalling in disease. Nat Rev Mol Cell Biol. 2008;9(2):162–76.

35. Hubler MJ, Kennedy AJ. Role of lipids in the metabolism and activation of immune cells. J Nutr Biochem. 2016;34(2):1–7.

36. Thijs JL, de Bruin-Weller MS, Hijnen DJ. Current and Future Biomarkers in Atopic Dermatitis. Immunol Allergy Clin North Am. 2017;37(1):51–61.

37. Thijs JL, Nierkens S, Herath A, Bruijnzeel-Koomen CAF, Knol EF, Giovannone B, et al. A panel of biomarkers for disease severity in atopic dermatitis. Clin Exp Allergy. 2015;45(3):698–701.